ABSTRACT

A TEST OF DIAGENETIC ORDERING IN SILICEOUS LITHOFACIES, MONTEREY FORMATION, SOUTHWESTERN CASMALIA HILLS, SANTA MARIA BASIN, CALIFORNIA

By

Idu Opral C. Ijeoma

December 2014

A study of 230 samples of porcelanite and siliceous mudstone from a single stratigraphic section containing all three silica phases in the Sisquoc and Monterey formations Casmalia Hills, California, tested established models of silica diagenesis. Analysis of composition, silica phase, and d_{101}-spacing using combined EDS/XRF and XRD documented a broad distribution of opal-CT d_{101}-spacing values rather than a linear progression for any particular compositional range predicted by prior studies. The data from this thesis study strongly suggest that other variables (e.g., carbonate, organic matter) besides burial depth/temperature and normalized silica:detritus ratios are critical to diagenetic ordering and that the opal-CT d_{101}-spacing and silica content of a single sample cannot be used as a geothermometer. Instead, the maximum opal-CT d_{101}-spacing in a set of samples for any normalized silica:detritus ratio in a stratigraphic interval may be useful to determine the minimum temperature or maximum burial depth reached prior to tectonic uplift.

A TEST OF DIAGENETIC ORDERING IN SILICEOUS LITHOFACIES, MONTEREY FORMATION, SOUTHWESTERN CASMALIA HILLS, SANTA MARIA BASIN, CALIFORNIA

A THESIS

Presented to the Department of Geological Sciences

California State University, Long Beach

In Partial Fulfillment

of the Requirements for the Degree

Master of Science in Geology

Committee Members:

Richard J. Behl, Ph.D. (Chair)
Gregory Holk, Ph.D.
Greg Hummel, M.S.

College Designee:

Robert D. Francis, Ph.D.

By Idu Opral C. Ijeoma

B.S., 2004, Texas Woman's University

December 2014

WE, THE UNDERSIGNED MEMBERS OF THE COMMITTEE,

HAVE APPROVED THIS THESIS

A TEST OF DIAGENETIC ORDERING IN SILICEOUS LITHOFACIES, MONTEREY FORMATION, SOUTHWESTERN CASMALIA HILLS, SANTA MARIA BASIN, CALIFORNIA

By

Idu Opral C. Ijeoma

COMMITTEE MEMBERS

Richard J. Behl, Ph.D. (Chair)	Geological Sciences
Gregory Holk, Ph.D.	Geological Sciences
Greg Hummel, M.S	Retired Geologist

ACCEPTED AND APPROVED ON BEHALF OF THE UNIVERSITY

Robert D. Francis, Ph.D.
Department Chair, Department of Geological Sciences

California State University, Long Beach

December 2014

ACKNOWLEDGEMENTS

I would like to take the time to thank everyone who supported me through my journey. To my advisor, Dr. Richard Behl, thank you for believing and allowing and me to be part of the Monterey and Related Sediments (MARS) team. You are a great inspiration and example of someone who is passionate about there work. You have showed me what it takes to be successful not just in my career, but in my life. To all the instructors and professors who helped me during my journey, your love and dedication to Geology is why I am where I am today. To all my friends that helped me along the way with their support, I thank you all. To Jim Fisher and all my coworkers at American Vanguard Corp thank you for all the support and encouragement over the years. The flexibility provided from this job allowed me to finish my course work in a timely manner and still be able to support myself financially. To my undergrad assistant Jessica Uglesich, I am so glad you were able to help me in the field. You are an awesome and amazing person with a positive attitude; I wish you luck in all of your future endeavors. To my family, from the beginning I have always had your support no matter what I have decided to do in my life. I am so lucky that I come from such a strong breed of hardworking people. I would also like to make a dedication to Greg Hummel, who despite current events in his life stayed with his commitment to my thesis, I cannot thank you enough.

TABLE OF CONTENTS

Page

ACKNOWLEDGEMENTS iii

LIST OF TABLES vi

LIST OF FIGURES vii

CHAPTER Page

1. INTRODUCTION 1

2. BACKGROUND 4

Siliceous Sediments 4
Siliceous Polymorphs 4
Silica Diagenesis 5
Rate Controlling Factors of Diagenesis 6
Oceanographic Setting of Siliceous Sedimentation 8
Monterey Formation 8
Lithology 9
Stratigraphy 10
Santa Maria Basin 13
Previous Studies 17

3. METHODS 31

Introduction 31
Field Methods 32
Stratigraphic Position of Samples 32
Mineralogic and Geochemical Analyses 36
X-Ray Diffraction 36
Energy Dispersive X-ray Spectroscopy/X-Ray Fluorescence 40

4. RESULTS 43

Data Description 43
Lower Sisquoc Formation 44
Upper Monterey Formation 45

CHAPTER Page

Middle Monterey Formation 45
Lower Monterey Formation 46

5. DISCUSSION 62

Summary and Explanation of Results 62
Summary and Explanation of Previous Studies 71
Assessment of Inconsistencies and Possible Explanations 87

6. CONCLUSIONS 96

5. RECOMMENDATIONS FOR FUTURE WORK 99

APPENDICES 101

A. X-RAY DIFFRACTION AND COMBINED ELECTRON SPECTROSCOPY/ X-RAY FLUORESCENCE DATA TABLES 102

B. COMBINED ELECTRON SPECTROSCOPY/X-RAY FLUORESCENCE METHOD 118

C. CALIBRATION ERROR 141

REFERENCES 144

LIST OF TABLES

TABLE Page

1. Table Showing Monterey Formation Sedimentary Components..... 41

2. Table Showing R^2 of Samples and Standards from Calibration and Actilabs Analysis..... 42

3. Table Showing Formation Name, Number of Samples, and Measured Stratigraphic Depth Range..... 46

LIST OF FIGURES

FIGURE Page

1. General relationships between siliceous lithologies and silica phase in the Monterey Formation 11

2. Composite geologic column and stratigraphic subdivision of the Monterey Formation for the coastal Santa Maria-Lompoc area 12

3. Geologic map of the Santa Maria basin area with the Casmalia Hills study are enclosed in the box..... 15

4. Geological map of the Casmalia Hills, which is outlined in black. Siquoc (Tsq), Upper Monterey (Tm), Middle Monterey cherts (Tmch), and Lower Monterey (Tml) 16

5. Variation in d_{101}-spacing of opal-CT with depth for porcelanite and chert at Chico Martinez Creek. 20

6. Opal-CT d_{101}-spacing in six wells from the Santa Maria oilfield shows a trend of decreasing value with depth 21

7. Three fields in the Santa Maria Basin showing a trend of decreasing d_{101}-spacing with depth..... 22

8. Map of Mussel Rock showing an irregular distribution of d_{101}-spacing 23

9. Distribution of opal-CT d_{101}-spacing with depth of samples from four DSDP sites from the north Pacific 24

10. The progressive ordering of d_{101}-spacing varying with composition along the Santa Barbara coast..... 27

11. The progression of opal-A to opal-CT to quartz with temperature scales..... 28

12. ODP sites from the deep West Pacific showing opal-CT d_{101}-spacing decreasing only generally with depth 29

FIGURE Page

13. Three ODP core holes from the deep West Pacific plotted by composition show very weak correlations with depth. 30

14. Dip-parallel profile of the field area with positions of samples projected on the profile represented by the inclined lines. 34

15. Shows a visual relationship of the bed direction, position of the samples, and their stratigraphic depth 35

16. Top and side view of slide and holder arrangement 38

17. Diffractogram showing the method used to measure the d_{101}- spacing of opal-CT relative to quartz standard 39

18. This X-ray diffractogram shows opal-CT porcelanite with a 4.10 Å d_{101}-spacing that consists of 75% diagenetic silica 48

19. X-ray diffractogram of opal-CT porcelanite with 4.07 Åd_{101}-spacing that consists of 91% silica 49

20. X-ray diffractogram of opal-CT siliceous shale with 4.04 Å) d_{101}-spacing that consists of 52% silica 50

21. X-ray diffractogram of a quartz-phase porcelanite that consists of 86% diagenetic silica 51

22. Graphs showing opal-CT d_{101}-spacing plotted versus stratigraphic depth in meters for narrow 10 percent silica ranges on a carbonate-, apatite-, and organic matter-free basis 52

23. Two stratigraphically similar beds from the upper Monterey showing variable composition and opal-CT d_{101}-spacing 53

24. Major oxides in samples from the lower Sisquoc Formation, measured by combined EDS/XRF 54

25. Major oxides in samples from the upper Monterey Formation, measured by combined EDS/XRF 55

26. Major oxides in samples from the middle Monterey Formation, measured by combined EDS/XRF 56

27. Major oxides in samples from the lower Monterey Formation, measured by combined EDS/XRF 57

FIGURE Page

28. Abundances of sedimentary components and opal-CT d_{101} - spacing of samples from the lower Sisquoc Formation, measured by combined EDS/XRF and XRD 58

29. Abundances of sedimentary components and opal-CT d_{101} - spacing of samples from the upper Monterey Formation, measured by combined EDS/XRF and XRD. 59

30. Abundances of sedimentary components and opal-CT d_{101} - spacing of samples from the middle Monterey Formation, measured by combined EDS/XRF and XRD. 60

31. Abundances of sedimentary components and opal-CT d_{101} - spacing of samples from the lower Monterey Formation, measured by combined EDS/XRF and XRD 61

32. Opal-CT d_{101}- spacing versus stratigraphic depth from the lower Sisquoc Formation plotted for narrow 10 percent silica ranges on a carbonate-, apatite-, and organic matter-free basis. 65

33. Opal-CT d_{101}- spacing versus stratigraphic depth from the upper Monterey Formation plotted for narrow 10 to 20 percent silica ranges on a carbonate-, apatite-, and organic matter-free basis 66

34. Opal-CT d_{101}- spacing versus stratigraphic depth from the middle Monterey Formation plotted for narrow 10 to 20 percent silica ranges on a carbonate-, apatite-, and organic matter-free basis 67

35. Opal-CT d_{101}- spacing versus stratigraphic depth from the lower Monterey Formation plotted for narrow 10 to 20 percent silica ranges on a carbonate-, apatite-, and organic matter-free basis 68

36. Data showing the correlation between opal-CT d_{101}- spacing and silica content in all the porcelanite samples from different Monterey Formation members 69

37. Initially opal-CT is varied, but with burial, the most poorly ordered crystallites become increasingly destabilized and are dissolved or removed from the system 70

38. The upper Monterey Formation is designated the Antelope Shale at Chico Martinez Creek and the Clayey-Siliceous member in the Santa Maria basin.. 77

FIGURE Page

39. Experimental results of opal-CT d_{101}-spacing vs. temperature during the hydrothermal transformation of silica from all experiments 78

40. Wells 12-15 from the Santa Maria Valley Field showing general trends of decreasing d_{101}-spacing with depth 79

41. Well 17 from the Bradley area showing a trend of decreasing d_{101}-spacing with depth with large step in middle of the succession 80

42. Wells 30-32 from the Orcutt Field showing weak or irregular trends of decreasing d_{101}-spacing with depth 81

43. Data showing the relationship between composition and opal-CT d101-spacing for closely spaced rock from different sites in the siliceous member 82

44. Data showing the relationship between composition and opal-CT d101-spacing in closely spaced rocks from different sites in the transition and upper calcareous shale members 83

45. Data showing the relationship between composition and opal-CT d101-spacing for closely spaced rock from the Gato and San Augustine Canyon sections... 84

46. Data from the San Augustine Canyon section showing opal-CT d_{101}- spacing plotted versus stratigraphic depth in meters for narrow 10 percent silica ranges on a carbonate-, apatite-, and organic matter-free basis 85

47. Data from the Gato Canyon section showing opal-CT d_{101}- spacing plotted versus stratigraphic depth in meters for narrow 10 to 30 percent silica ranges on a carbonate-, apatite-, and organic matter-free basis 86

48. Model for diagenetic ordering with growth of opal-CT lepispheres 93

49. With increased burial higher opal-CT d_{101}-spacing values dissolve and re-precipitate as more ordered opal-CT with increased silica content..... 94

50. Silica migration and reprecipitation between layers at lamination to bed scale results in changes in silica concentration and opal-CT d_{101}-spacing 95

CHAPTER 1

INTRODUCTION

Highly siliceous sediment makes up much less than 1 percent of the sedimentary record (Tucker, 2010). These rocks are unusually significant because of their association with other important resources such as, petroleum, iron, manganese, barite, phosphorite, and uranium (Iijima et al, 1983; Hein and Scholl, 1978). Such biosiliceous deposits occur in polar regions, the equatorial belt, and in coastal areas where cold nutrient-rich water upwells (Iijima et al., 1983; Hein and Scholl, 1978). Biosiliceous sediments have existed throughout the Phanerozoic, with a primarily radiolarian composition in the Paleozoic and Mesozoic and mostly diatomaceous component in the Cenozoic (Hein, 1978).

Siliceous sediments undergo a unique and complex diagenesis with two steps and three polymorphic phases (Bramlette, 1946). Along with the change in silica polymorph, there are tremendous stepwise changes in porosity, rock strength, and fluid expulsion with great implications for basin hydrology, geochemical reorganization and petroleum geology (Eichhubl and Behl, 1998). The process starts with opal-A (x-ray amorphous hydrous silica) in the form of biogenic siliceous oozes; which with burial converts to opal-CT (hydrous silica with disordered stacking of cristobalite and tridymite). These phases with continued burial, convert to stable anhydrous quartz (Bramlette, 1946;

Murata and Larson, 1975; Hein and Scholl, 1978). This progressive ordering of the phases has been linked to burial depth, temperature, and time. Several studies such as Murata and Larson (1975), Pisciotto (1978), and Isaacs (1980) have concluded that the progressive crystallographic ordering of opal-CT can be used as a geothermometer, which would be useful for basin analysis, tectonic burial and uplift history, and for modeling the thermal maturity of potential hydrocarbon source rocks. Silica diagenesis has been intensely studied in the Monterey Formation in California (Bramlette, 1946; Murata and Larson, 1975; Pisciotto, 1978; Isaacs, 1980), Miocene-Pliocene formations in Japan (Iijima et al., 1983) and in the Bering Sea (Hein and Scholl, 1978; Hein and Parrish, 1987) and West Pacific (Behl and Smith, 1992).

The purpose of this study is to test the diagenetic models of Isaacs (1980), studies led by Murata (1974, 1975, 1977) and Pisciotto (1978) in a new field area, and to test natural variability in crystallographic ordering of opal-CT at high spatial resolution. Past studies were based on limited or scattered samples, so this study was done with a very dense array of samples collected from a single stratigraphic succession to test these trends. The results from this study will be used to answer the following questions: (1) How variable are the indications of diagenetic state at a single maximum burial depth for a specific compositional range; (2) What is the compositional variability along a single distinct bed; and (3) Is crystallographic ordering a linear progression with depth when analyzed at high-spatial resolution?

The southwestern Casmalia Hills was chosen as the field area for this study because Woodring and Bramlette (1950) described it as the best continuous exposure of siliceous section of the Monterey Formation in the Santa Maria basin, California. Two

hundred and thirty outcrop and road-cut samples were collected and analyzed for composition, silica phase, and d_{101}-spacing using combined Electron Dispersive Spectroscopy/X-Ray Fluorescence (EDS/XRF) and X-Ray Diffraction (XRD) methods. This is the first detailed study of opal-CT d_{101} ordering in a single stratigraphic section. It has 20 times more samples than any published study of a single succession published in the public domain. The findings of this study are not consistent with the simple diagenetic progression in crystallographic ordering of opal-CT that is predicted by previous workers (Murata and Nakata, 1974; Murata and Larson, 1975; Murata et al., 1977; Pisciotto, 1978; Isaacs, 1980). While not necessarily refuting the conceptual model of increased ordering (decreased d_{101}-spacing) with burial depth, this study strongly suggests that other variables beside burial depth/temperature and composition are critical to the detailed progression of diagenesis.

CHAPTER 2

BACKGROUND

Siliceous Sediments

Cenozoic fine-grained, marine siliceous deposits are composed primarily of biogenic silica (SiO_2) derived from opaline debris of diatoms, radiolarians, silicoflagellates, and sponge spicules (Iijima et al., 1983). These sediments undergo a complicated pathway of diagenesis, which entails a two-step dissolution/reprecipitation process (Bramlette, 1946; Murata et al., 1977; Kastner et al., 1977). Biogenic opal-A silica converts with time and burial to metastable opal-CT, which transforms to diagenetic quartz (Bramlette, 1946; Murata and Larson, 1975; Pisciotto, 1978; Isaacs, 1980; Hesse, 1988). This process is responsible for the lithification of these sediments and for dramatic changes in their physical properties.

Silica Polymorphs

Silica exists in multiple polymorphs in sediments and sedimentary rocks (Hesse and Schacht, 2011). *Opal-A* is x-ray amorphous biogenic hydrous silica that occurs primarily as diatoms, radiolarians and sponge spicules, with some occurring from altered volcanic debris (Hein and Scholl, 1978; Williams et al., 1985). *Opal-A'* is a more stable, less soluble form of opal-A sourced from altered tuffaceous siliceous sediments and partially recrystallized diatoms (Hein and Scholl, 1978; Williams et al., 1985); it can precipitate as overgrowth on partially dissolved siliceous tests, but mostly it is an intermediate phase between opal-A and opal-CT (Hein and Scholl, 1978).

Opal-CT also consists of hydrous silica, but with interstratified domains of disordered cristobalite and tridymite. It precipitates within tests and pore spaces as cement and matrix replacement, lepispheres (spherical aggregates of intersecting platy or bladed euhedral crystals), or blades (Wise and Kelts, 1972; Keene, 1976; Kastner, 1979; Williams et al., 1985). *Opal-C* (low cristobalite) is a hydrous form of a well-ordered high-temperature polymorph of cristobalite with minor evidence of tridymite stacking (Jones and Segnit, 1971; Kastner, 1979); it occurs as an intermediate between opal-CT and quartz in some cases (Williams et al., 1985). *Quartz* precipitates first as poorly ordered chalcedony/cryptocrystalline quartz (fibrous structure), which is followed by a neomorphism to microcrystalline quartz (crystals less than 20um) (Kastner, 1979; Williams and Crerar, 1985) or macroquartz with the approach of metamorphic conditions.

Silica Diagenesis

Silica diagenesis is a two-step dissolution-reprecipitation process that generally converts opal-A to opal-CT to quartz (Bramlette, 1946; Murata and Larson, 1975; Kastner et al., 1977) as in Figure 1. The precipitation of each phase is dependent on its equilibrium solubility (Kastner et al., 1977); opal-A is ~60-130 ppm, cristobalite (proxy for opal-CT) is ~20-30 ppm, and quartz is ~6-10 ppm at Standard Temperature and Pressure (Williams et al., 1985). During the transformation of opal-CT to quartz, crystallographic ordering gradually increases with burial; this is shown by the progressive decrease in d_{101}-spacing from about 4.11Å to 4.04 (Mizutani, 1977; Williams et al., 1985). For burial conditions, the temperature ranges required for opal-A to opal-CT transformation are ~40-50ºC and ~65-85ºC for opal-CT to quartz (Williams and Crerar, 1985). In deep-sea settings where sedimentation is slower the temperature ranges

required for opal-A to opal-CT transformation are ~8-35ºC and ~30-68ºC for opal-CT to quartz, but require longer timespans (Siever, 1983).

Rate-Controlling Factors of Diagenesis

The rates of these transformations are controlled by many factors, such as differences in solubility of polymorphs, surface area, temperature, bulk composition, pore water chemistry, pH, salinity, pressure, and grain size (Williams et al., 1985). Surface area, which is especially large in very small, very porous, or irregularly shaped particles or crystallites, affects the solubility and rate of diagenesis (Williams et al., 1985). The pH and pressure can also affect silica solubility, when pH is >9 or there is an increase in pressure, the solubility of silica increases (Volosove et al., 1972; Willey, 1974; Walther and Helgeson, 1977; Iler, 1979; Williams and Crerar, 1985). Temperature also affects the solubility of biogenic SiO_2 and consequently the kinetics of the reactions (Lawson et al., 1978; Kamatani and Riley, 1979; Kamatani et al., 1980; Kamatani, 1982; Van Cappellen and Qiu, 1997a; Van Cappellen and Qiu, 1997b; Lourcaides, 2009). Higher temperatures increase silica solubility, silica concentration in pore fluids, and rates of diagenetic reactions (Ernest and Calvert, 1969; Stein and Kirkpatrick, 1976; Williams and Crerar, 1985).

Sediment composition is another important controlling factor; the kinetics and average temperature of silica-phase transformations varies with the relative abundance of terrigeneous detritus (Isaacs, 1983). Opal-CT forms at slightly lower temperature in rocks containing relatively less detritus will have a larger $d\text{-}_{101}$ spacing, and diagenetic quartz forms at slightly lower temperatures in sediments with greater detritus (Williams and Crerar, 1985; Isaacs, 1980). The relationship between the abundance of terrigeneous

detritus and temperatures of silica-phase transformations may be caused by the influence of smectite on the chemistry of pore waters during diagenesis (Kastner et al., 1977; Keller and Isaacs, 1985). The presence of smectite retards the silica conversion rate of opal-A to opal-CT, while the opal-CT to quartz transformation is accelerated (Williams and Crerar, 1985; Isaacs, 1980). The opal-A to opal-CT transformation is enhanced by the presence of Mg^{++} and $(OH)^{-}$ (Kastner et al., 1977; Brueckner and Snyder, 1985), but smectites compete by taking up Mg^{++}, thus retarding the precipitation of opal-CT. In the presence of dissolving carbonates, formation of complexes such as $Mg(OH)_2$ can act as a catalyst to nucleate opal-CT (Williams and Crerar, 1985). Also, the presence of dissolved carbonates increases the alkalinity, which raises the pH, thereby increasing the solubility of silica (Williams and Crerar, 1985; Isaacs, 1980). Experimental evidence suggests that the rate of silica diagenesis is reduced in organic-rich sediments, especially if the organic material present produces large quantities of organic acids (Hinman, 1990). While Siever and Scott (1963) predicted that the initial degradation of organic matter would increase the pH of pore fluids and promote silica diagenesis by increasing dissolution of silica, the results of Hinman (1990) suggest that later organic maturation and organic acid dissociation actually *decrease* the pH of solutions, thereby reducing the inorganic alkalinity and reducing the rate of silica diagenesis. These findings imply that in rocks with higher organic content, opal-CT will be produced more slowly and therefore have a lower $d\text{-}_{101}$ spacing when precipitated than the opal-CT that formed in rocks with lower organic carbon content (Hinman, 1990).

Oceanographic Setting of Siliceous Sedimentation

Large accumulations of siliceous sediments can be found along the Pacific Rim in and offshore of Korea, Japan, Kamchatka as well as the Pacific coast of North America, south to the Tres Marias Islands off central Mexico (Ingle, 1973, 1981) and along and offshore of the Pacific coast of South America (Martinez and Caro, 1980; Ingle, 1981). The primary global locus of biogenic silica deposition shifted from the Caribbean and low-latitude North Atlantic to the North Pacific during the middle Miocene, following tectonic opening of oceanic circulation gateways and increased upwelling intensity that provided the necessary silica and nutrients for these siliceous organisms to thrive in the Pacific, particularly in the Monterey Formation of the California margin (Barron, 1986). The change in ocean circulation was also related to severe cooling and buildup of the Antarctic ice sheet that provided a source of cold bottom-water and increased latitudinal thermal gradient to accelerate winds and intensify coastal upwelling (Ingle, 1981).

Monterey Formation

One of the best-studied areas of the Northern Pacific siliceous deposits is the Miocene Monterey Formation in California, a highly diatomaceous deposit and a major source and reservoir of petroleum (Bramlette, 1946). The Monterey Formation was deposited from approximately 17.5 Ma to 6.2 Ma into basins that formed as a consequence of the change of the California margin from a convergent to transform setting (Barron, 1986). The Monterey Formation is primarily composed of fine-grained siliceous sediments with a mix of detrital, organic-rich matter, and calcareous constituents (Bramlette, 1946; Pisciotto and Garrison, 1981). These siliceous sediments are predominantly composed of diatoms, with less significant amounts of siliceous

sponge spicules, radiolarians and silicoflagellates (Bramlette, 1946; Isaacs, 1980). The terrigeneous detritus in the outer basins is primarily mixed-layer illite-montmorillonite, with some detrital quartz, plagioclase feldspar, potassium feldspar, mica, and rarer chlorite (Isaacs, 1981c); inner basins contain proportionately more feldspar and mica. The organic-rich matter is mostly type II kerogen–marine algae. The carbonate is derived from coccoliths and foraminifers (Isaacs, 1983; Isaacs and Petersen, 1987).

Lithology

The Monterey Formation in California contains a diverse suite of lithologies, which include: calcareous, diatomaceous and siliceous mudrocks, dolomite, porcelanite, and chert (Bramlette, 1946; Keene, 1975; Murata and Larson, 1975; Isaacs, 1981c). Calcareous and siliceous mudrocks are fine-grained, predominantly siliciclastic rocks that contain coccoliths, foraminifers, and diatoms (Bramlette, 1946; Keene, 1975; Murata and Larson, 1975; Isaacs, 1981c). Siliceous mudstones contain diagenetic silica and are fine-grained rocks that are less siliceous than chert or porcelanite, have a grainy surface texture, and are generally free of carbonate (Bramlette, 1946; Keene, 1975; Murata and Larson, 1975; Isaacs, 1981c). Cherts are aphanitic rocks with a waxy to vitreous surface have a hardness ≥ 5 and are brittle and break with a conchoidal fracture (Bramlette, 1946; Keene, 1975; Murata and Larson, 1975; Isaacs, 1981a). Porcelanites are siliceous sedimentary rocks with a dull or matte luster resembling that of unglazed porcelain, which are less hard and less dense than chert and commonly have lower silica content (Pisciotto, 1981b). Porcelanites have a hardness ≤ 3 due to their greater porosity and clay content and fracture irregularly with a rough splintery to blocky surface (Isaacs, 1981c). Porcelanites and siliceous shales were chosen as the main lithology analyzed for this

study because previous studies indicate that they have a simpler burial diagenetic pathway than cherts (Behl and Garrison, 1994) and display the full range of d_{101}-spacings (Pisciotto, 1978). It is important to note that there is a relationship between siliceous lithologies and silica phase: diatomaceous mudstones/shales contain opal-A silica, whereas siliceous shales, porcelanites, and cherts can contain opal-CT or quartz (e.g., Bramlette, 1946; Pisciotto, 1981a; Isaacs, 1981c; Fig. 1).

Stratigraphy

The Monterey Formation can generally be divided into three main lithostratigraphic units; in ascending stratigraphic order, these are the calcareous, phosphatic, and siliceous members (Pisciotto and Garrison, 1981). Locally, different areas, like the Santa Maria basin, have a more complex version of this stratigraphy (Isaacs, 1981a; Mackinnon, 1989; Fig. 2). The lower calcareous member is composed primarily of foraminifera and coccolithic shale and mudstone with abundant biogenic and authigenic carbonate (Isaacs, 1981a), and contains both calcareous and dolomitic rocks. The middle phosphatic member is composed chiefly of organic-rich, phosphatic calcareous shale and mudstone, which is cyclically interbedded with siliceous or dolomitic rocks (Pisciotto, 1981a). In the Santa Maria basin, the middle section also includes the purest cherts (Woodring and Bramlette, 1950). The upper siliceous member is composed primarily of both biogenic and diagenetic silica and fine detritus (mostly clay), mainly as siliceous mudstone or shale, diatomaceous mudstone or shale, porcelanite, and chert (Isaacs, 1981a).

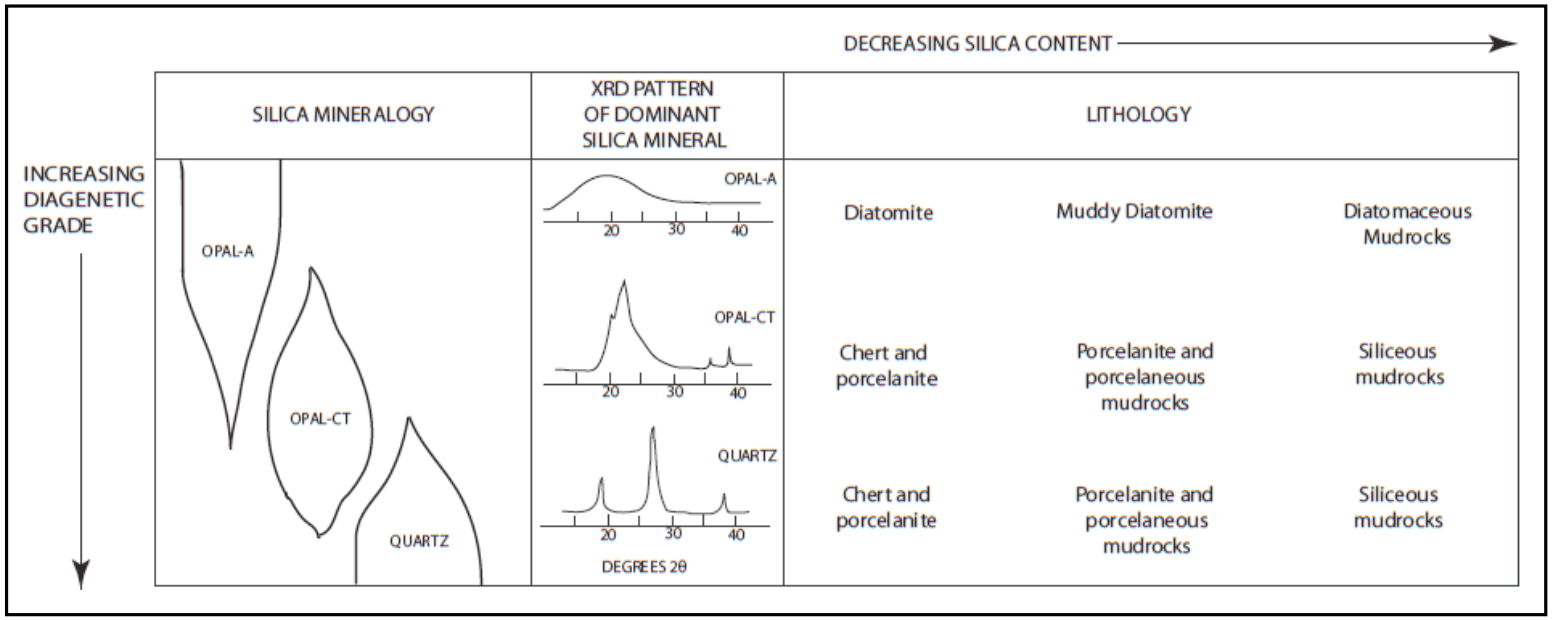

FIGURE 1. General relationship between siliceous lithologies and silica phase in the Monterey Formation. (After Pisciotto, 1981a)

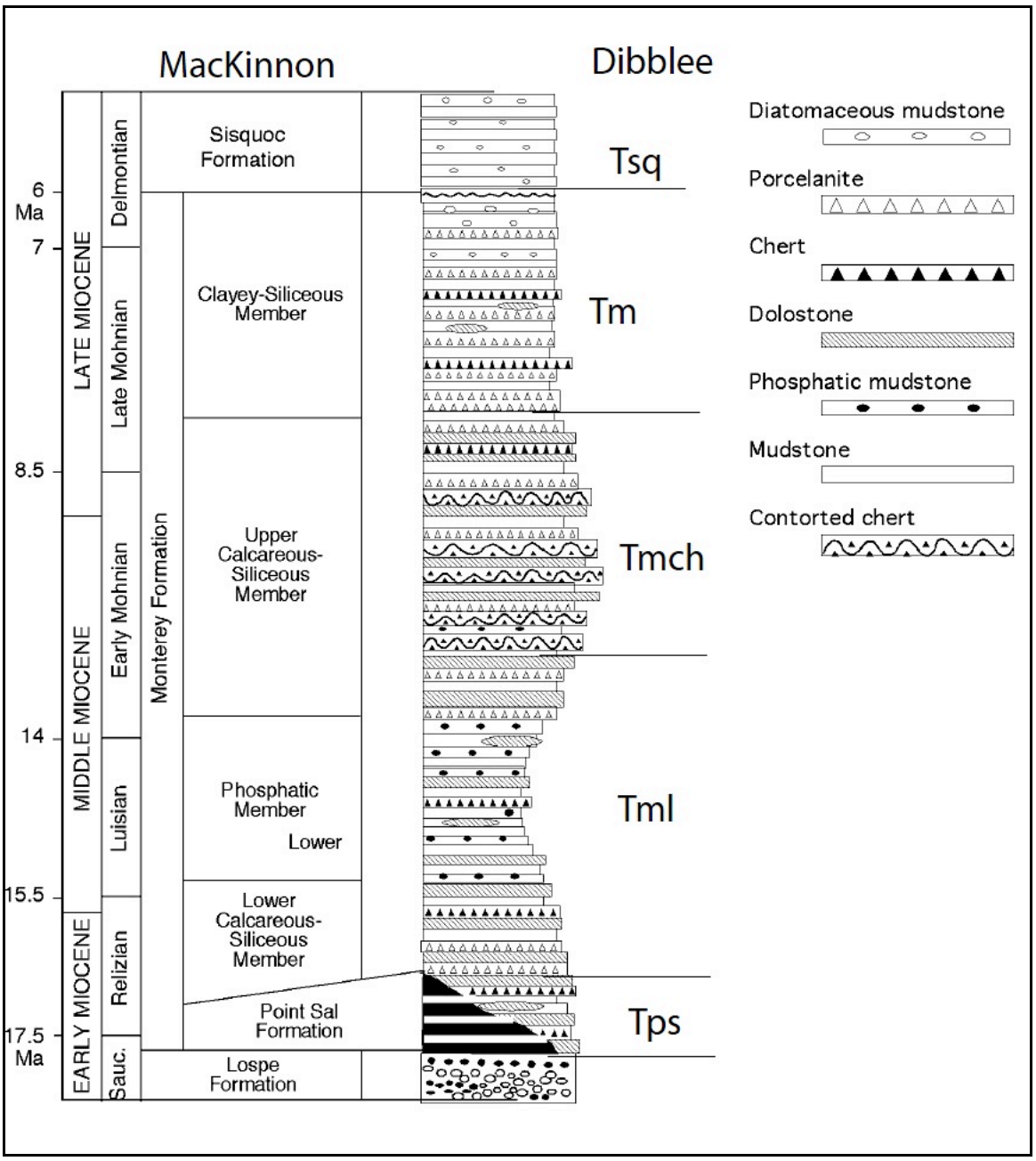

FIGURE 2. Composite geologic column and stratigraphic subdivision of the Monterey Formation for the coastal Santa Maria-Lompoc area (modified MacKinnon (1989) and correlated to Dibblee (1989a, 1989b)

Santa Maria basin

One of the finest surface exposures to show the opal-A to opal-CT to quartz transition in the Monterey Formation is the southwestern Casmalia Hills, Santa Maria basin, California. The onshore Santa Maria basin is a triangular-shaped basin located in the southern Coast Ranges of central California; it is bound by the Hosgri fault to the west, the Nacimiento-Rinconada fault to the northeast and, the Western Transverse Ranges to the south (Woodring and Bramlette, 1950; Fig. 3). The formation of the basin was directly related to the onset of the North American-Pacific transform margin and rotation of the Western Transverse Ranges. The Farallon plate was subducted eastward underneath the central California part of the North American plate during the early Cenozoic (McCrory et al., 1995), which led to the Pacific-Farallon ridge colliding with North American plate after 30 Ma (Atwater, 1970; McCrory et al., 1995). The new interaction of the Pacific and North American plates, and consequent geometric realignment of the Californian Margin, led to the formation of numerous basins and transition from subduction to strike-slip tectonics (Blake et al., 1978). The Santa Maria basin underwent numerous basin tectonic stages from the late Oligocene to the present (McCrory et al., 1995). Between ~18 to 16 Ma, the basin underwent transtension and rapid subsidence (Stanley et al., 1992; McCrory et al., 1995) followed by a slower phase of subsidence from 16 to 7 Ma (McCrory, 1995), which allowed for deposition of sediments. The clockwise rotation of the Western Transverse Ranges eventually caused transpression and shortening that continues to the present (McCrory et al., 1995). The Santa Maria basin contains up to 4.5 km of Miocene and younger strata including the Monterey and Sisquoc formations (Woodring and Bramlette, 1950; McCrory et al., 1995),

which overlie the Point Sal Ophiolite, Franciscan Complex, and Great Valley sequence basement rocks (McLean, 1991; McCrory et al., 1995).

Interest in the Santa Maria area was amplified by the discovery of oil in August 1901 by the Western Oil Company, which led to geological studies by Arnold and Anderson (1907), Woodring and Bramlette (1950), and Pisciotto (1981a), among others. The study area for this thesis research is in the Casmalia Hills (Fig. 4), a northwest-southeast-trending emergent anticlinal structure located north of the east-west-trending Western Transverse Ranges in western Santa Barbara County. The outcrops in these hills expose a complete section of the of the Monterey formation between the underlying Point Sal Formation and overlying Sisquoc Formation.

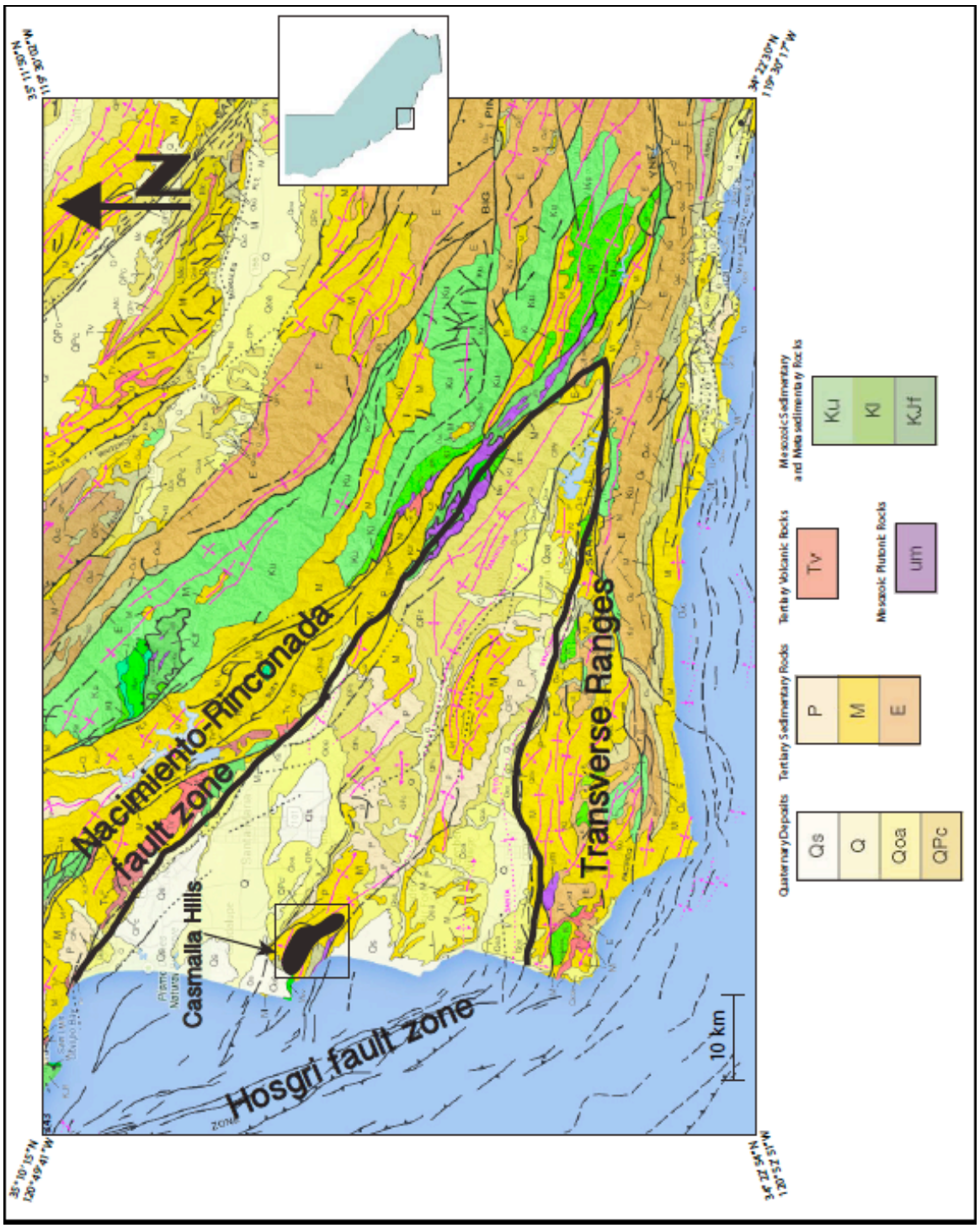

FIGURE 3. Geological map of the Santa Maria basin area with the Casmalia Hills study area enclosed in the box (http:// http://ngmdb.usgs.gov/maps/mapview/).

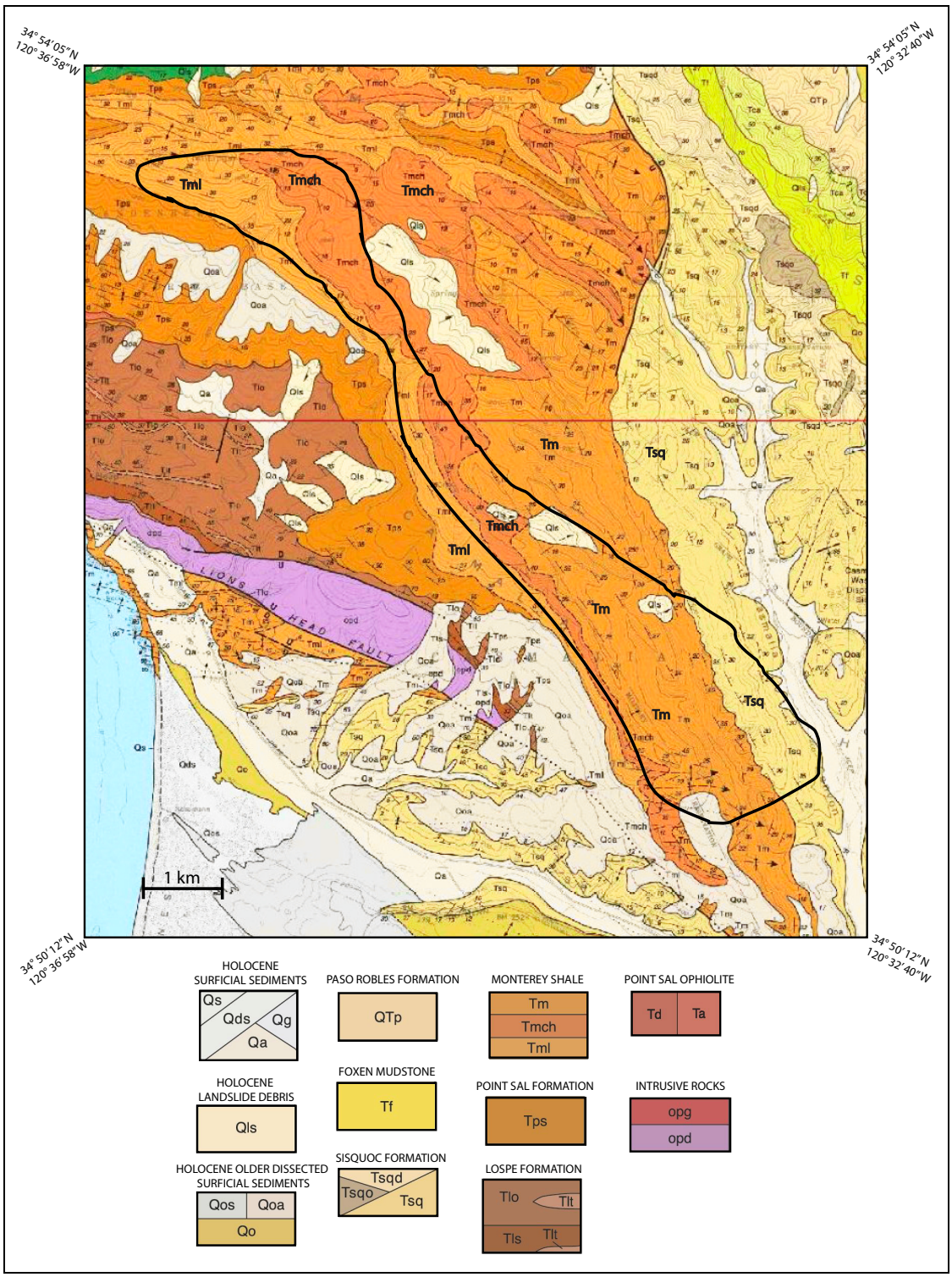

FIGURE 4. Geological map of the Casmalia Hills, which is outlined in black. Siquoc (Tsq), Upper Monterey (Tm), Middle Monterey cherts (Tmch), and Lower Monterey (Tml) after Dibblee (1989a & 1989b).

Previous Studies

Bramlette (1946) first recognized the significance of the siliceous rocks of the Monterey Formation and that they underwent diagenesis with burial. In his classic paper, he studied numerous basins that contained the Monterey shale, including the Santa Maria basin, and completed a detailed paleontologic and stratigraphic study that characterized the different facies and lithologies by observation of field relationships and thin sections, and by comparison of stratigraphic successions. He also presented minor geochemical analysis of silica and alumina ratios (Bramlette, 1946). Bramlette developed important, early ideas about silica transformations involved in the formation of chert and porcelanite and their relationship to burial diagenesis of diatomaceous sediment. Since then, a number of key studies detailed below continued to advance understanding of the process of silica diagenesis, explored the influence of composition on silica diagenesis, timing and temperature of phase transitions, changes in crystallographic ordering with depth, and changes in rock properties.

About thirty years later, a series of studies by Murata and colleagues (1974, 1975, 1977) focused on the siliceous facies in the Chico Martinez Creek area, San Joaquin basin, using texture to characterize the cherts and porcelanites, and x-ray diffraction (XRD) to determine their mineralogy (Murata and Larson, 1975). They documented the progressive ordering of opal-CT as represented by decreasing d_{101}- spacing of cristobalite with depth in a single stratigraphic section. The trend was shown for both chert and porcelanite, but with only a few samples (N=30) and without geochemical information on rock composition. Opal-CT-phase samples were from the Antelope Shale member, which is equivalent to the Upper Clayey-Siliceous member in the Santa Maria basin. The

diagenetic conversions of opal-CT in chert and porcelanite have different paths and timing (Behl and Garrison, 1994) and at any given depth, the d_{101}-spacing of porcelanite is 0.001–0.015 angstroms smaller than that of associated chert (Murata and Nakata, 1974; Fig. 5). Oxygen isotope ratios indicate that the initial temperature of formation for cristobalite was about 48°C and about 80°C for microquartz (Murata et al., 1977).

A few years later, Pisciotto (1978, 1980, 1981a, 1981b), examined lithofacies and silica diagenesis in the Santa Maria basin; this was done by XRD and thin-section petrography of outcrop and core samples from oil wells (Pisciotto, 1981b). Only porcelanites and siliceous mudrocks (non-cherts) were used to investigate the spatial distribution of diagenetic silica minerals (Pisciotto, 1981a). Six wells from the Santa Maria Valley field in a homoclinally-dipping section showed a general trend of a progressively decreased d_{101}-spacing with depth and overburden in individual stratigraphic successions (Pisciotto, 1978; Fig. 6). Other oil fields (Bradley and Orcutt) in the basin also show the same general trend but with minor differences (Pisciotto, 1981b; Fig. 7). However, Pisciotto also found that the diagenetic trend from outcrop samples of porcelanite, siliceous shale and chert from Mussel Rock (middle Monterey) was not a regular progression and showed an irregular pattern of d_{101}-spacing (Fig. 8). Pisciotto confirmed that temperature is an important control of silica transformation and can reflect past and present differences in thermal gradients of an area (Mizutani, 1977). He also calculated the temperature ranges for silica phase transformations from present geothermal gradients, and depths of burial for intact sections of the Monterey and other Neogene siliceous rocks in the Pacific region; these values were compared to temperature ranges calculated from oxygen isotopic data (Pisciotto, 1978). His combined isotopic and

calculated temperatures of transformation for opal-CT yielded the following ranges: 29-49°C for opal-CT and 42-75°C for quartz.

Hein and Scholl (1978) studied silica diagenesis in cores from Deep Sea Drilling Project (DSDP) Leg 19 in the far northwest Pacific and the Bering Sea. Petrographic microscopy, XRD, scanning electron microscopy (SEM), and energy dispersive X-ray spectroscopic (EDX) techniques were utilized to identify the mineralogy, silica phase, opal-CT d_{101}-spacing, and elemental composition of samples (Hein and Scholl, 1978). The results demonstrated that the d_{101}-spacing of opal-CT did indeed decrease with depth of burial at one site–DSDP Site 192–but showed no such trend at Sites 184, 185, and 188 (Hein and Scholl, 1978; Fig. 9). These results do not support the findings of the previous studies of Murata and Larson (1975) and Pisciotto (1978).

Isaacs (1980, 1981a, 1981b, 1981c, 1983) conducted a study along the Santa Barbara coast, which has 55 km of continuous exposure of Monterey rocks that had been progressively buried to greater depths from east to west. The purpose of her study was to characterize the lithologic variation in terms of composition and diagenetic state and to evaluate lateral and vertical trends related to burial environment. XRD and Atomic Absorption were utilized for mineralogy and chemical analysis. Combined mineralogic and geochemical data helped her to develop formulas to calculate ratios of biogenic + diagenetic silica to total detritus (Isaacs, 1980). She identified different lithologies, compared their field characteristics and assembled them into 5 lithologic members of the Monterey Formation: uppermost Siliceous member (carbonate-free), upper Calcareous Shale member, Transition member, Organic Shale member, and the lower Calcareous Shale member. Isaacs (1983) later renamed these units to better reflect their composition

to the Clayey-siliceous, Upper Calcareous-siliceous, Transitional marl-siliceous, Carbonaceous marl, and Lower calcareous-siliceous members, respectively. Isaacs used closely associated rocks that exist at different silica phases to assess the importance of composition (Isaacs, 1980). Figure 10 displays how silica and detrital ratios affect opal-CT d_{101}-spacing. At all locations studied, opal-CT ordering varied with composition in a very consistent way (Isaacs, 1980). Isaacs found that burial depth (and inferred temperature) and composition (detrital content) were major controls of diagenesis and the ordering of opal-CT. As the detrital content increased, opal-CT formed progressively later and quartz formed progressively earlier (Isaacs, 1980). The results from this study were combined into a model for the silica diagenesis progression that should apply to any stratigraphic succession of a particular compositional range. The temperature scales for silica diagenesis were subsequently calibrated based on two points from the average geothermal gradient from the Point Conception COST Well (Keller and Isaacs, 1985; Fig. 11). With this data, opal-CT d_{101}-spacing was inferred to have potential use as a geothermometer and indication of maximum burial depth (e.g., Behl and Morita, 2007).

Finally, Behl and Smith (1992) studied the diagenesis of siliceous rocks recovered during Ocean Drilling Program (ODP) Leg 129 in the Mariana and Pigafetta basins of the western Pacific. This study was of much older middle Jurassic to lower Miocene strata compared to the other workers' study of middle to upper Miocene rocks. Analysis of core samples from ODP Sites 800A, 801A, and 802A demonstrated that for all compositions, opal-CT d_{101}-spacing decreased only generally with depth with wide scatter (Fig. 12). When these same results were plotted with compositional control they showed only a very weak correlation with depth (Fig. 13)

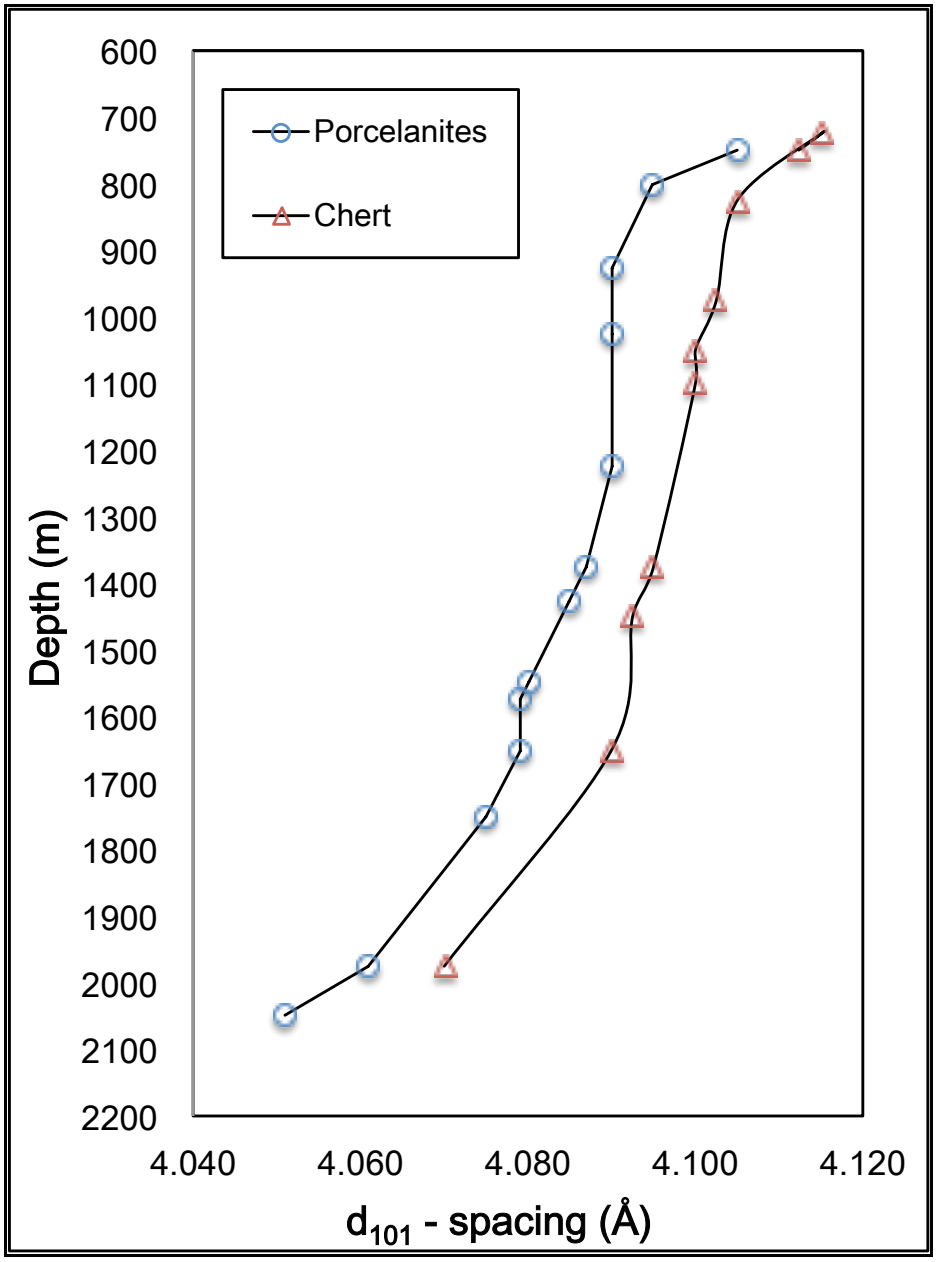

FIGURE 5. Variation in d_{101}-spacing of opal-CT with depth for porcelanite and chert at Chico Martinez Creek. Data from Murata and Nakata (1974).

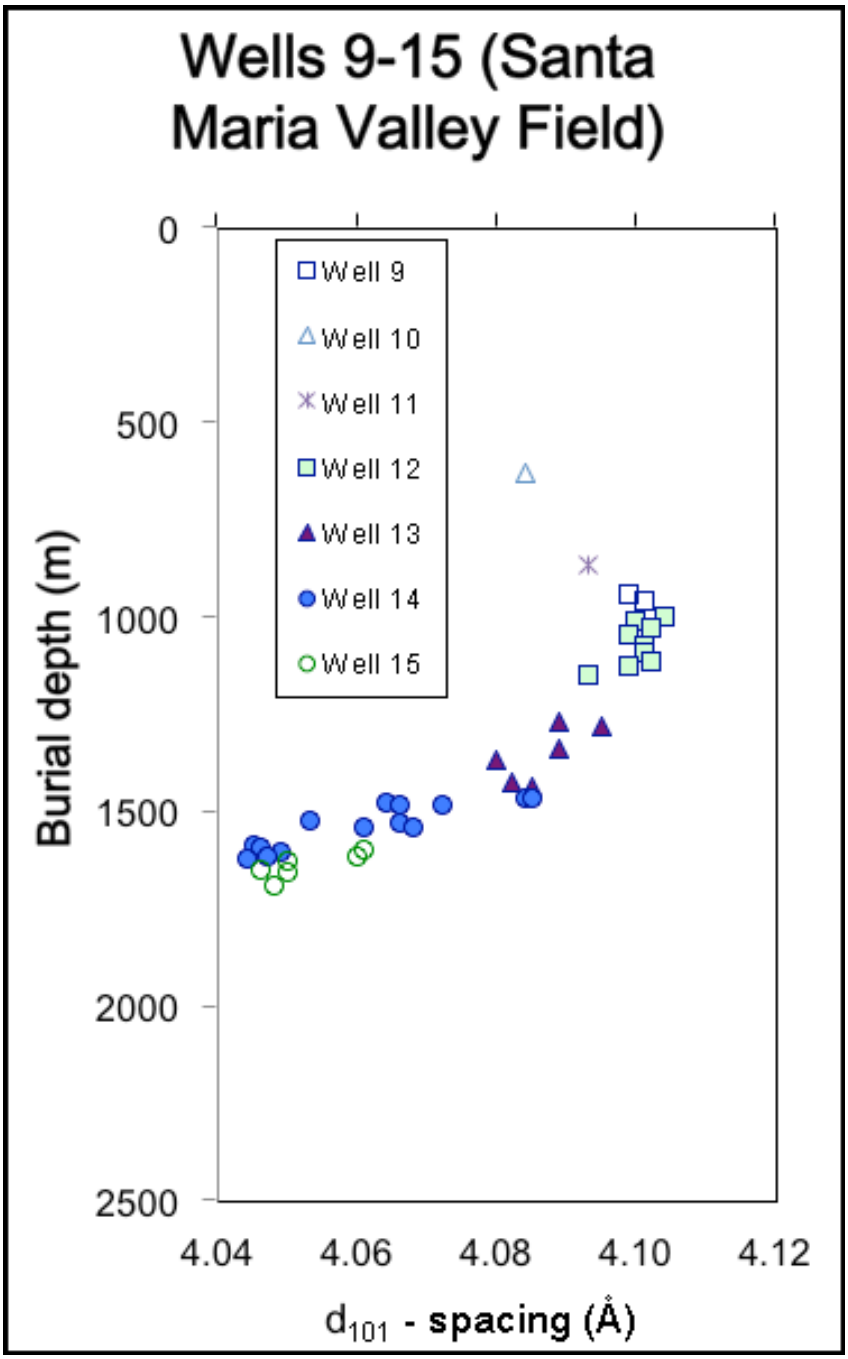

FIGURE 6. Opal-CT d_{101}-spacing in six wells from the Santa Maria oilfield shows a trend of decreasing value with depth. Data from Pisciotto (1978).

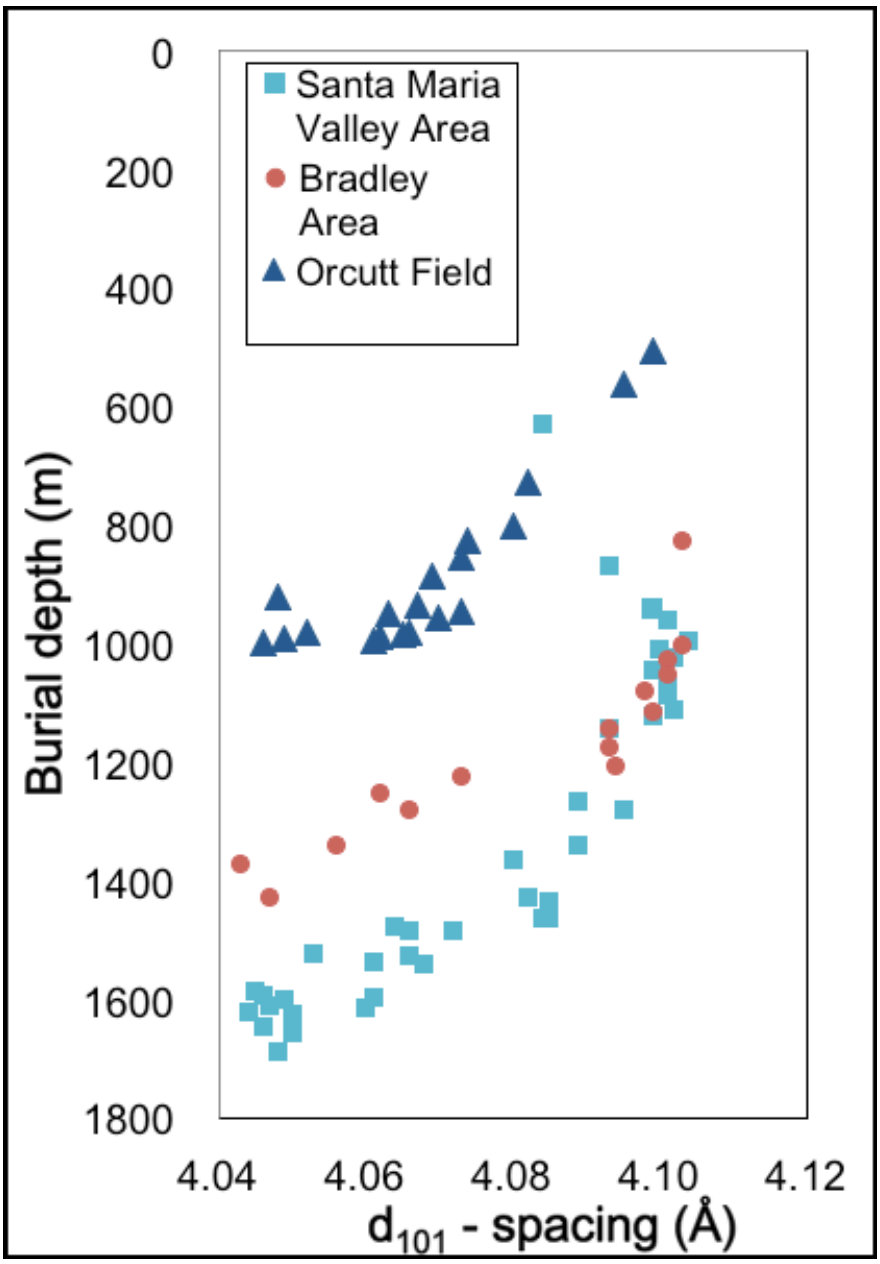

FIGURE 7. Three fields in the Santa Maria Basin showing a trend of decreasing d_{101}-spacing with depth. Data from Pisciotto (1981a).

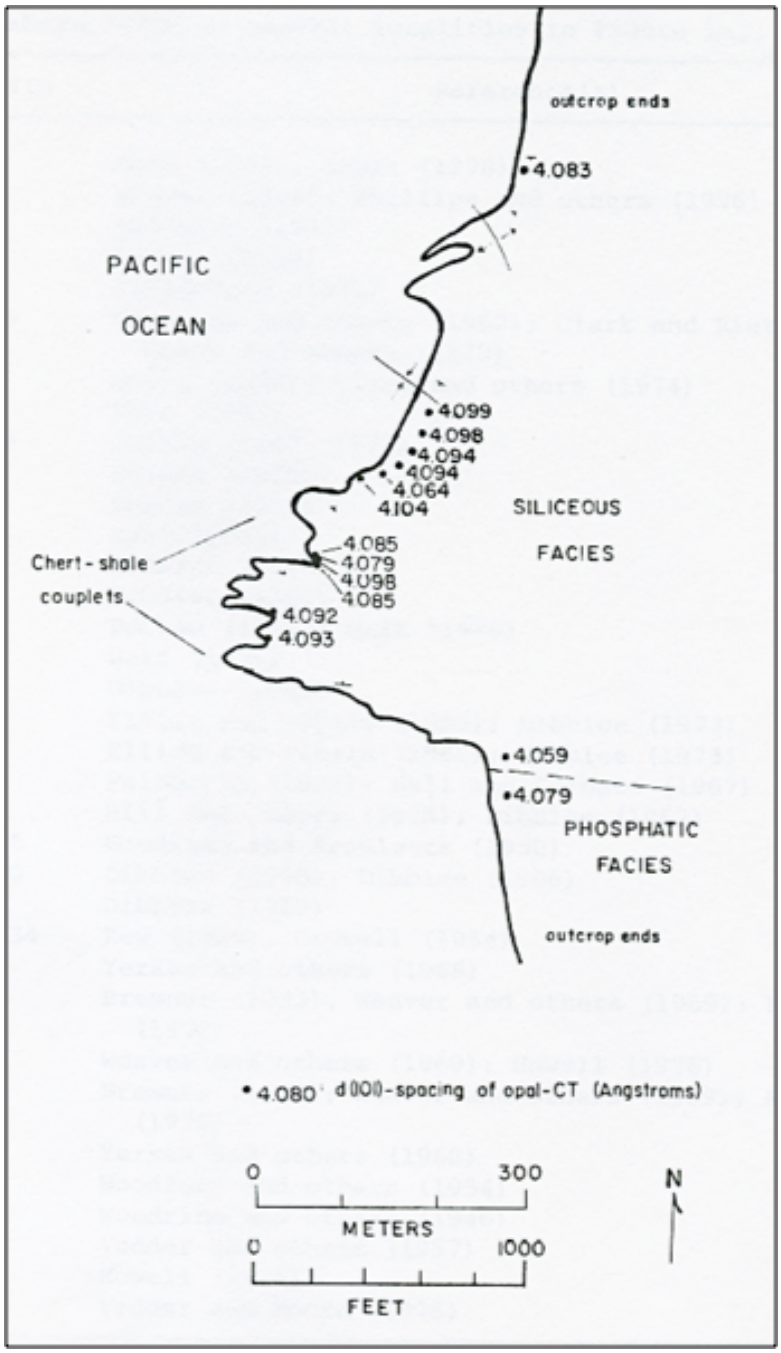

FIGURE 8. Map of Mussel Rock showing an irregular distribution of d_{101}-spacing. Downsection is to the southwest in the section analyzed. (Pisciotto, 1978)

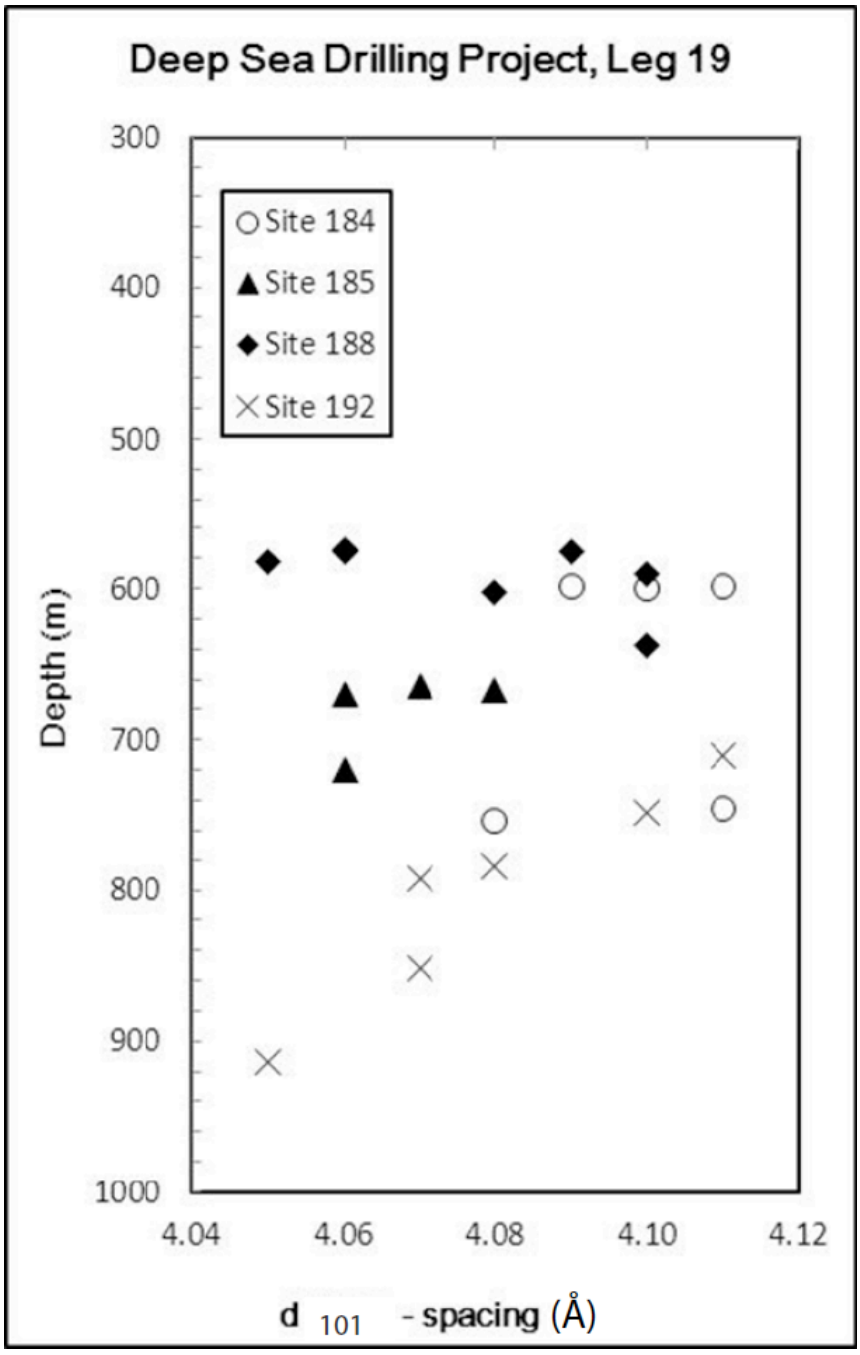

FIGURE 9. Distribution of opal-CT d_{101}-spacing with depth of samples from four DSDP sites from the north Pacific. Site 192 is the only one that shows a decreasing trend with depth. Data from Hein and Scholl (1978).

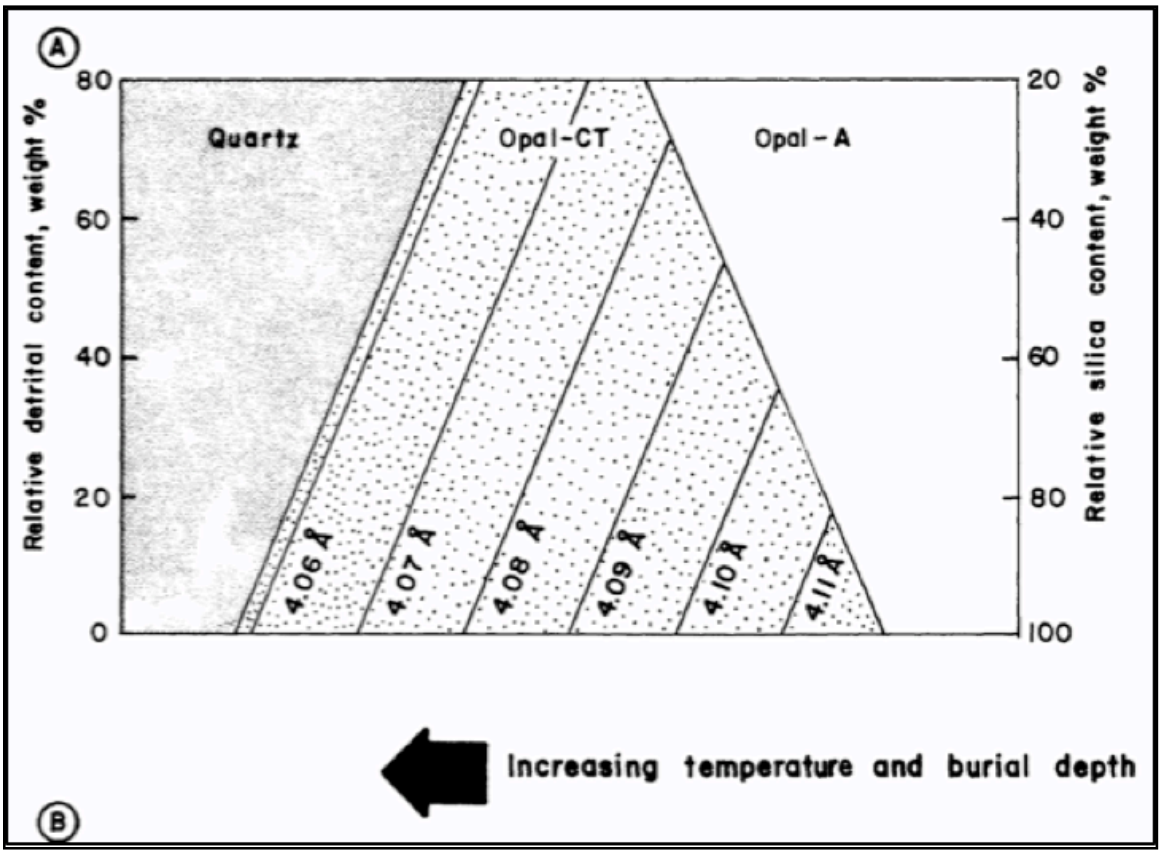

FIGURE 10. The progressive ordering of d_{101}-spacing varying with composition along the Santa Barbara coast (Isaacs, 1980).

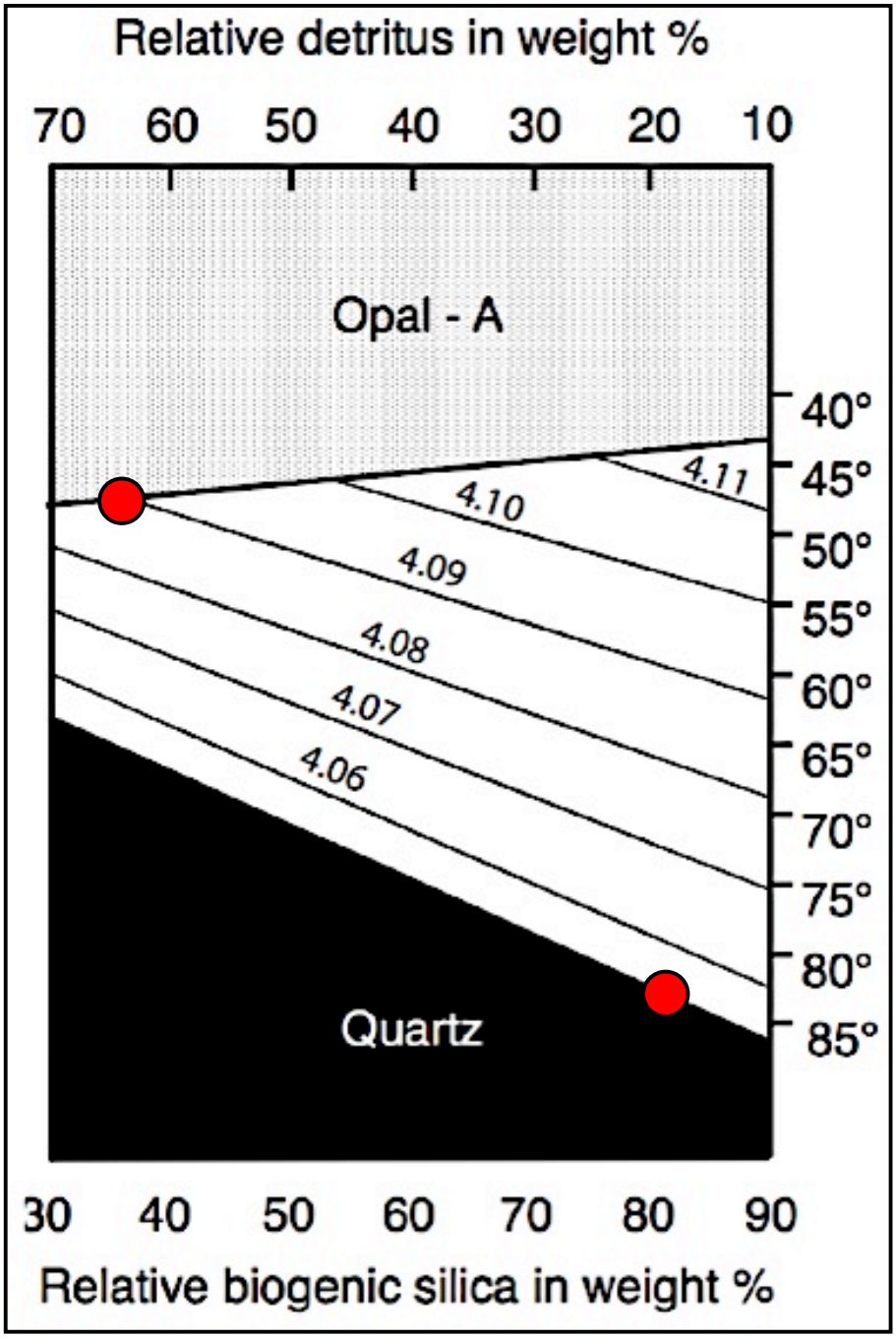

FIGURE 11. The progression of opal-A to opal-CT to quartz with temperature scales (Isaacs and Keller, 1985).

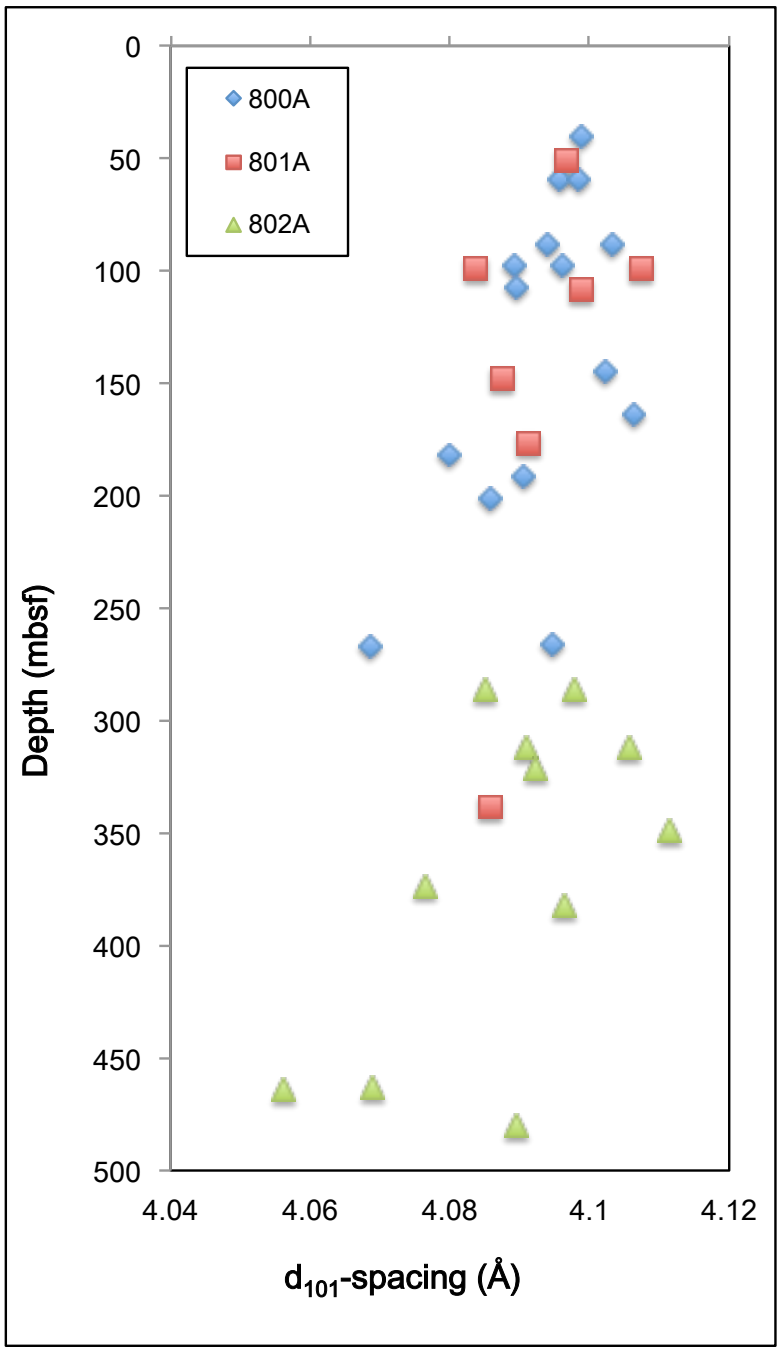

FIGURE 12. ODP sites from the deep West Pacific showing opal-CT d_{101}-spacing decreasing only generally with depth. Data from Behl and Smith (1992).

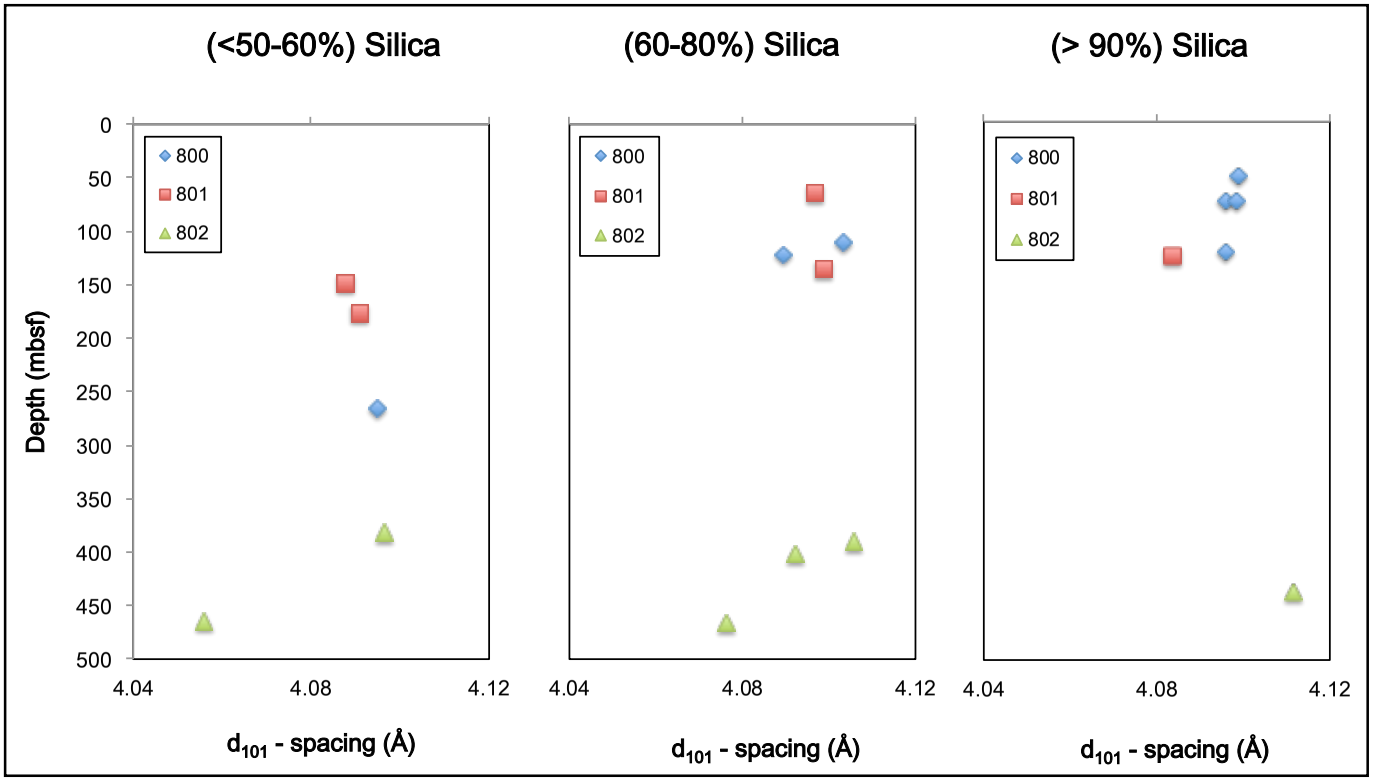

FIGURE 13. Three ODP core holes from the deep West Pacific plotted by composition show very weak correlations with depth. Data from Behl and Smith (1992).

CHAPTER 3

METHODS

Introduction

The focus of this study was to densely sample and characterize the siliceous facies of the Monterey Formation and lower Sisquoc Formation in the southwestern Casmalia Hills, Santa Maria basin, California. This research involved two field sessions during which a total of two hundred and thirty samples were collected. Sampling targeted porcelanite rocks, which were identified by their hardness, matte texture and earthy to procelaneous luster (Bramlette, 1946; Isaacs, 1981a, 1981b, 1981c) to restrict complications of variable composition on diagenesis. Twenty-three samples from two adjacent porcelanite beds at approximately 450 m from the upper Monterey were used to test the compositional variability along a single bed (Fig. 22). Two 1:24,000-scale geologic maps of the Casmalia-Orcutt and Point Sal-Guadalupe quadrangles (Dibblee, 1989a, 1989b) and satellite images from Google Earth were used in the field for location and to provide stratigraphic context. GPS location and bedding attitude were recorded for most samples collected. The samples were ordered stratigraphically and analyzed for bulk mineralogy and chemical compositions using X-ray diffraction (XRD) and energy dispersive X-ray spectroscopy/X-ray fluorescence (EDS/XRF). The following sections describe the field and laboratory methods in more detail.

Field Methods

Prior to fieldwork, specific locations that could potentially provide the best outcrops and most continuous stratigraphic succession were determined by review of previous studies by Bramlette (1946), Pisciotto (1978, 1981), and Dibblee (1989a, 1989b). In particular, Dibblee's geologic maps (Point Sal/Guadalupe and Casmalia/Orcutt quadrangles) were extremely useful. These maps were scanned and imported into Google Earth where they were draped over the Casmalia Hills to better understand terrain and to locate landmarks and access routes to the targeted locations.

The study area was partially on private land (Bognuda Ranch) and partially on Vandenberg Air Force Base. Neither area is open to access without prior permission that can take weeks to months to obtain. Access to the Bognuda Ranch had to be arranged through a series of personal connections, whereas access to Vandenberg required a formal application to the Public Affairs Office of the 30th Space Wing and a security check to visit. Field trips on base are usually escorted, but extended independent work can be arranged in certain areas.

Stratigraphic Position of Samples

Due to discontinuous exposure, samples were collected over a wide area with broad lateral extent (~2 km NE-SW by 4 km NW-SE). On average, the strata dip approximately 16° to the northeast throughout the field area which was previously described as a homocline by Woodring and Bramlette, 1950. Consequently, the original method was to collapse all the samples laterally along strike onto a single dip-parallel profile as shown in (Fig. 14). However, it became apparent that there was sufficient structural curvature of strata over the broad lateral extent (especially in the northwestern

portion of the study area) that the samples could not be accurately projected onto a single plane. Nonetheless, this projection was adequate enough to help identify stratigraphic gaps in the first field session to guide sampling during the following fieldwork. The second approach identified separate portions of the field area where samples could be traced along beds to form short, composite stratigraphic successions spanning 10's of meters of stratigraphic section. Stratigraphic distance between samples was calculated trigonometrically using horizontal and elevation measurements determined from Google Earth. These groups were then placed into a relative stratigraphic position by tracing them parallel along strike to more continuous and prominent beds, which were inline with the dip direction. Their approximate stratigraphic offset was also calculated by trigonometry taking into account stratigraphic dip, slope angle, elevation differences, and the direction of offset. The following equations apply to Figure 15, which is a visual representation of depth:

$\alpha = \tan^{-1}$ (horizontal distance/elevation difference)
$c = \sqrt{}$(horizontal distance^2 + elevation difference^2)
If sloping eastward is $\beta = \alpha$ – Dibblee
If sloping westward is $\beta = \alpha$ + Dibblee dip
Depth (d) = $\sin\beta$ x c

Mineralogic and Geochemical Analyses

All analyzed samples were crushed with a porcelain mortar and pestle to less then about 250-micron mesh and collected into 8 ml vials. The fine powders were then prepared accordingly for separate XRD and EDS/XRF analyses, which are outlined in the following sections.

X-ray Diffraction (XRD)

A few tenths of a gram of the powdered sample was further ground with a mortar and pestle and then mixed into slurry with a few drops of methanol. The slurry was then smeared uniformly onto a circular clean glass slide and then placed in a round aluminum holder. Three small pieces of modeling clay were placed between the slide and holder to level the sample to the top of the holder (Fig. 16). The samples were air-dried and then loaded six at a time into the sample holder inside of a Rigaku MiniFlex X-ray diffractometer, which was operated at 30 kV and 15 mA with X-rays generated from a copper anode target. Each sample was scanned from 15° to 40° 2θ at 0.2 steps for 2 seconds/step. Diffractograms were processed using PANalytical X'Pert High Score Plus ® software. The position of the d_{101}-spacing peak of cristobalite occurs at about 22° 2θ was used to measure the degree of ordering of opal-CT (Pisciotto, 1978). Because the sedimentary rocks usually contain some amount of either detrital or diagenetic quartz, the quartz peak position of 26.65° 2θ was used as an internal standard (Pisciotto, 1978). Use of these peak positions follows similar studies by Isaacs (1980) and Pisciotto (1978). The precise numerical position of the peaks were determined a few different ways and compared for reproducibility when possible: (1) If the peak was symmetrical and the top came to a single point, the center of the highest point was used; (2) If the peak was symmetrical and the top was narrow but flat, the midpoint of 90% of the peak height was used; (3) If the peak was skewed and broad, the midpoint of 50% of the peak height was used. Once the opal-CT d_{101} peak positions were measured, the measured quartz 2θ was subtracted from the known quartz standard 2θ. The difference was then subtracted from

the opal-CT 2θ giving the new corrected 2θ for the opal-CT d_{101}-spacing (Fig. 17). The d_{101}-spacing of each peak was then obtained using Bragg's Law:

$$2d(\sin \theta) = n\lambda$$

Variable d is the spacing between planes in the crystal lattice in angstroms, θ is the angle of incidence between the x-ray and the lattice plane taken from 2θ reported on the diffractograms, and λ is 1.54056 angstroms, which is the wavelength of the Cu Kα incident wave.

Energy Dispersive X-ray Spectroscopy/X-Ray Fluorescence (EDS/XRF)

The same sample set that was analyzed by XRD was used for EDS/XRF analysis. Sample powders were compressed into pellets with a hydraulic pellet press and 13 mm diameter DIE. Approximately 0.5 grams of each sample was added to the die, which was placed in to the hydraulic press and 10 ton/ psi applied. The product was a circular pellet with a diameter of 13 mm and thickness of 3-5 mm. The prepared samples were placed in a desiccator until they were ready to be analyzed. A FEI Quanta 200 Environmental Scanning Electron Microscope (ESEM) coupled with IXRF Iridium Ultra energy dispersive X-ray and X-Ray fluorescence spectroscopy system was used for the combined EDS/XRF analysis. A set of 11 international geochemical standards (U.S. Geological Survey and South African) were used for calibration and analyzed as unknowns. The results were given in major oxides, Na_2O, Si_2O, CaO, Fe_2O_3, Al_2O_3, MgO, P_2O_5, Ti_2O, K_2O, and MnO, which were then converted to their sedimentary components using formulas developed by Isaacs, 1983 (Table1).

Procedures for the calibration were developed with the help of iXRF Iridium Ultra staff support and are detailed in Appendix B. To check the error of the calibration the Actual Concentrations (documented) and Calculated Concentrations (calculated from calibration) were plotted for the major element oxides (Appendix B). Twenty-five samples plus the standards were sent to an outside lab (Actlabs) for analysis. The R^2 results of the calibration and the Actlab analysis are shown in Table 2. Actlabs used ICP-MS as the method of analysis, which is comparable to XRF, but has higher sensitivity.

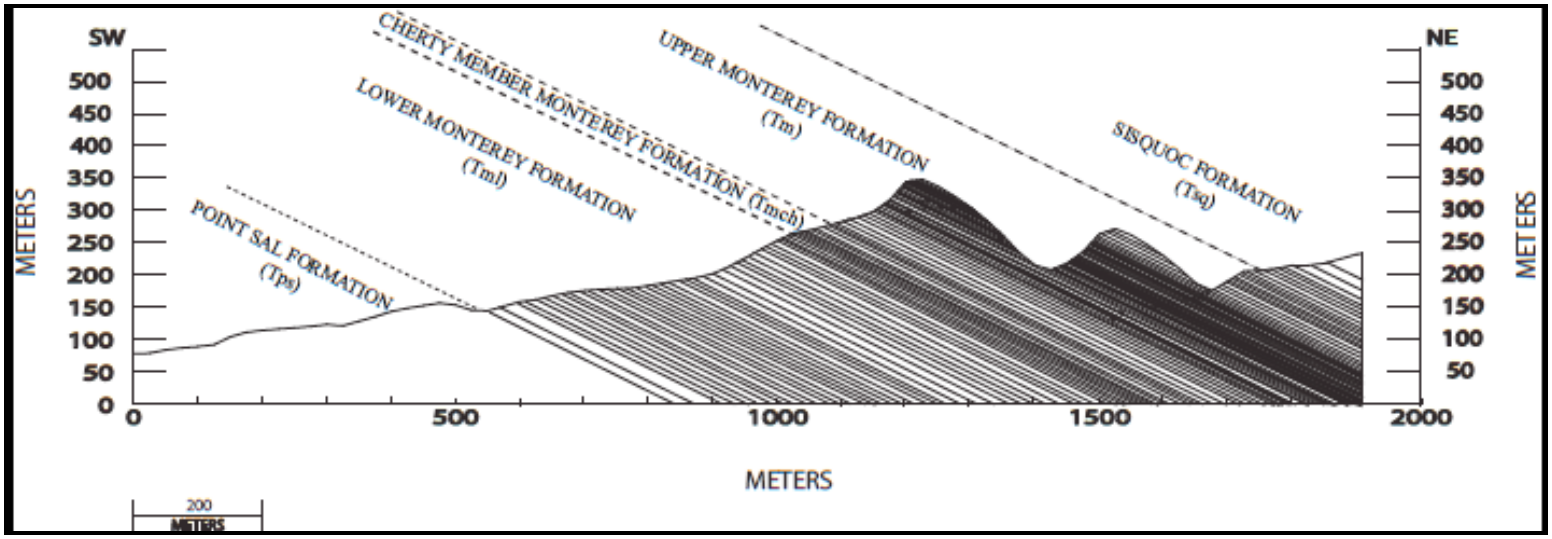

FIGURE 14. Dip-parallel profile of the field area with positions of samples projected on the profile represented by the inclined lines.

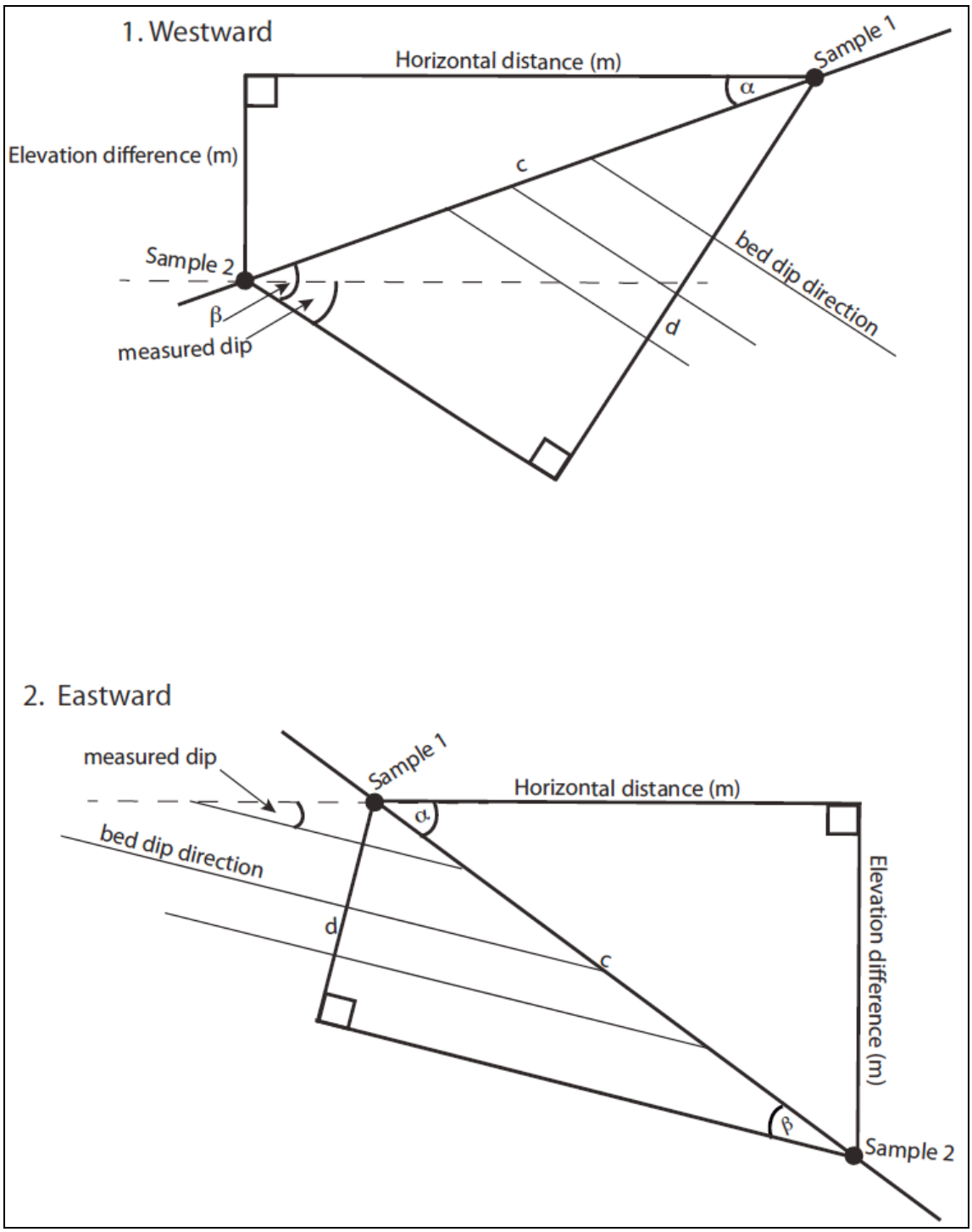

FIGURE 15. Shows a visual relationship of the bed direction, position of the samples, and their stratigraphic depth.

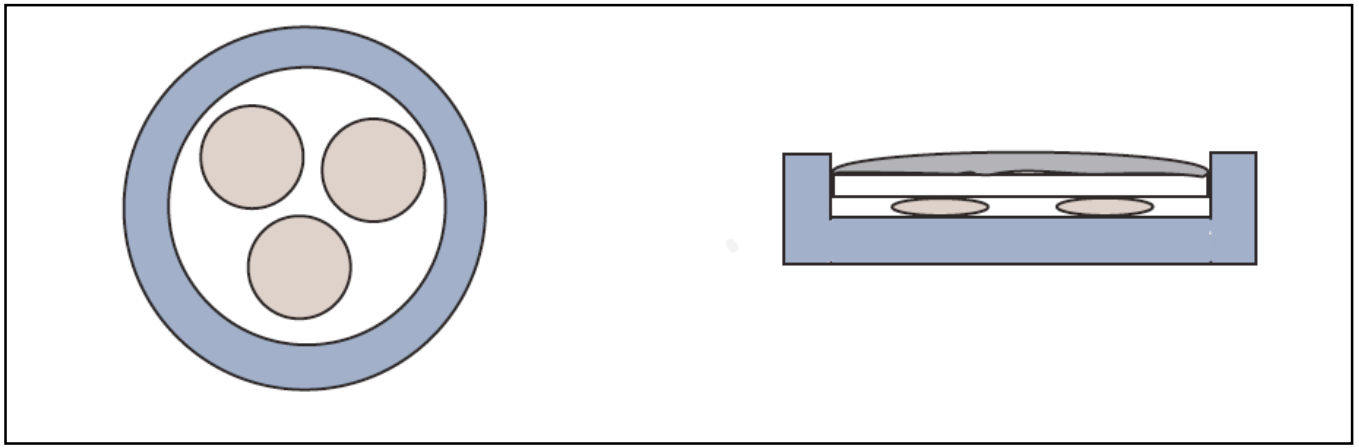

FIGURE 16. Top and side view of slide and holder arrangement.

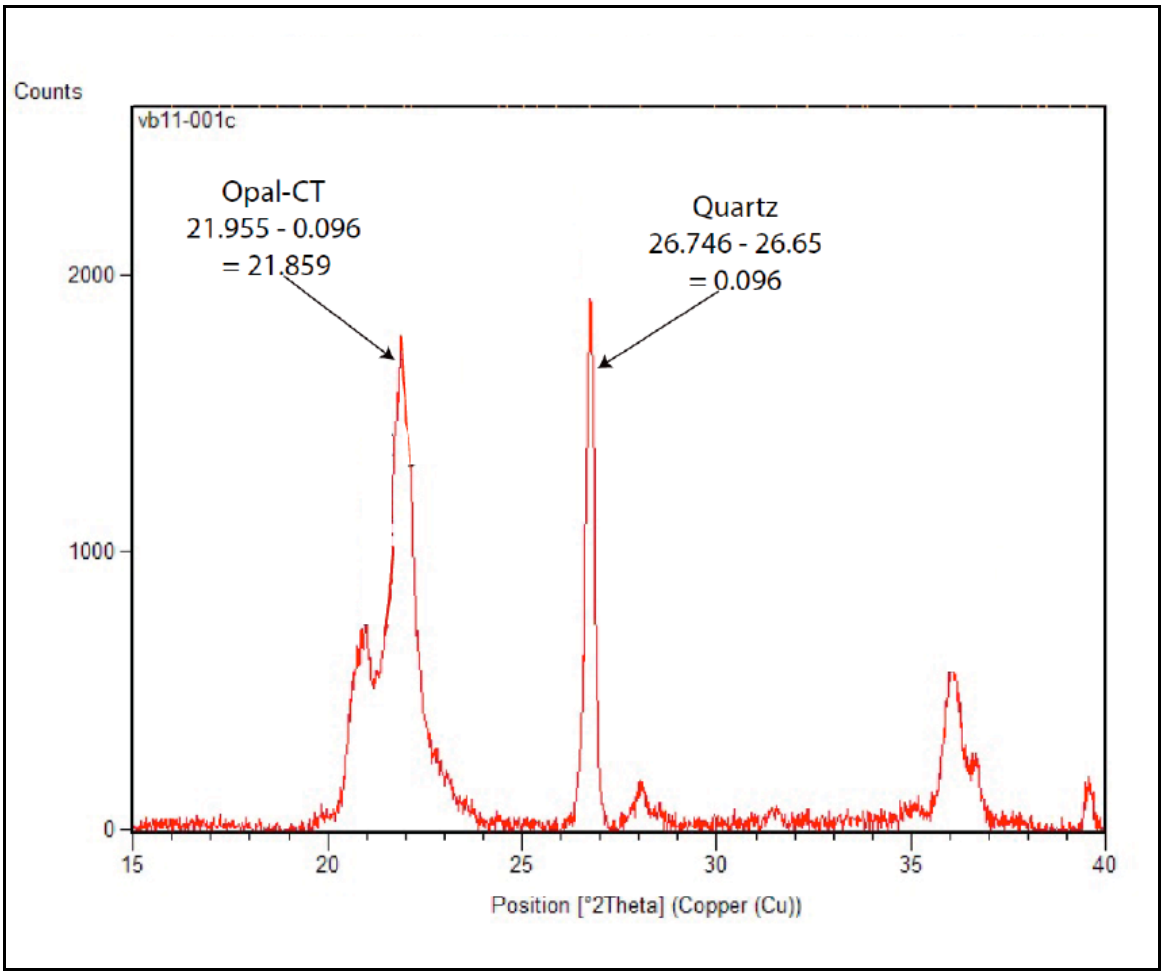

FIGURE 17. Diffractogram showing the method used to measure the d_{101}- spacing of opal-CT relative to quartz standard.

TABLE 1. Table Showing Monterey Formation Sedimentary Components (After Isaacs et al., 1983).

Quantity	Explanation	Formula
Detritus Aluminosilicates Detrital quartz	Equals aluminosilicates + detrital quartz Based on Al_2O_3 content Based on a proportion of aluminosilicates	5.6 x Al_2O_3 4.2 x Al_2O_3 Aluminosilicates / 3
Silica (biogenic and diagenetic)	Based on SiO_2 content adjusted for amounts in detritus	$SiO_2 – (3.5 \times Al_2O_3)$
Apatite	Based on P_2O_5 content adjusted for 0.7% P_2O_5 in aluminosilicates and assuming 42.4% P_2O_5 in apatite	$[P_2O_5 – (0.032 \times Al_2O_3)] / 0.424$
Dolomite	Based on MgO content adjusted for 2.6% MgO in aluminosilicates and assuming 21.9% MgO in dolomite	If MgO <= (0.11 x Al_2O_3): dolomite = 0 Otherwise: $[MgO – (0.11 \times Al_2O_3)] / 0.219$
Calcite	Based on CaO content adjusted for 1.9% CaO in aluminosilicates, 55.5% CaO in apatite, and 30.4% CaO in dolomite, and assuming 56.0% CaO in calcite	$[CaO – (0.08 \times Al_2O_3 –$ (0.555 x apatite) – (0.304 x dolomite)] / 0.56

TABLE 2. Table Showing R^2 Of Samples And Standards From Calibration And Actlabs Analysis.

	CSULB vs. Actilabs Samples and Standards (R^2)
SiO_2	0.97
Al_2O_3	0.89
Fe_2O_3	0.92
MnO	0.89
MgO	0.98
CaO	0.99
Na_2O	0.90
K_2O	0.99
TiO_2	0.96
P_2O_5	0.99

CHAPTER 4

RESULTS

Data Description

A total of 230 outcrop and road-cut samples were analyzed using XRD and combined EDS/XRF. Examples of some of the diffractograms used to determine silica phase and opal-CT ordering are presented in Figures 18 through 21. They are examples of the major rock types studied in this thesis, which are porcelaneous mudstone (Fig. 20), high detritus porcelanite (Fig. 18), and low detritus porcelanite (Fig. 19 & Fig. 21). The XRD data provided was used along with the stratigraphic depth in meters to construct Figure 22, which displays the data in narrow 10-weight-percent silica (SiO_2) ranges on a carbonate-, apatite-, and organic matter-free basis. The silica (SiO_2) was calculated with formulas from Table 1 and normalized with detritus to 100 percent. Major oxides (combined EDS/XRF) are presented in Figures 24 through 27. The sedimentary components were calculated using the formulas of Issacs (1983; Table 1) and the major oxides from the combined EDS/XRF analysis. The sedimentary components and opal-CT d_{101}–spacing versus stratigraphic depth (XRD) is represented in Figures 28 through 31 for each member. See Appendices A for data tables for XRD and combined EDS/XRF measurements values.

Twenty-three samples from two adjacent porcelanite beds at approximately 450 m from the upper Monterey were used to test the compositional variability along single beds

(Fig. 23), a wide of compositions was found. The results showed that for bed 1 the silica ranged from 61-76 % (mean 70) and 36-83% (mean 65) for bed 2.

The major oxides from the samples in the southwestern Casmalia hills varies throughout the section. Aluminium oxide (Al_2O_3) ranges from 1.4 to 17.4 wt. % (mean 5.8). Sodium oxide (Na_2O) ranges 0.04 to 5.4 wt. % (mean 0.6). Silicon oxide (SiO_2) ranges from 26.0 to 96.3 wt. % (mean 85.4). Iron oxide (Fe_2O_3) ranges from 0.24 to 8.2 wt. % (mean 1.8). All of the previous five reached their maximum value in the upper Monterey Formation (Fig. 25). Phosphorous pentoxide (P_2O_5) ranges from < 0.1 to 29.8 wr. % (mean 1.1). Calcium oxide (CaO) ranges from < 0.1 to 57.6 wt. % (mean 2.7). Titanium oxide (TiO_2) ranges from < 0.1 to 3.7 (mean 0.3). P_2O_5, CaO, TiO_2 all reached their maximum value in the middle Monterey Formation (Fig. 26). Magnesium oxide (MgO) ranges from 0.4 to 13.0 wt. % (mean 1.4) and increases to its maxmum value in the lower Monterey formation (Fig. 27). Mangenese oxide (MnO_2) ranges from < 0.1 to 0.5 wt. % (mean 0.02). Both reached their maximum value in lower Monterey Formation (Fig. 27).

Lower Sisquoc Formation

This section and the members of the Monterey were characterized and identified by map location according to Dibblee (1989a), descriptions from Woodring and Bramlette (1950) and MacKinnon (1989), and by their composition. The Sisquoc Formation has two main lithologic facies: diatomaceous mudstones and porcelaneous mudstones (Woodring and Bramlette, 1950). Fifteen samples from the lower Sisquoc Formation span a stratigraphic depth range from 0 to 275 meters. Abundances of sedimentary components (Fig. 28) were calculated from the major oxide data displayed in

Figure 24. Detritus content ranges from 28 to 72 wt. % (46.4 mean), silica from 26 to 70 wt. % (53.1 mean), and calcite from <1 to 2 wt. % (0.5 mean) for the section. The measured d_{101}-spacing varies from 4.05 to 4.09 Å (4.06 mean).

Upper Monterey Formation

The upper Monterey is made up of platy porcelaneous shale (Woodring and Bramlette, 1950) with a higher amount of detritus (30-50%). One hundred twenty-eight samples from the upper Monterey Formation were acquired from a stratigraphic depth range of 275 to 500 meters. Abundances of total detritus, biogenic + diagenetic silica and calcite (Fig. 22) were calculated from the major oxide data shown in Figure 25. Detrital content ranges from 10 to 97 wt. % (35.5 mean), silica from 11 to 90 wt. % (65.4 mean), and calcite from <1 to 2 wt. % (0.2 mean) for the section. The measured d_{101}-spacing ranged from 4.04 to 4.11 Å (4.07 mean).

Middle Monterey Formation

The middle Monterey consists of chert and cherty shale interbedded with porcelaneous shale with low-detritus (10-30%; Woodring and Bramlette, 1950). Thirty-five samples from the upper Monterey Formation were taken from the narrow stratigraphic range of 500-530 meters. The mineralogical abundances (Fig. 30) were calculated from the major oxide data shown in Figure 26. Detritus content ranges from 11 to 92 wt. % (26.5 mean), silica ranges from 47 to 87 wt. % (71.2 mean), and calcite varies from <1 to 45 wt. % (3.7 mean) for the section. The measured opal- CT d_{101}-spacing ranges from 4.05 to 4.10 Å (4.07 mean).

Lower Monterey Formation

The lower Monterey Formation is made up of phosphatic shale, silty shale, porcelaneous shale, dolostone and limestone (Woodring and Bramlette, 1950). Forty-five samples from the lower Monterey Formation were acquired from a stratigraphic depth range of 530-700 meters. The mineralogical abundances (Fig. 31) were calculated from the major oxide data displayed in Figure 27. Detritus content ranges from 9 to 60 wt. % (22.7 mean), silica from 24 to 89 wt. % (65.5 mean), and calcite from <1 to 75 wt. % (17.5 mean) for the section. The measured opal-CT d_{101}-spacing ranges from 4.04 to 4.10 Å (4.06 mean).

TABLE 3. Table Showing Formation Name, Number of Samples, and Measured Stratigraphic Depth Range.

Formation/Section	Number of Samples	Measured Stratigraphic Depth Range (m)
Sisquoc	15	0-275
Upper Monterey	128	275-500
Middle Monterey	35	500-530
Lower Monterey	45	530-700

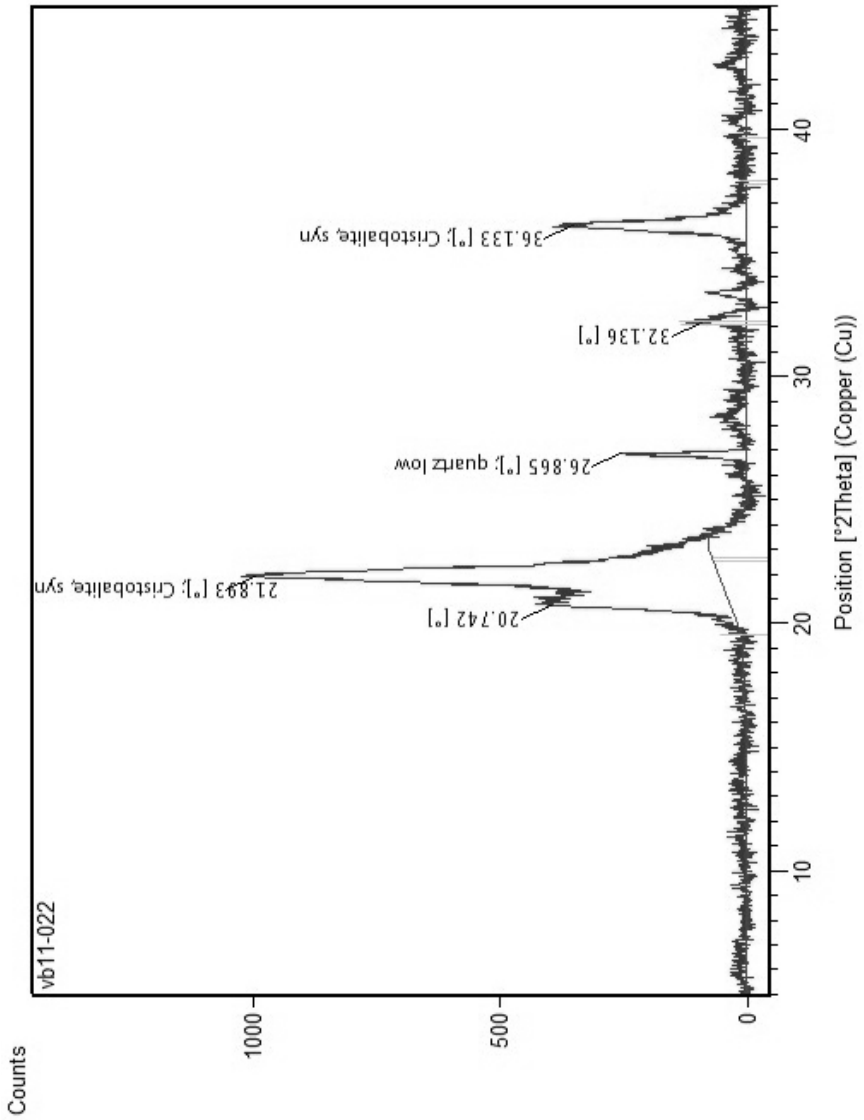

FIGURE 18. This X-ray diffractogram shows opal-CT porcelanite with a 4.10 Å d_{101}-spacing that consists of 75% diagenetic silica.

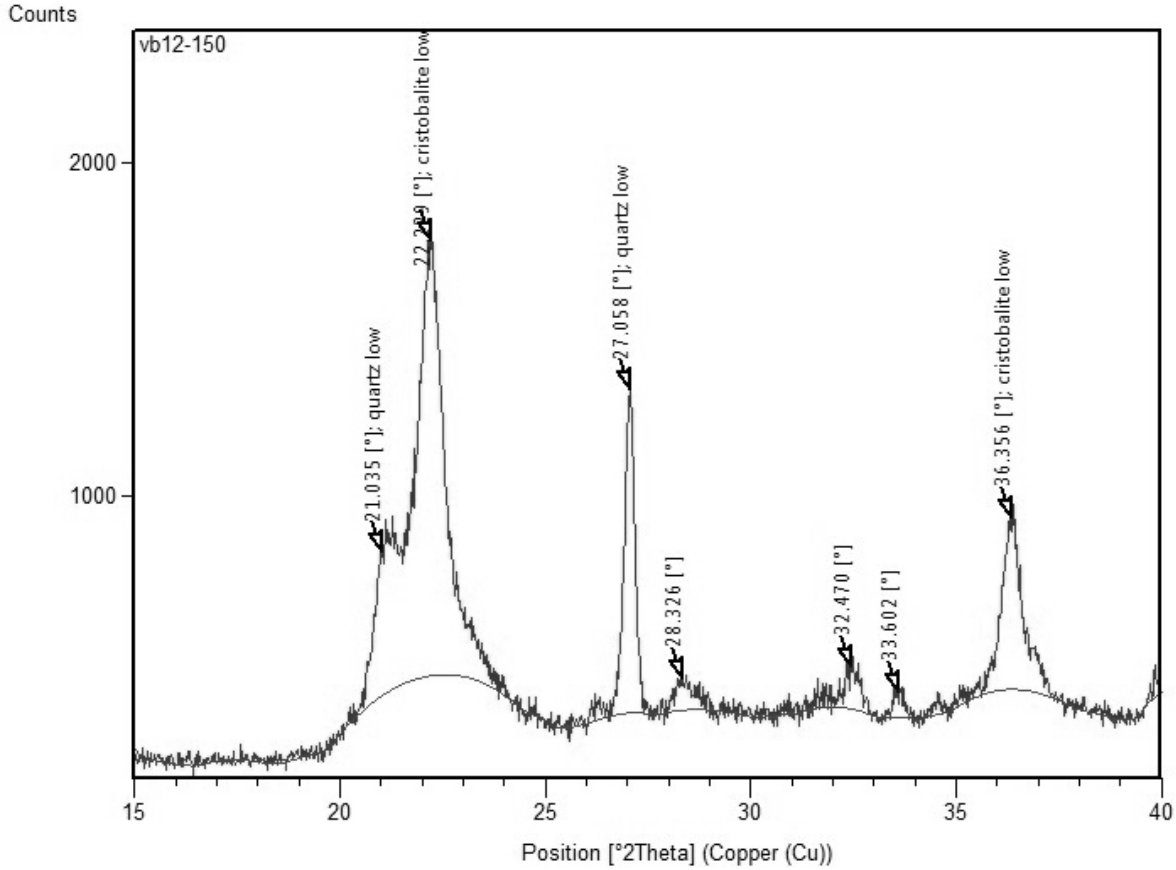

FIGURE 19. X-ray diffractogram of opal-CT porcelanite with 4.07 Åd_{101}-spacing that consists of 91% silica.

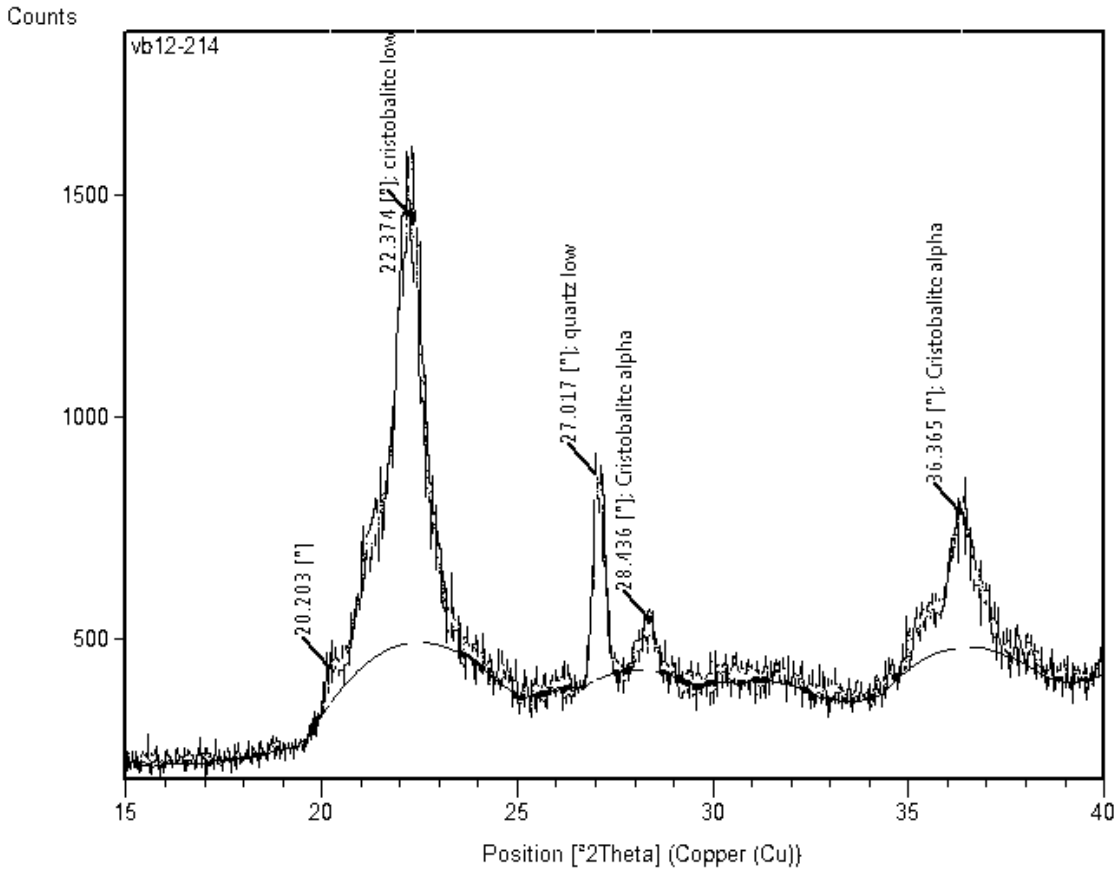

FIGURE 20. X-ray diffractogram of opal-CT siliceous shale with 4.04 Å) d_{101}-spacing that consists of 52% silica.

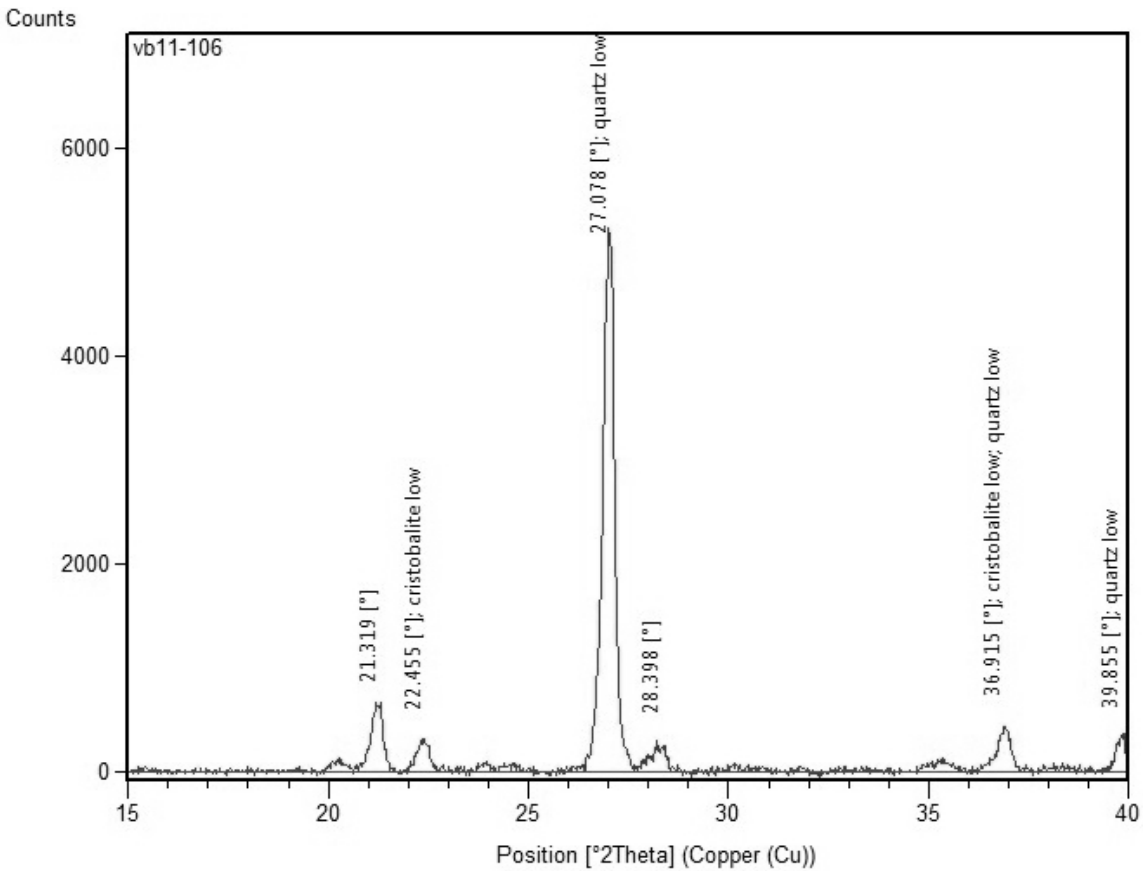

FIGURE 21. X-ray diffractogram of a quartz-phase porcelanite that consists of 86% diagenetic silica.

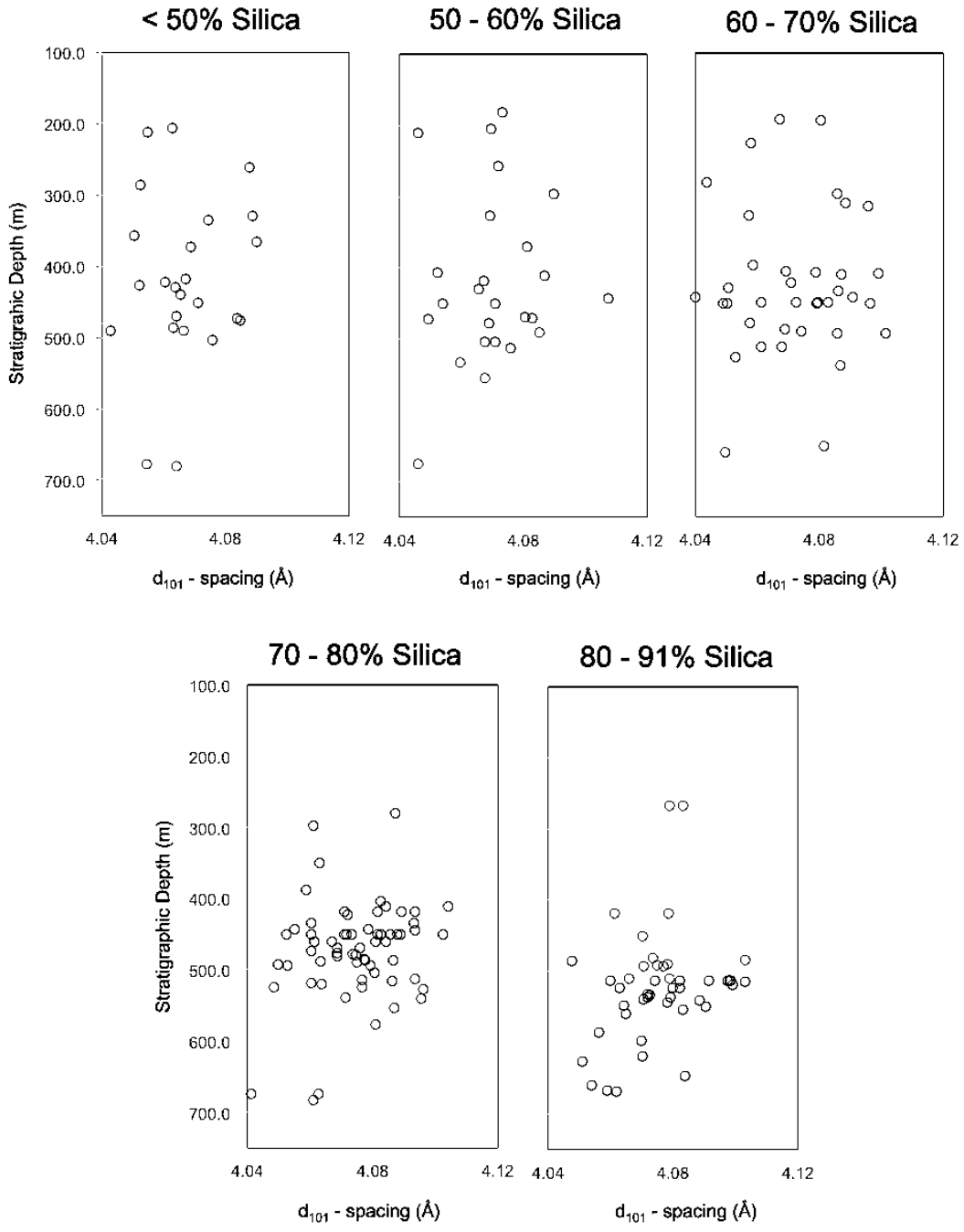

FIGURE 22. Graphs showing opal-CT d_{101}-spacing plotted versus stratigraphic depth in meters for narrow 10 percent silica ranges on a carbonate-, apatite-, and organic matter-free basis.

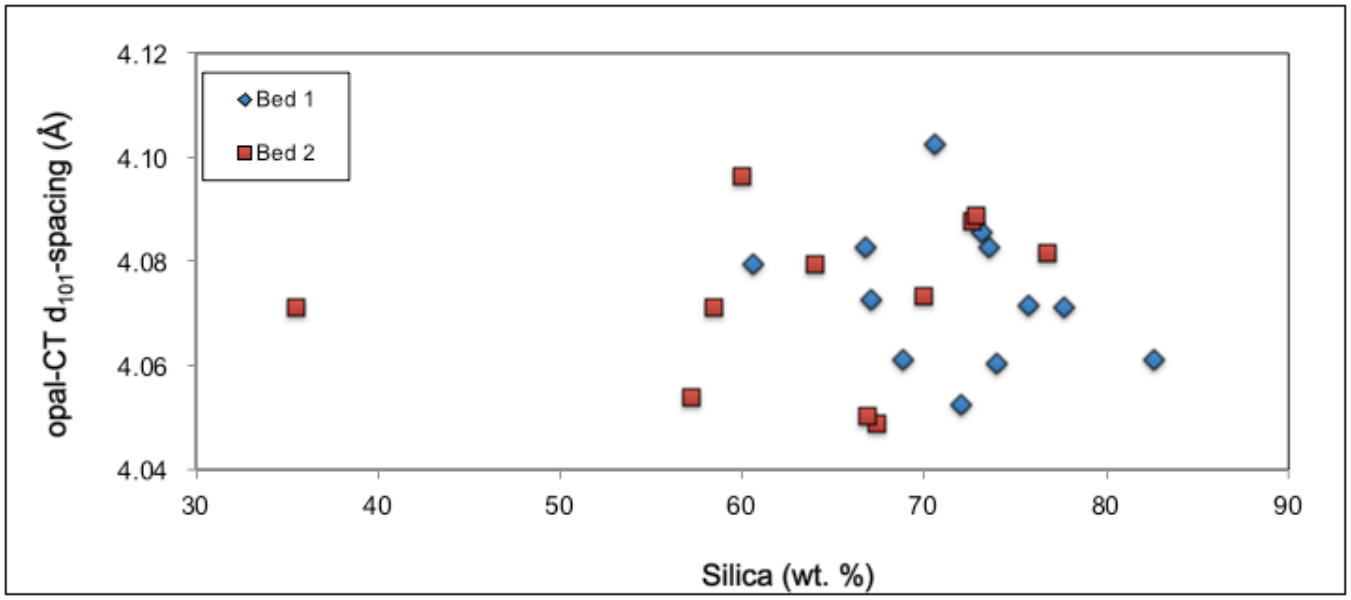

FIGURE 23. Two stratigraphically similar beds from the upper Monterey showing variable composition and opal-CT d_{101}-spacing.

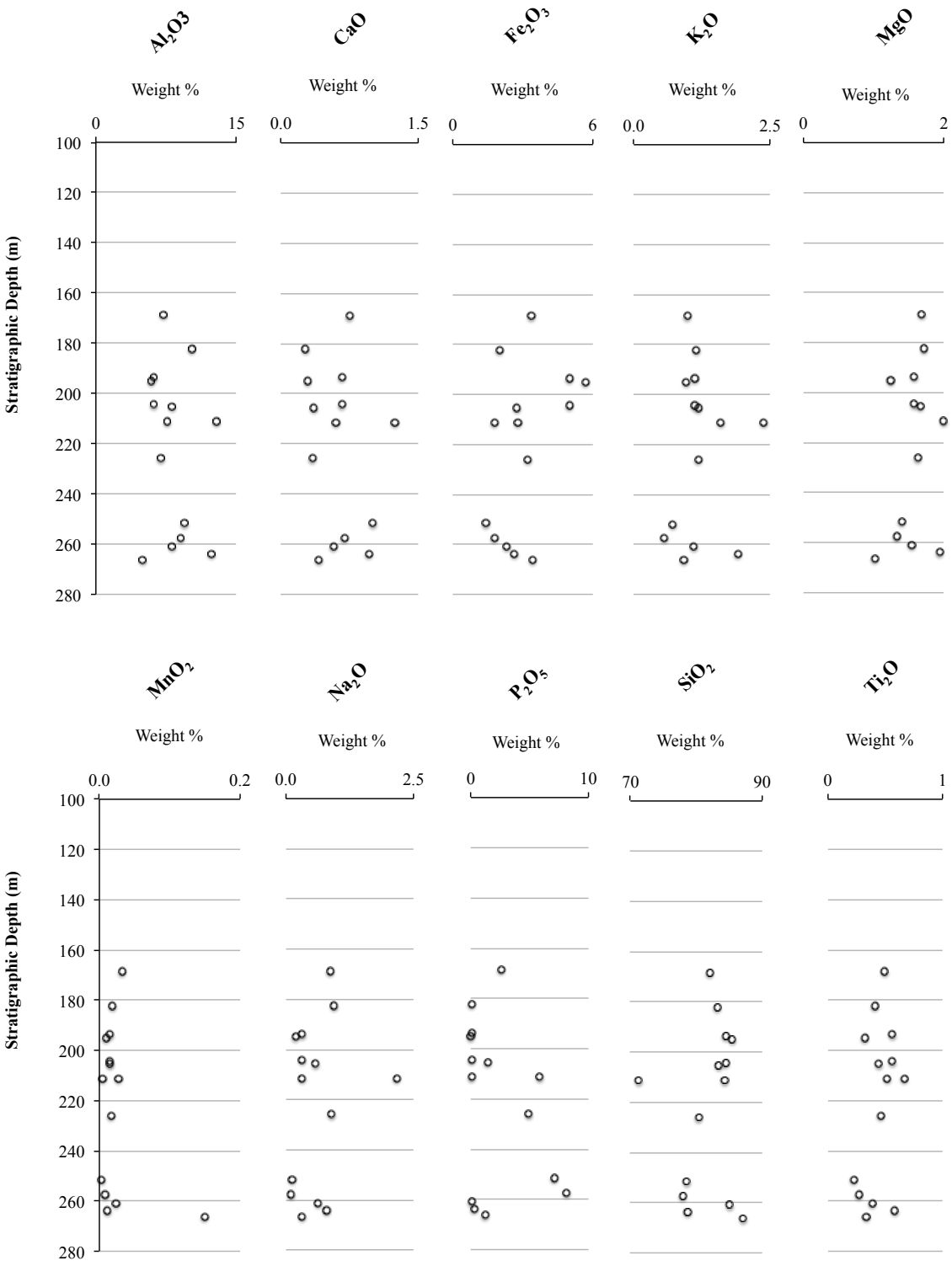

FIGURE 24. Major oxides in samples from the lower Sisquoc Formation, measured by combined EDS/XRF. Note scales vary.

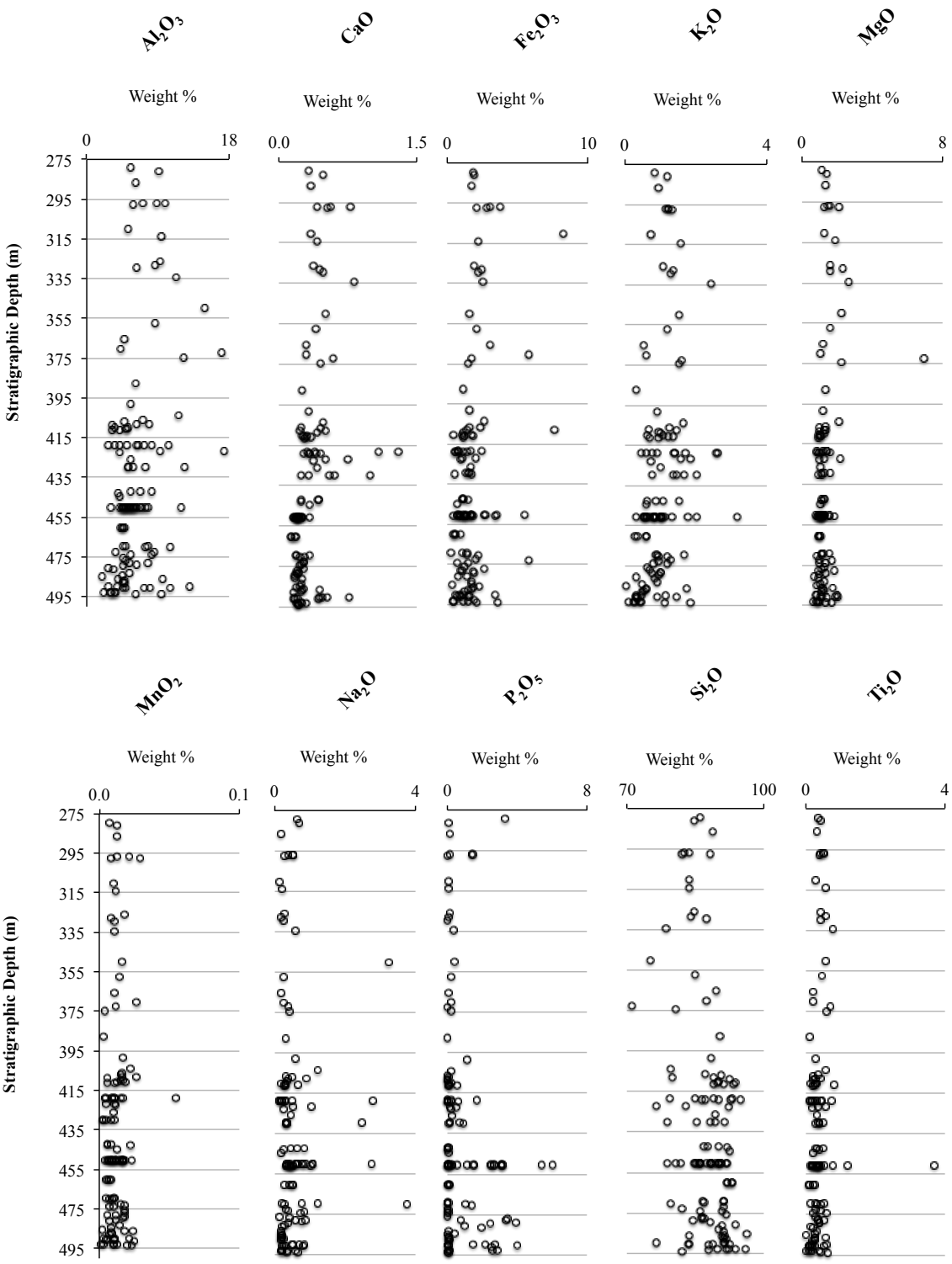

FIGURE 25. Major oxides in samples from the upper Monterey Formation, measured by combined EDS/XRF. Note scales vary.

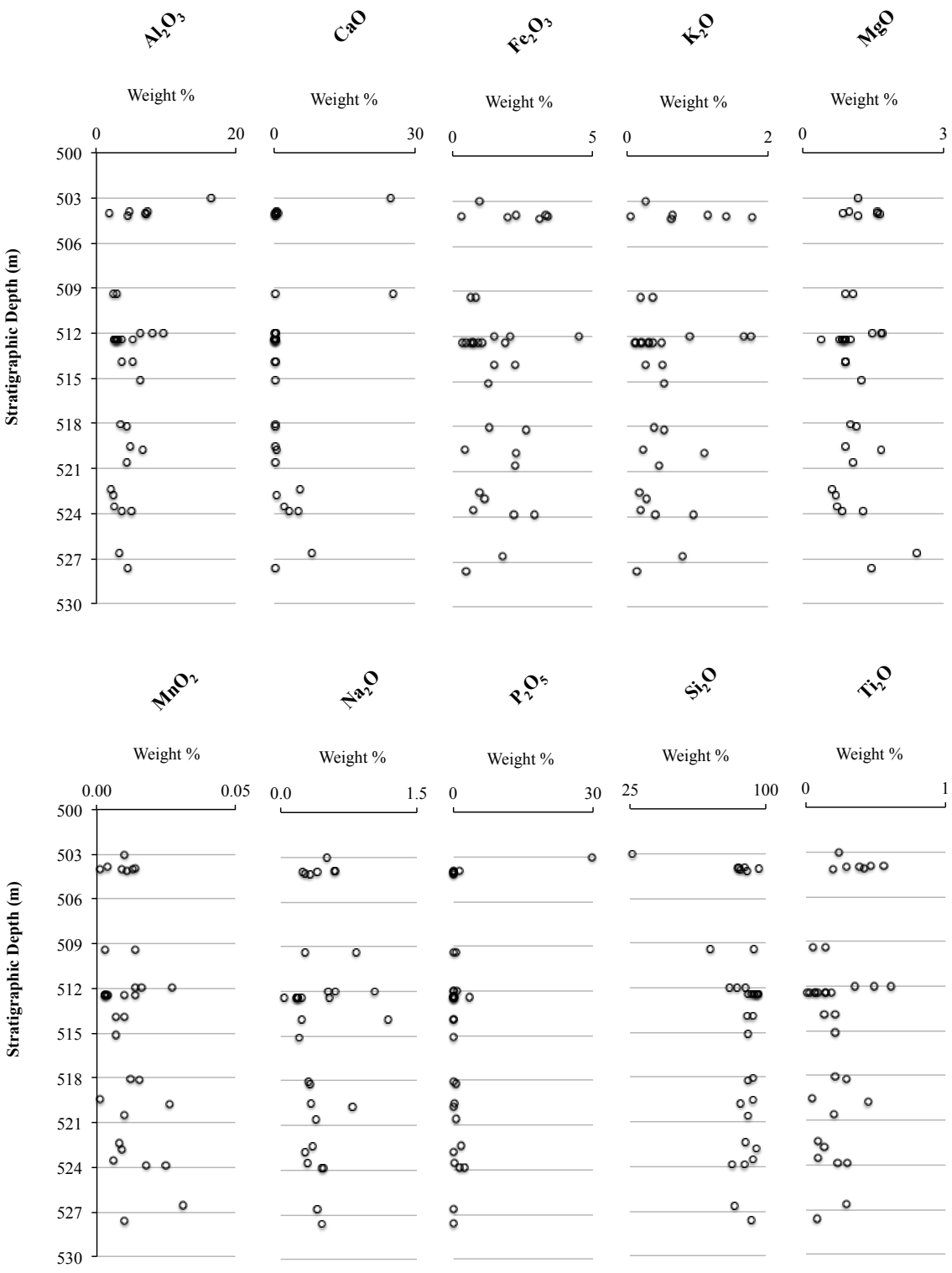

FIGURE 26. Major oxides in samples from the middle Monterey Formation, measured by combined EDS/XRF. Note scales vary.

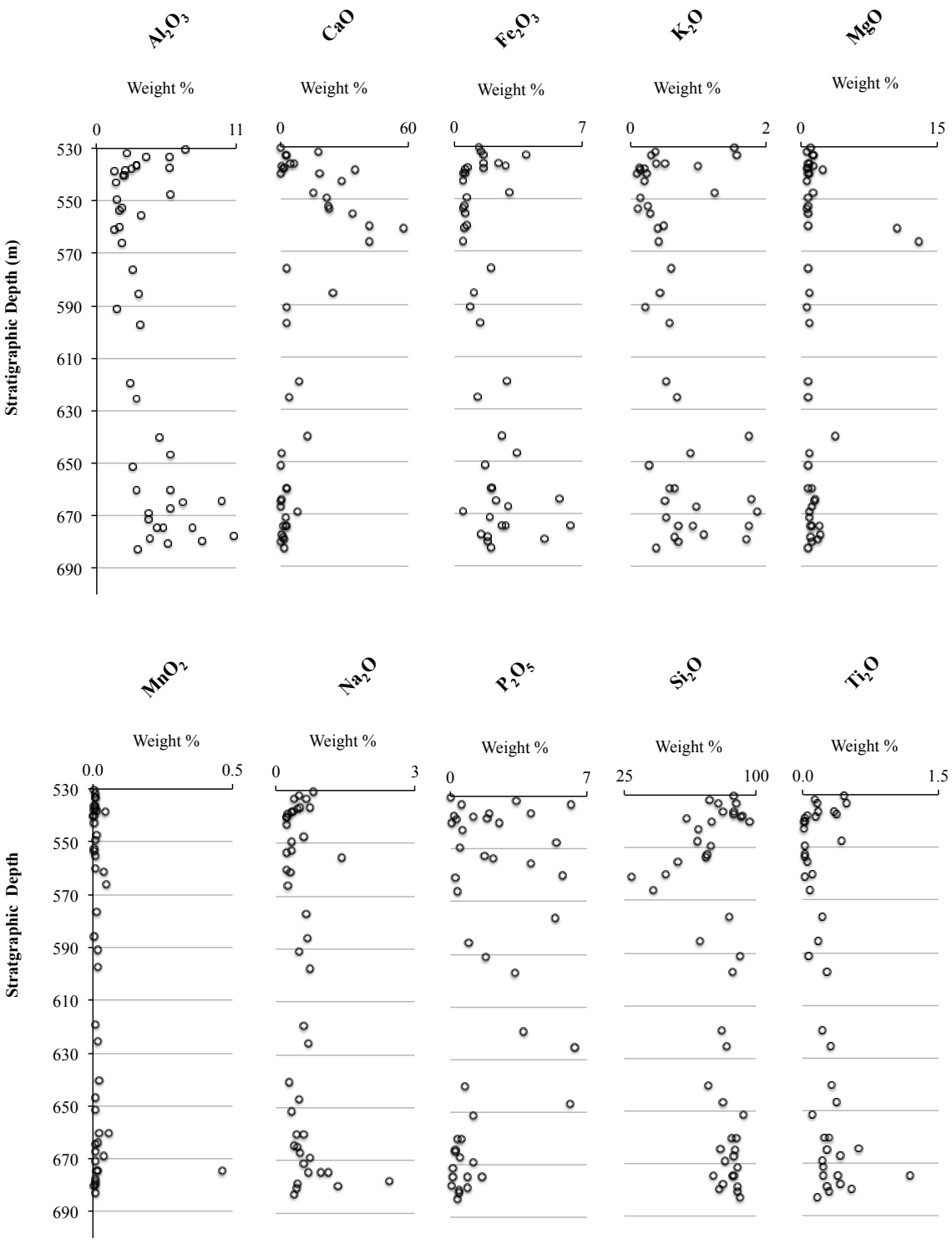

FIGURE 27. Major oxides in samples from the lower Monterey Formation, measured by combined EDS/XRF. Note scales vary.

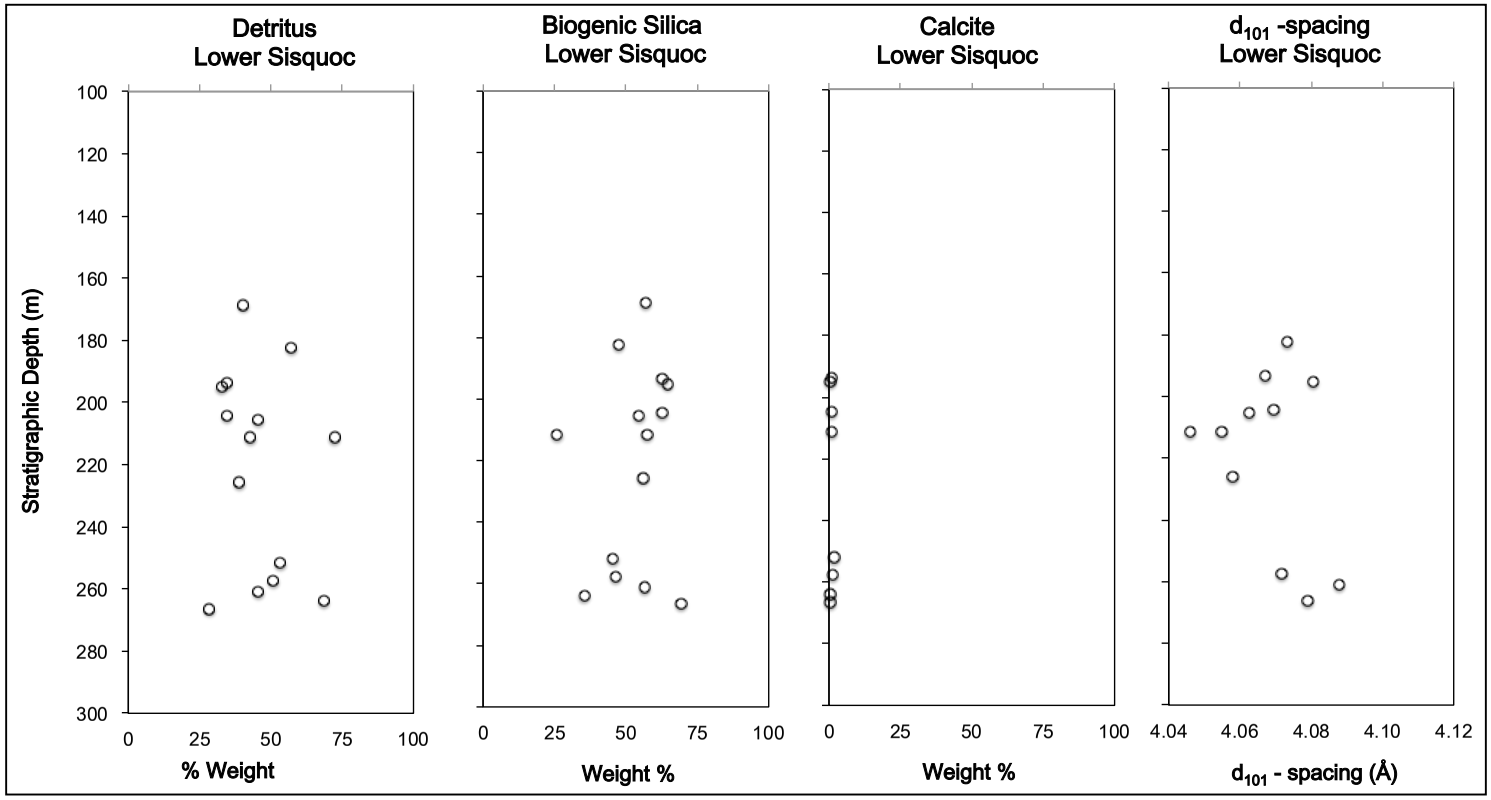

FIGURE 28. Abundances of sedimentary components and opal-CT d_{101} - spacing of samples from the lower Sisquoc Formation, measured by combined EDS/XRF and XRD.

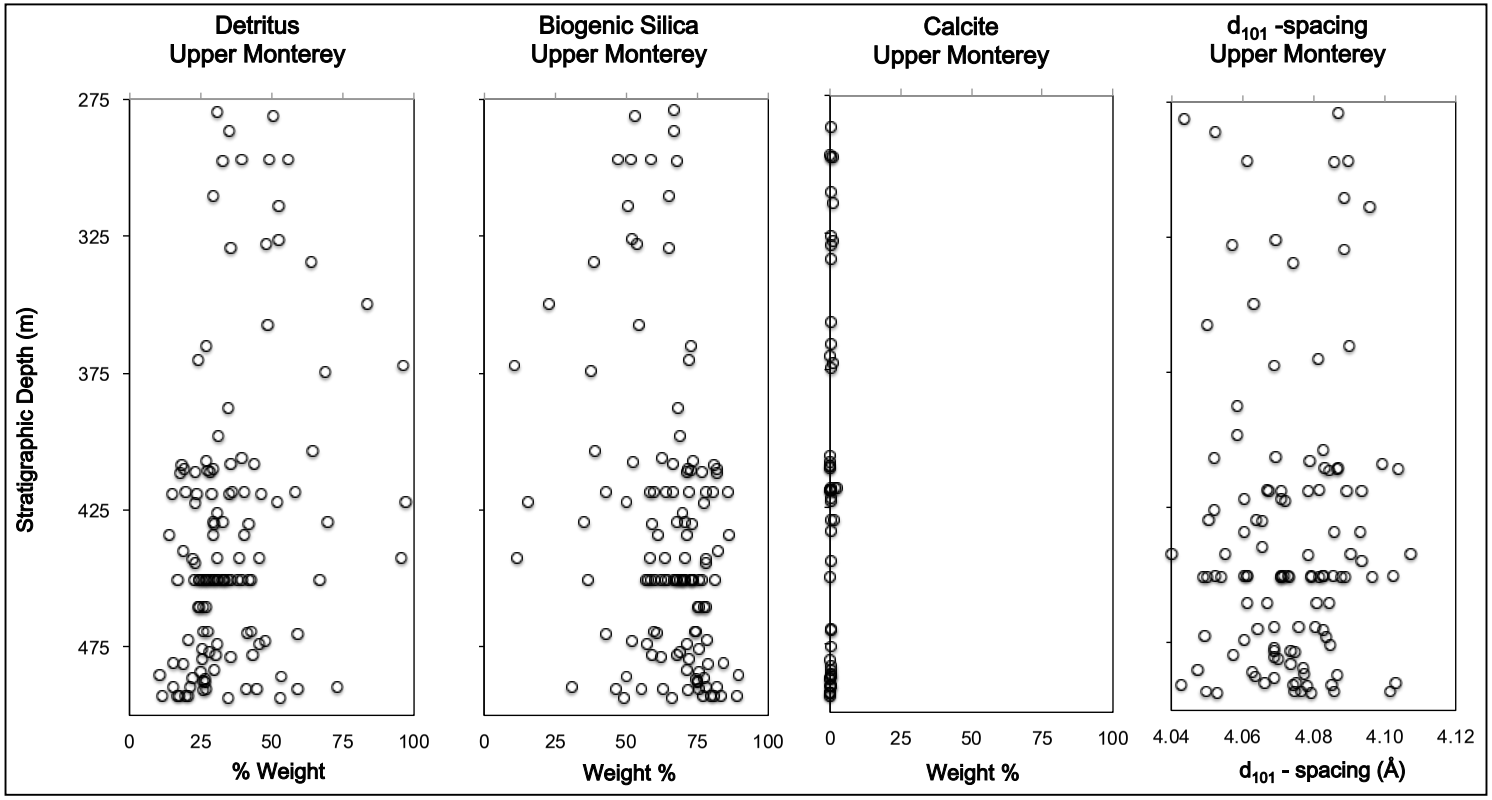

FIGURE 29. Abundance of sedimentary components and opal-CT d_{101} - spacing of samples from the upper Monterey Formation, measured by combined EDS/XRF and XRD.

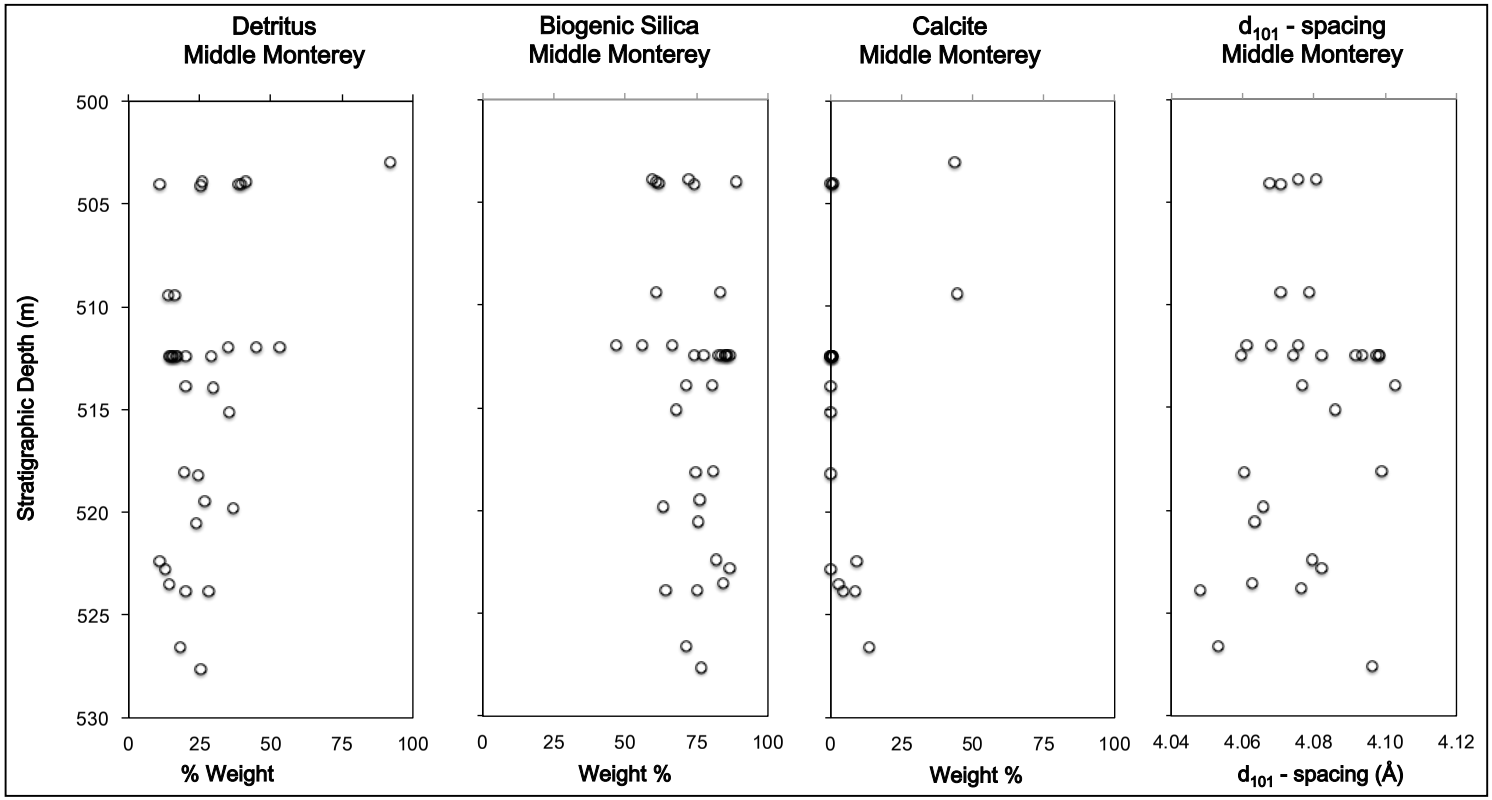

FIGURE 30. Abundances of sedimentary components and opal-CT d_{101} - spacing of samples from the middle Monterey Formation, measured by combined EDS/XRF and XRD.

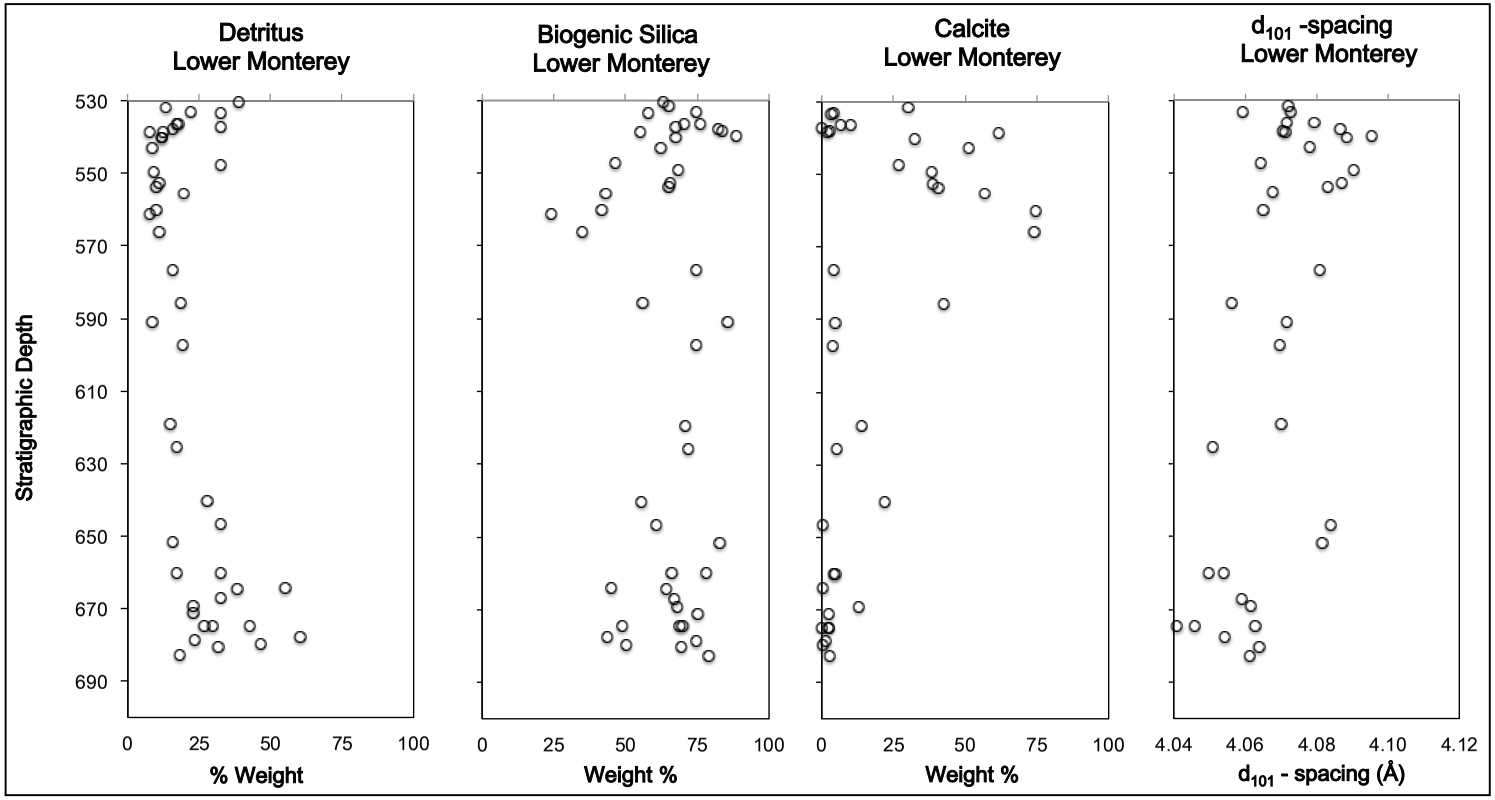

FIGURE 31. Abundances of sedimentary components and opal-CT d_{101} - spacing of samples from the lower Monterey Formation, measured by combined EDS/XRF and XRD.

CHAPTER 5

DISCUSSION

The elemental and mineralogic data from siliceous rocks of the Monterey and Sisquoc formations in the southwestern Casmalia Hill show a wide range of opal-CT d_{101} spacing for all depths and compositional ranges. These results do not show a simple trend of decreased d_{101}-spacing with burial as would be predicted by the well-cited studies described in Chapter 2. Surprisingly, this even holds true for most individual narrow compositional ranges. As described in Chapter 3, an external laboratory was used to confirm our geochemical results in a blind test. Additionally, multiple approaches to determine the opal-CT d_{101}-spacing were tested and compared. Consequently, we have good confidence in the accuracy of the data. Therefore, the results of this study need to be carefully assessed in terms of the similarities and differences with previous work to propose explanations. A full analysis of the limitations and actual findings of the previously published work follows the Summary. This is then followed by proposed explanations.

Summary and Explanation of Results

The results of this thesis do not fully support the claim that the ordering of opal-CT d_{101}-spacing is a simple linear progression with depth, as found by Murata and Larson (1975), Murata and Nakata (1974), and predicted by Isaacs (1980). Even when the data is plotted and evaluated in different ways (i.e., by single beds, by members) the expected linear trend is rarely present or well developed.

The data is plotted both as a whole (Fig. 23) and by individual Monterey Formation members (Fig. 32–Fig. 35) in narrow 10-percent silica ranges on a carbonate-, apatite-, and organic matter-free basis, to illustrate potential trends in the relationship between stratigraphic depth and opal-CT d_{101}-spacing when compositional variation is limited. Within the succession as a whole, the opal-CT d_{101}-spacing vs. depth displays no distinct trends for rocks of any compositional range (Fig. 23). Individual members show slightly more coherent structure. The data for the uppermost interval–the lower Sisquoc Formation-is limited in both number of samples and compositional range, but shows a very weak trend of increasing opal-CT d_{101}-spacing with depth (Fig. 32), the opposite of that predicted by previous studies. The upper Monterey Formation displays a wide scatter with no trend present with stratigraphic depth except for the greater than 80% silica range that presents the predicted trend of decreasing opal-CT d_{101}-spacing with depth (Fig. 33). In the middle Monterey, the < 50%-60%, and 60%-70% silica ranges are small sample sets that show very weak trends of decreasing opal-CT d_{101}-spacing with stratigraphic depth, while the 70%-80% and > 80% silica showed no apparent trends with a wide scatter (Fig. 34). For the lower Monterey, all the compositional ranges show slight to moderate trends of decreasing opal-CT d_{101}-spacing with stratigraphic depth (Fig. 35). These highly scattered data with generally only weak trends are not at all similar to the smooth linear to curvilinear progressions shown by Murata and co-workers (1974, 1975) or suggested by Isaacs (1980). For the entire Sisquoc-Monterey section, or for any individual members in the section, there is broad scatter in opal-CT d_{101}-spacing when plotted against % silica. The data showed a very weak trend of decreasing opal-CT d_{101}-

spacing with stratigraphic depth for certain narrow compositional ranges within individual members of the Monterey Formation.

Although the graphs plotted for different members by d_{101}-spacing vs. silica content show a lot of scatter, all members display a distinct upper cut-off for almost all data that has a trend of decreasing opal-CT d_{101}-spacing with decreasing silica (Fig. 36). This suggests a somewhat different crystallographic ordering process with depth than previously proposed from field and experimental studies. This new data suggests that d_{101}-spacing at initial opal-CT precipitation may be quite varied, but with burial, the most poorly ordered crystallites become increasingly destabilized and are dissolved or removed from the system, where they are re-precipitated as more ordered opal-CT crystals (Fig. 37). The slope of the limit-line suggests that the progression into instability is influenced by composition in a similar manner as proposed by previous workers (e.g., Kastner et al., 1977; Isaacs, 1980), but represents dissolution of opal-CT with large d_{101}-spacing instead of progressive solid-state conversion of existing poorly ordered opal-CT. The following section will examine these previous studies in depth to see exactly what were the conditions of measurement and if the widely cited models and conclusions were as unequivocally demonstrated as believed. A new model will then be discussed afterwards.

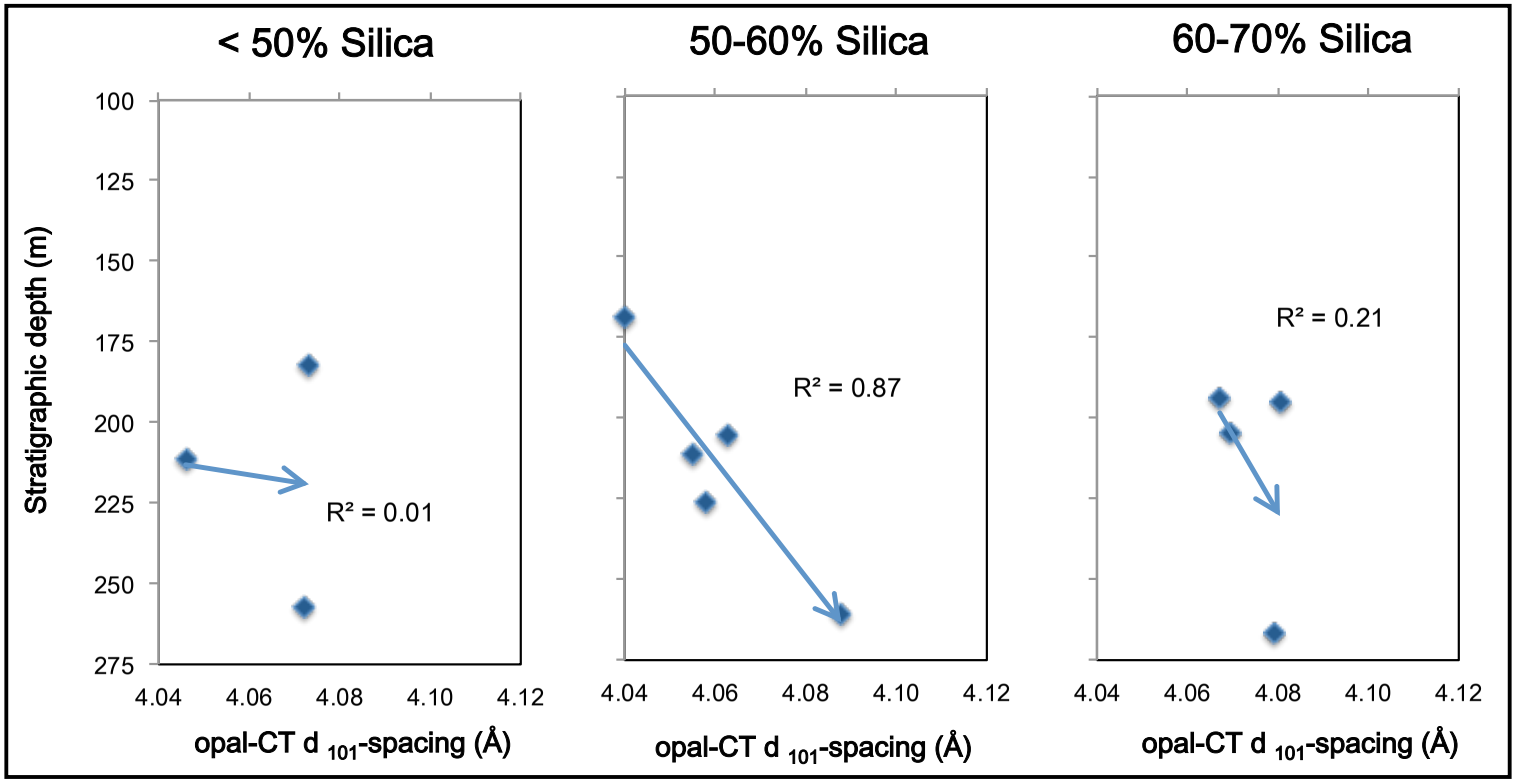

FIGURE 32. Opal-CT d_{101}- spacing versus stratigraphic depth from the lower Sisquoc Formation plotted for narrow 10 percent silica ranges on a carbonate-, apatite-, and organic matter-free basis.

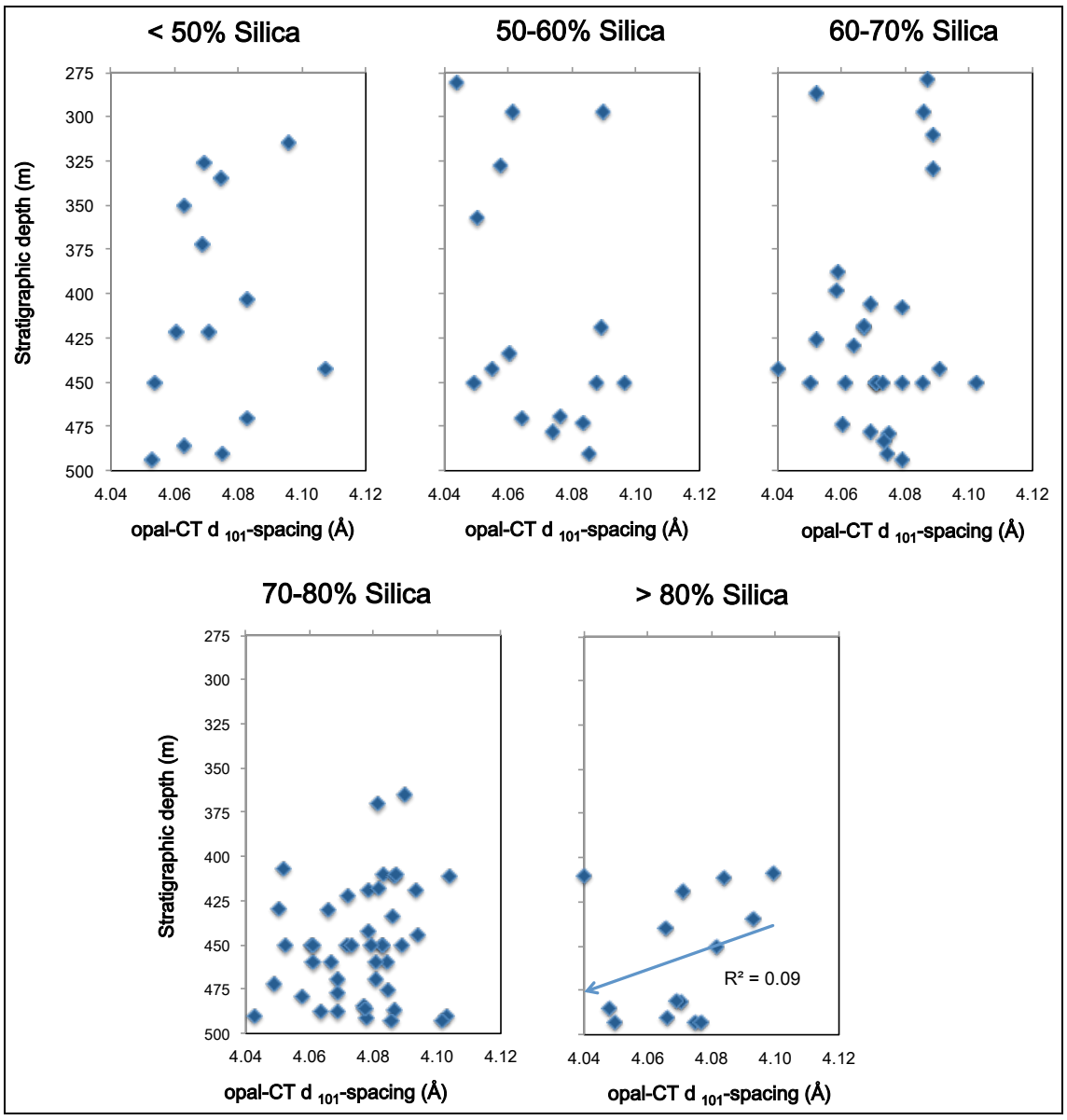

FIGURE 33. Opal-CT d_{101}- spacing versus stratigraphic depth from the upper Monterey Formation plotted for narrow 10 to 20 percent silica ranges on a carbonate-, apatite-, and organic matter-free basis.

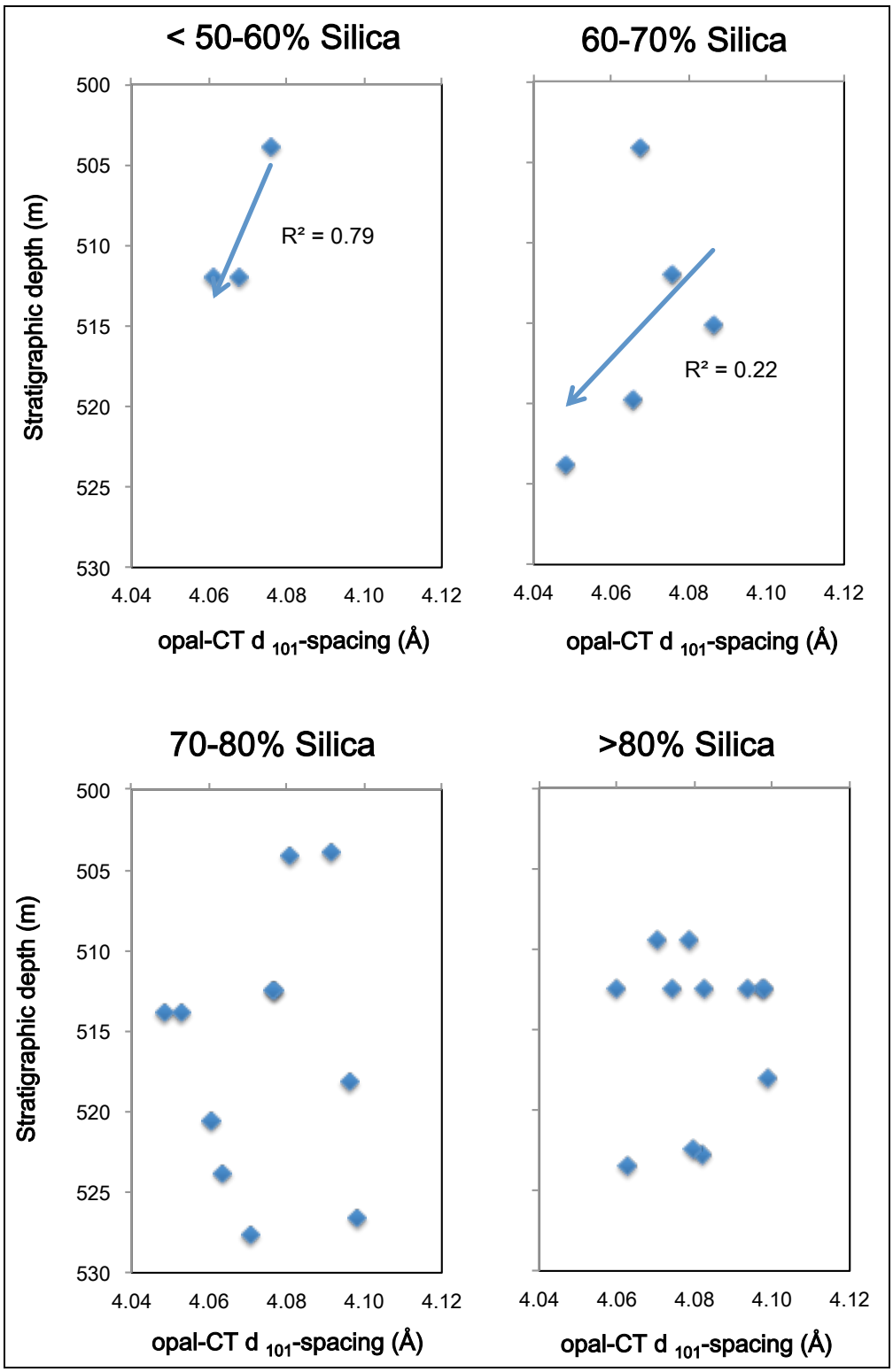

FIGURE 34. Opal-CT d_{101}- spacing versus stratigraphic depth from the middle Monterey Formation plotted for narrow 10 to 20 percent silica ranges on a carbonate-, apatite-, and organic matter-free basis.

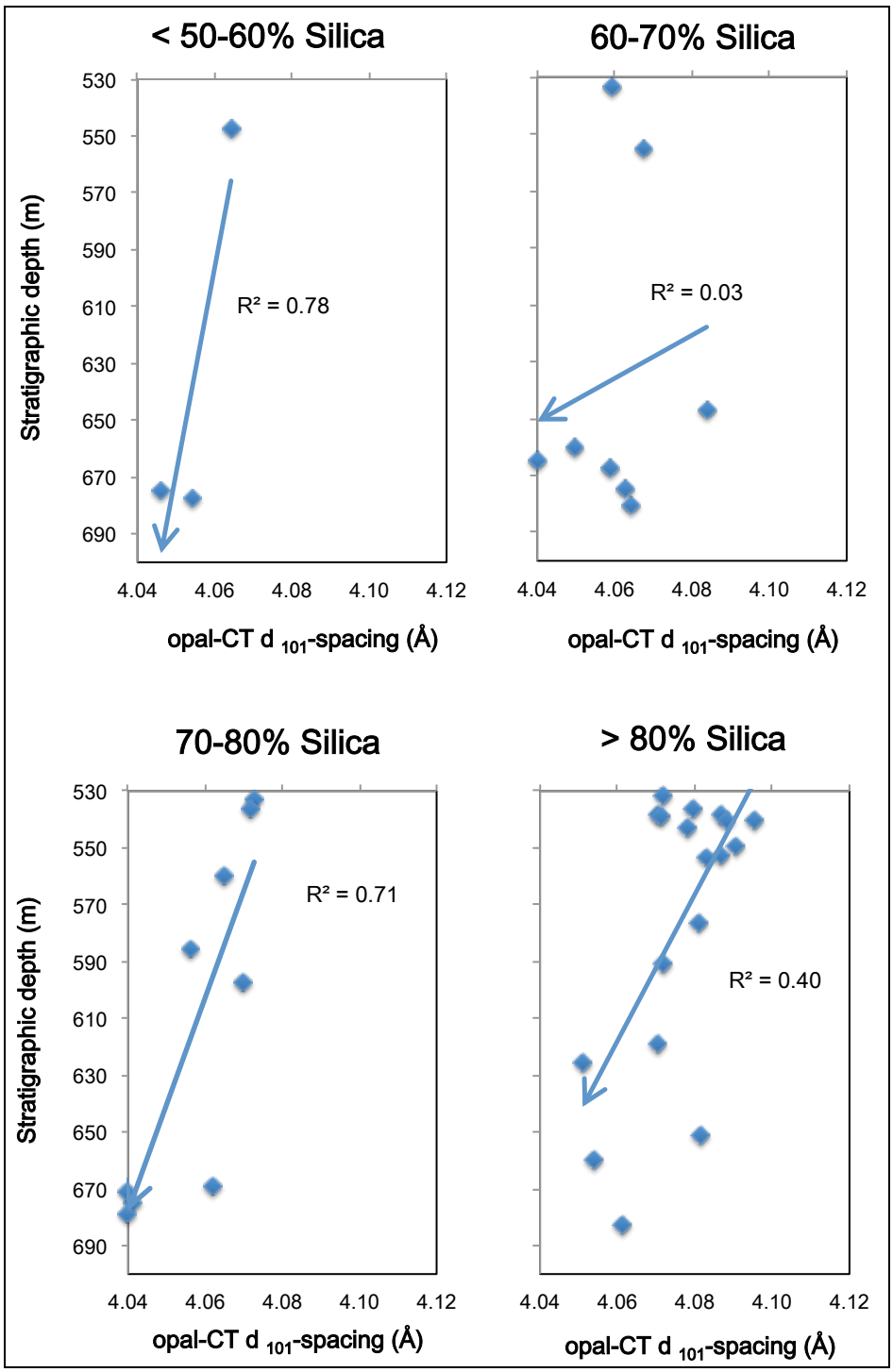

FIGURE 35. Opal-CT d_{101}- spacing versus stratigraphic depth from the lower Monterey Formation plotted for narrow 10 to 20 percent silica ranges on a carbonate-, apatite-, and organic matter-free basis.

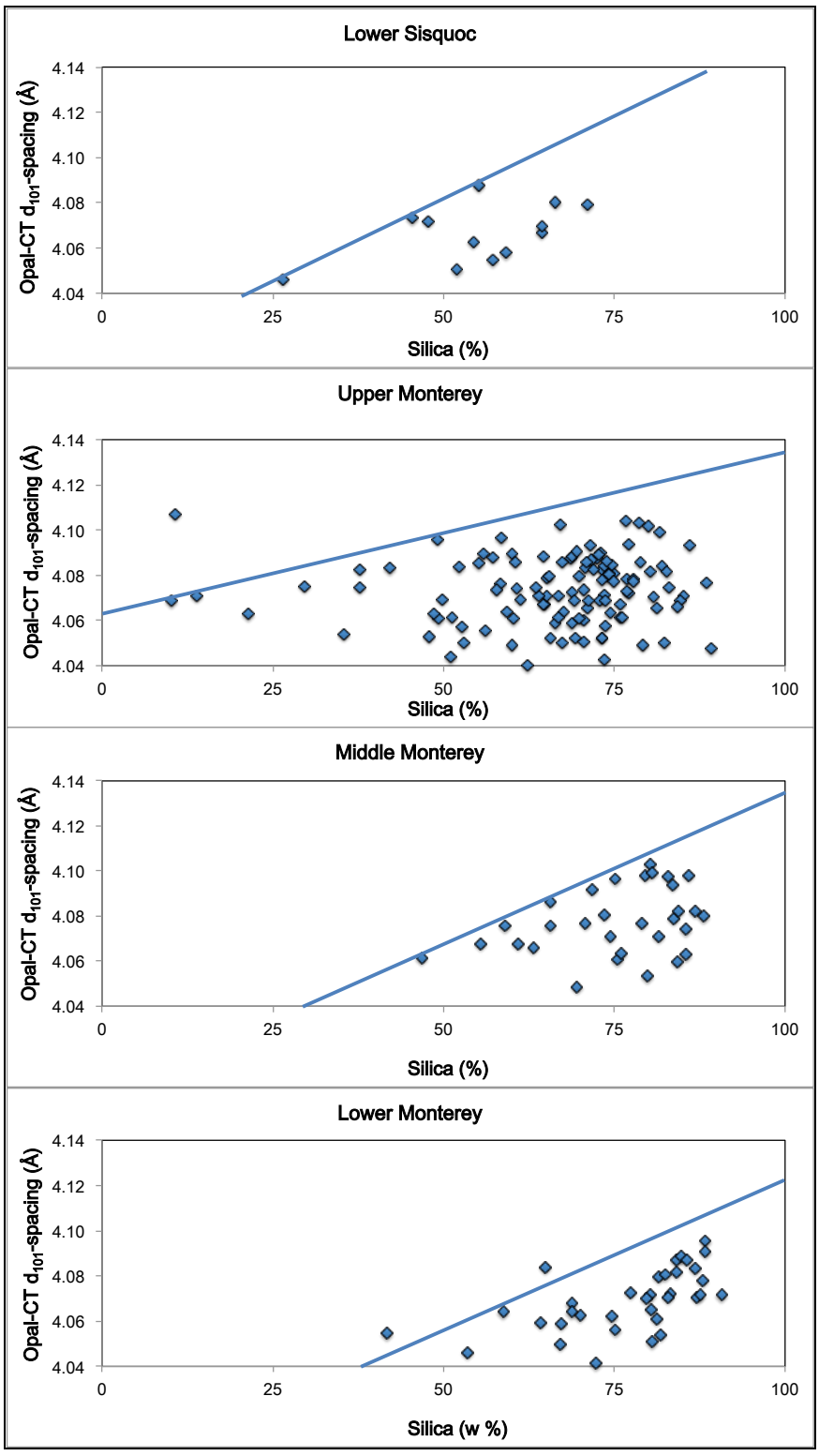

FIGURE 36. Data showing the correlation between opal-CT d_{101}- spacing and silica content in all the porcelanite samples from different Monterey Formation members. Note upper limit of opal-CT d_{101}- spacing for all members.

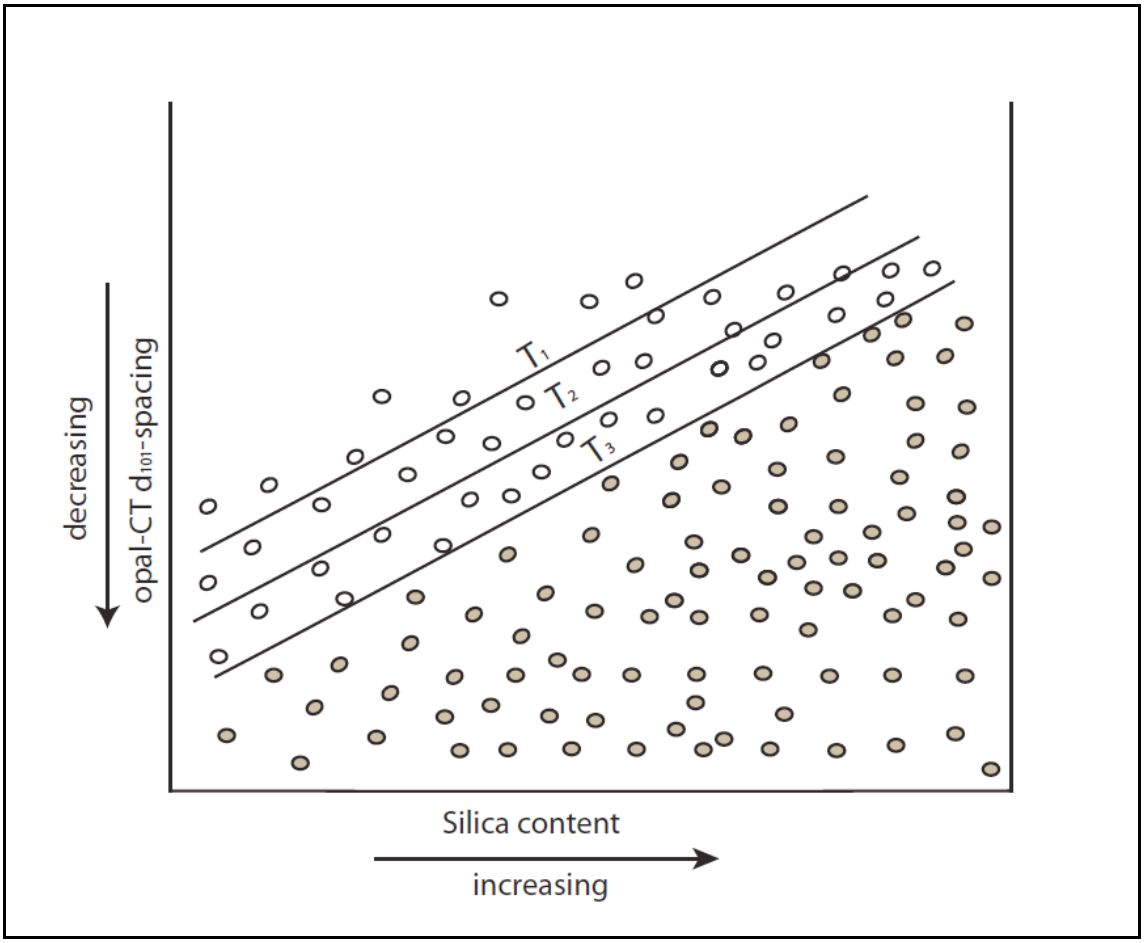

FIGURE 37. Initially opal-CT is varied, but with burial, the most poorly ordered crystallites become increasingly destabilized and are dissolved or removed from the system. T_1 thru T_3 represent the limit lines at different burial depths. The unfilled in circles are the poorly ordered crystals that are being removed from the system.

Summary and Explanation of Previous Studies

Murata and Nakata (1974) and Murata and Larson (1975) observed a curvilinear progression of decreased opal-CT d_{101}-spacing with depth in a single uplifted stratigraphic section at Chico Martinez Creek (Fig. 5), but with much fewer samples than this study and without compositional constraint except to visually separate chert from porcelanite samples. They sampled a ~1,300-meter thick section of the Antelope Shale, which is equivalent to the Upper Monterey (Dibblee, 1989) or Upper Clayey Siliceous member (MacKinnon, 1989) in the Santa Maria area (Fig. 38). This area was tilted and uplifted to the surface from its maximum burial depth. This succession is composed chiefly of varying amounts of fine detritus and diagenetic silica, resulting in a simple interbedding of siliceous mudstone and porcelanite, with minor sandstone and chert. Samples from this succession are generally lacking in calcareous or phosphatic composition and are not especially organic-rich, consequently are not representative of the heterogeneity of the whole Monterey Formation. Murata and colleagues inferred that the major control of diagenetic ordering was temperature (and possibly pressure) as a function of burial depth (Murata and Larson, 1975). Their study's tight trend of curvilinear progression of decreasing opal-CT d_{101}-spacing with depth is inconsistent with my results that show a broad scatter of opal-CT d_{101}-spacing with stratigraphic depth and only weak trends in certain members of the Monterey or within specific compositional ranges.

Mizutani (1966, 1967, 1977) observed decreased opal-CT d_{101}-spacing with increased temperature and time in hydrothermal experiments (Fig. 39). His study identified temperature and time as controlling factors in the diagenetic ordering of opal-

CT. His experiments took place in a simple, controlled environment and were intended study the progressive ordering of cristobalitic silica during diagenesis without chemical complexities. Although run at an unnaturally high temperature to increase kinetics, it provided direct observational evidence that temperature and time influence the natural progression of opal-CT d_{101}-spacing. At lower temperatures, no trend in opal-CT d_{101}-spacing was observed. However, at higher temperature ranges, opal-CT d_{101}-spacing was shown to decrease with increased reaction time. It should be noted that these experiments only strictly apply to sediments with a specified pore fluid composition, uninfluenced by other factors such as variable detrital content, organic content, or pore water chemistry.

Pisciotto (1978, 1981) measured the range of opal-CT d_{101}-spacing in porcelanites through the entire thickness of the Monterey in a number of oil wells and noted a progressive decrease in the midpoint of the range where the formation was buried to increasingly greater depths (Fig. 7). Although most wells showed a slight trend, Pisciotto (1978, 1981) did not observe a smooth curvilinear decrease in d_{101}-spacing with depth in any single stratigraphic succession as described by Murata and colleagues (1974, 1975) at Chico Martinez Creek. Many of the wells showed abrupt shifts instead of a gradual ordering, or had only one or two samples with lower opal-CT d_{101}-spacing at their base. The wells from the Santa Maria Valley show an irregular pattern of decreasing opal-CT d_{101}-spacing with depth (Fig. 40). The one well from the Bradley area shows the best overall trend of decreasing opal-CT d_{101}-spacing in a single stratigraphic section, but with little to no change in the upper half followed by a distinct break in slope for the lower part of the section (Fig. 41). The wells from the Orcutt field show patterns of decreasing

d_{101}-spacing with depth, but with a smaller sample set and distinct jumps to lower d_{101}-spacing at their bases (Fig. 42). The Orcutt oil wells have a more complicated burial history than those from the Santa Maria Valley field or Bradley area due to late Neogene uplift. Pisciotto (1981a) also collected surface samples from outcrops in the Mussel Rock area spanning the more heterogeneous middle Monterey (Fig. 8). The data from this area showed a very irregular pattern of opal-CT d_{101}-spacing with depth in cherts, porcelanites, and siliceous shales (Pisciotto, 1981a), possibly reflecting the more complex diagenetic environment provided by interbedded organic-rich mudstone, marlstone and dolomite. In sum, Pisciotto found an overall progressive decrease in the average opal-CT d_{101}-spacing of entire sections buried to greater depth than more shallowly buried correlative sections of the Monterey Formation, but only complex and irregular patterns of decrease within any one stratigraphic section.

Hein and Scholl (1978) studied cores from Deep Sea Drilling Project (DSDP) Leg 19 in the far northwest Pacific and the Bering Sea and found that d_{101}-spacing decreased with depth of burial only at one (DSDP Site 192) of four sites studied (Fig. 9). These workers concluded that important controls of silica diagenesis were temperature and time, but also surface area, pore water chemistry, sediment permeability, and the host sediment (Hein and Scholl, 1978). These samples, unlike those of the previously described studies, were taken from deep marine settings likely at their maximum burial depth. The lithologies of all the sites are very similar and comparable to the upper Clayey-Siliceous member from Santa Maria Basin or the Antelope Shale of the San Joaquin Basin. Samples from the three sites without clear trends consisted of upper Miocene clay- or silt-rich diatom ooze with interbedded with diatom-rich mudstone and shale (Supko, 1971).

There were only 4 to 6 samples analyzed from each site. The data from the one location that shows a linear trend of decreasing opal-CT d_{101}-spacing with depth (Site 192) consisted of five lower Pliocene to lower middle Miocene samples with silt- and clay-bearing diatom ooze overlying porcelanite and calcareous mudstone (Supko, 1971). The succession at this location spans a longer time interval than the other sites and accumulated on top of the Meji Guyot seamount while the others are on the deeper basin floor.

Isaacs (1980, 1981) observed decreased opal-CT d_{101}-spacing with increased detrital content (decreased silica content) within sets of samples from single locations and narrow stratigraphic levels along the Santa Barbara coastline. Like Pisciotto, she observed that the average opal-CT d_{101}-spacing decreased for the same stratigraphic level in sections that she inferred were buried to greater depths (Isaacs, 1980). She found that the silica:detritus ratios affected the timing of opal-CT precipitation and the progression of opal-CT d_{101} ordering (Isaacs, 1980); as the ratio decreases (more detrital-rich) in individual beds, opal-CT is formed later. This was interpreted to result in an initially lower d_{101}-spacing, starting the opal-CT maturation sequence closer to that at which quartz will form, leading to earlier quartz formation (Isaacs, 1980). More than 100 samples of porcelanite, siliceous shale/mudstone, cherty porcelanite, chert, calcareous mudstone, and organic-rich shale were collected from all the members at multiple locations along the coast. The crystallographic and geochemical data from the siliceous member, upper calcareous, and transitional members, in particular, were used to construct a well-known conceptual model of silica diagenesis and opal-CT ordering (Fig.10).

Isaacs (1980) examined closely associated sets of samples from individual members at different locations. She considered each set to have been exposed to the same burial history and maximum temperature. Within each set, she noted smaller d_{101}-spacing for samples with greater detrital content. For each site farther to the west, she found that the same member had greater diagenetic ordering, expressed either as lower opal-CT d_{101}-spacing values or by the conversion to quartz (Fig. 43 & Fig. 44). However, she did not show a linear trend in opal-CT d_{101}-spacing for any one stratigraphic succession (Fig. 45). This subtlety is lost on most geologists who assume the model was developed from and should be applicable to individual stratigraphic successions. To demonstrate this, I plotted Isaacs' data from the two sections with the greatest number of samples-San Augustine Canyon (Fig. 46) and the Gato Canyon (Fig. 47) in narrow 10-percent silica ranges on a carbonate-, apatite-, and organic matter-free basis, to illustrate the trend of the relationship between stratigraphic depth and opal-CT d_{101}-spacing when composition is controlled. They display very weak trends of decreasing opal-CT d_{101}-spacing with depth, but not the linear trends inferred from her oft-referenced model.

Behl and Smith (1992) studied cores from the Deep Sea Drilling Project (DSDP) Leg 129 in the Pigafetta and East Mariana Basins of the Western Pacific and found the trend of opal-CT d_{101}-spacing decreased only generally with depth and age (Fig. 12). They noted that the burial depth (temperature) and age (time) were important controlling factors of silica diagenesis, but noted that differences of the opal-CT d_{101}-spacing occurred between samples at the same depth, likely reflecting the effects of compositional variations on the primary sediment (Behl and Smith, 1992). When the data from this study was plotted by composition it still showed very weak trends with

depth (Fig. 13). The siliceous samples were from much older middle Jurassic to lower Miocene strata than the California or Bering Sea studies and contained minor to moderate amounts of clay minerals (mainly smectite), calcite, zeolites (clinoptilite), and iron/manganese oxides/hydroxides (Behl and Smith, 1992).

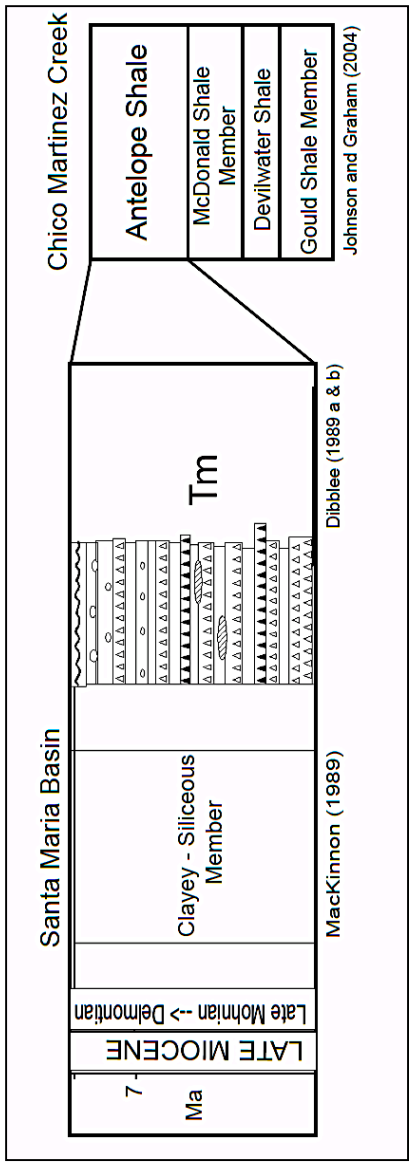

FIGURE 38. The upper Monterey Formation is designated the Antelope Shale at Chico Martinez Creek and the Clayey-Siliceous member in the Santa Maria basin. Modified from Johnson and Graham (2004) and MacKinnon (1989).

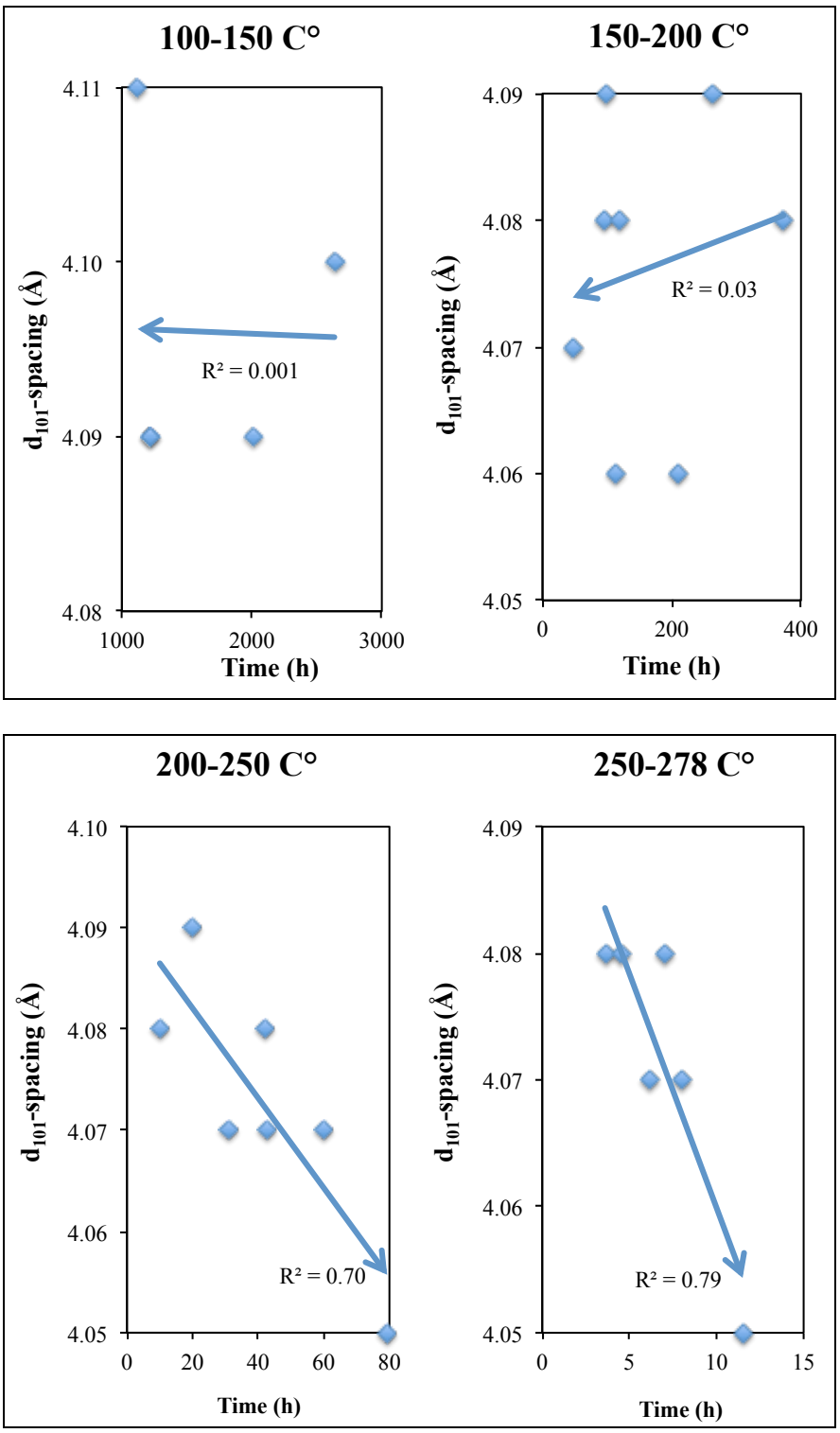

FIGURE 39. Experimental results of opal-CT d_{101}-spacing vs. temperature during the hydrothermal transformation of silica from all experiments. Samples reacted at higher temperature ranges showed better correlation of opal-CT d_{101}-spacing with length of reaction time (after Mizutani, 1977).

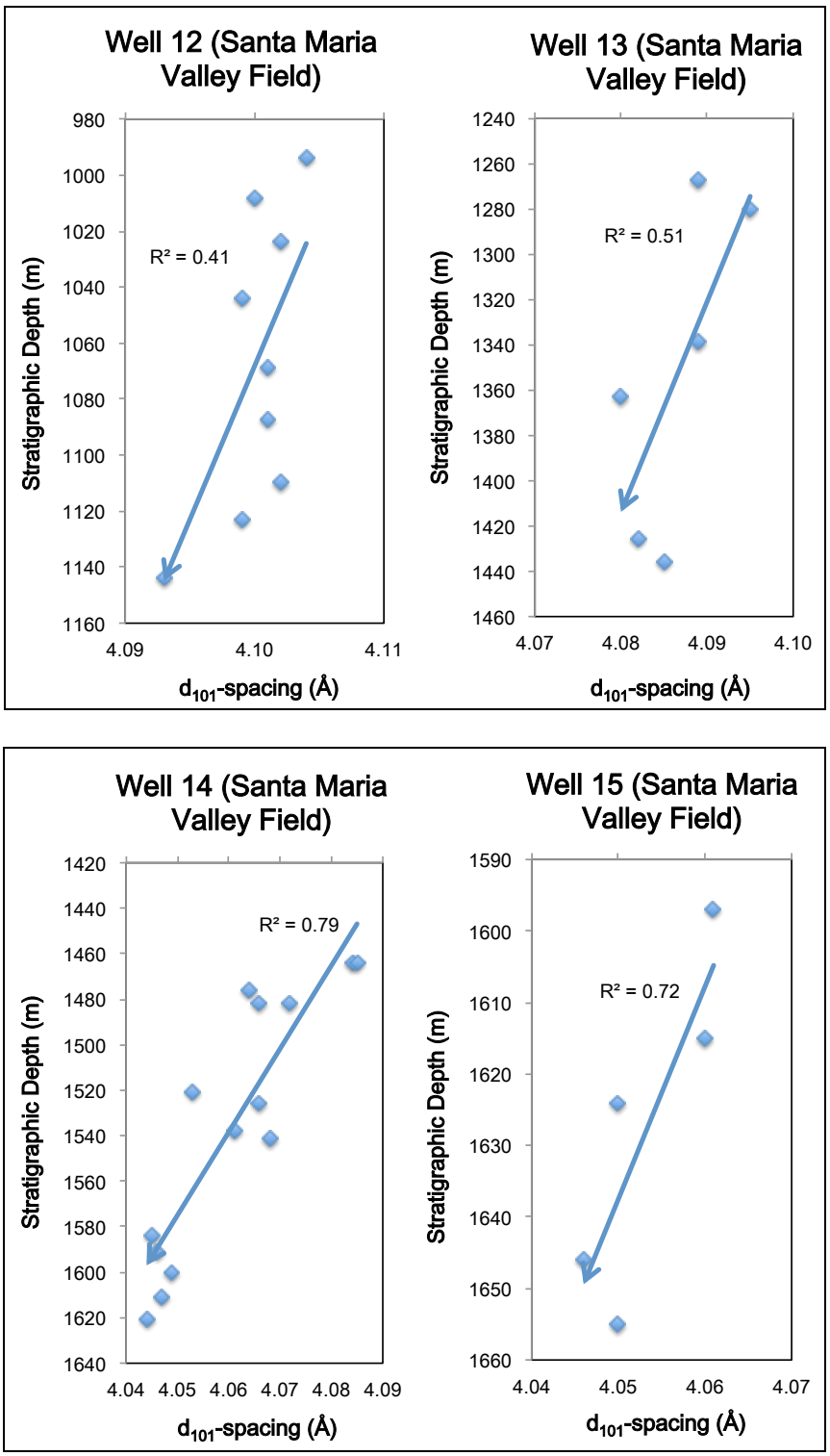

FIGURE 40. Wells 12-15 from the Santa Maria Valley Field showing general trends of decreasing d_{101}-spacing with depth. Data from Pisciotto (1978)

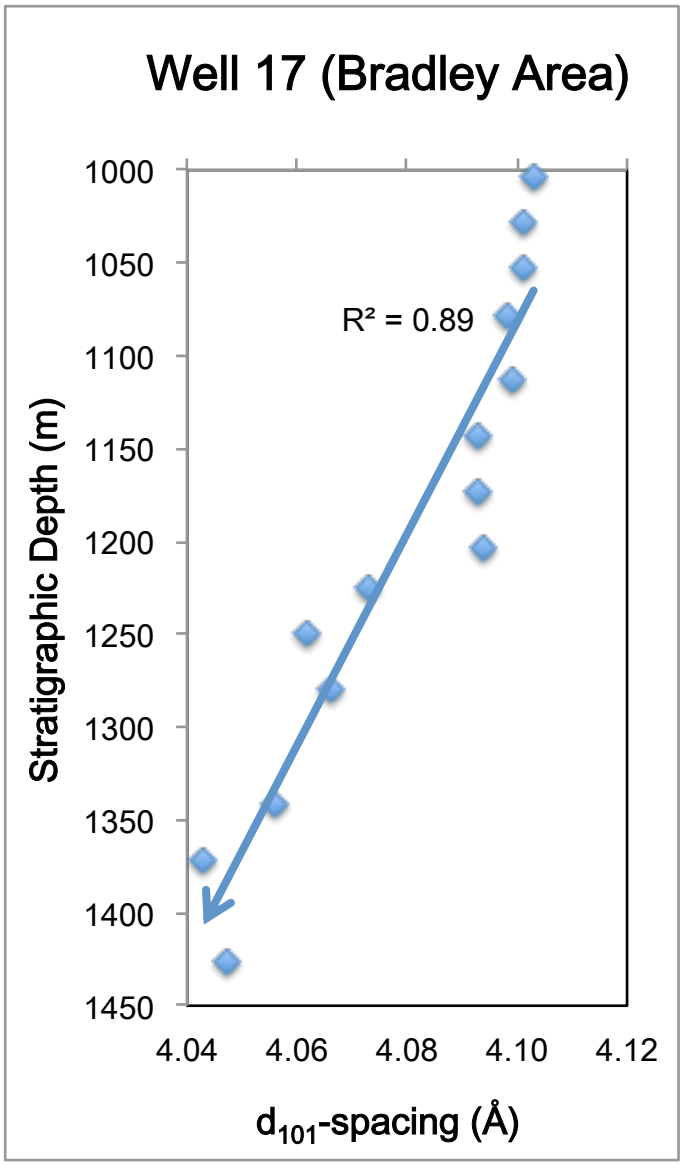

FIGURE 41. Well 17 from the Bradley area showing a trend of decreasing d_{101}-spacing with depth with large step in middle of the succession. Data from Pisciotto (1978).

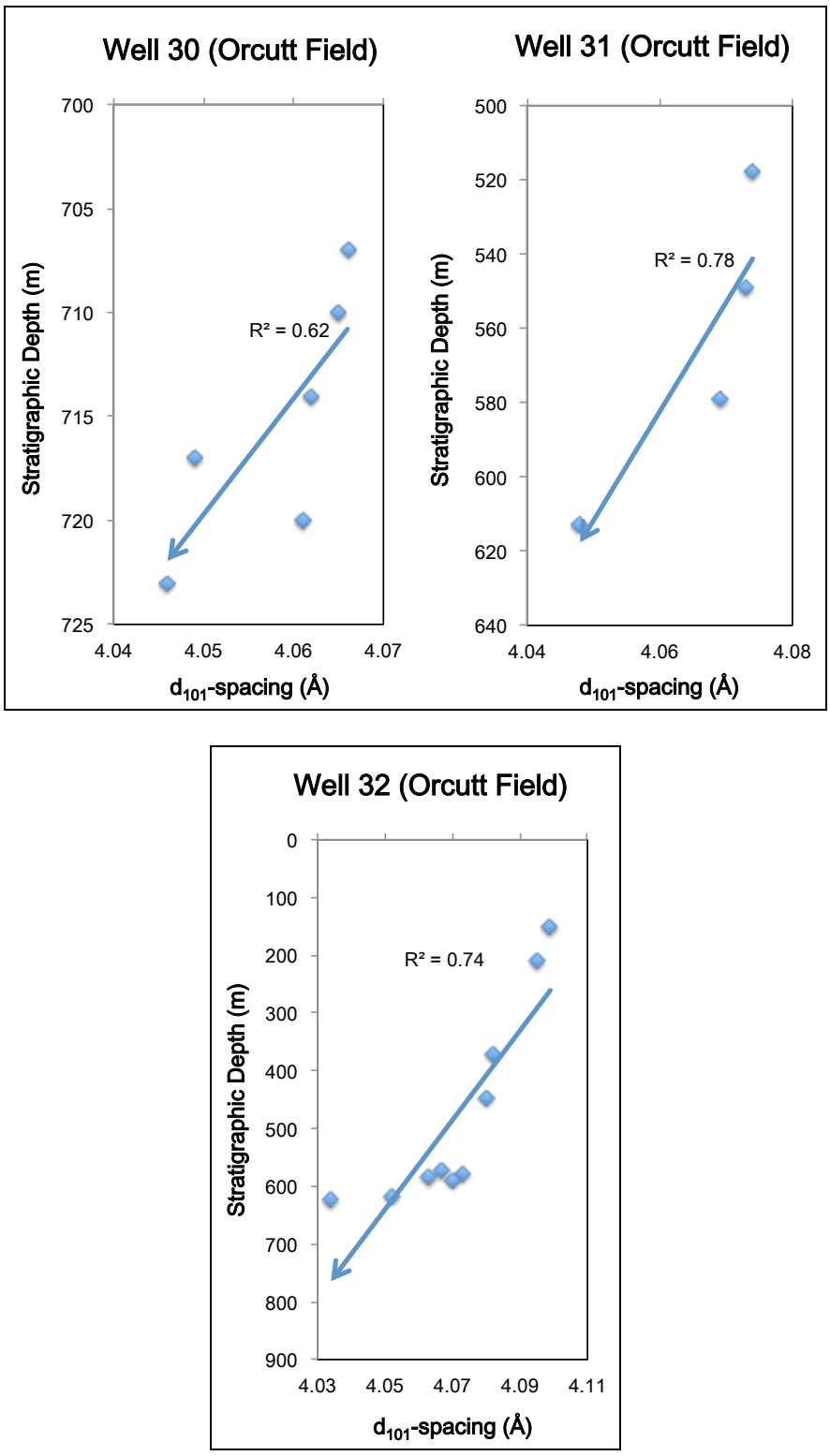

FIGURE 42. Wells 30-32 from the Orcutt Field showing weak or irregular trends of decreasing d_{101}-spacing with depth. Data from Pisciotto (1978).

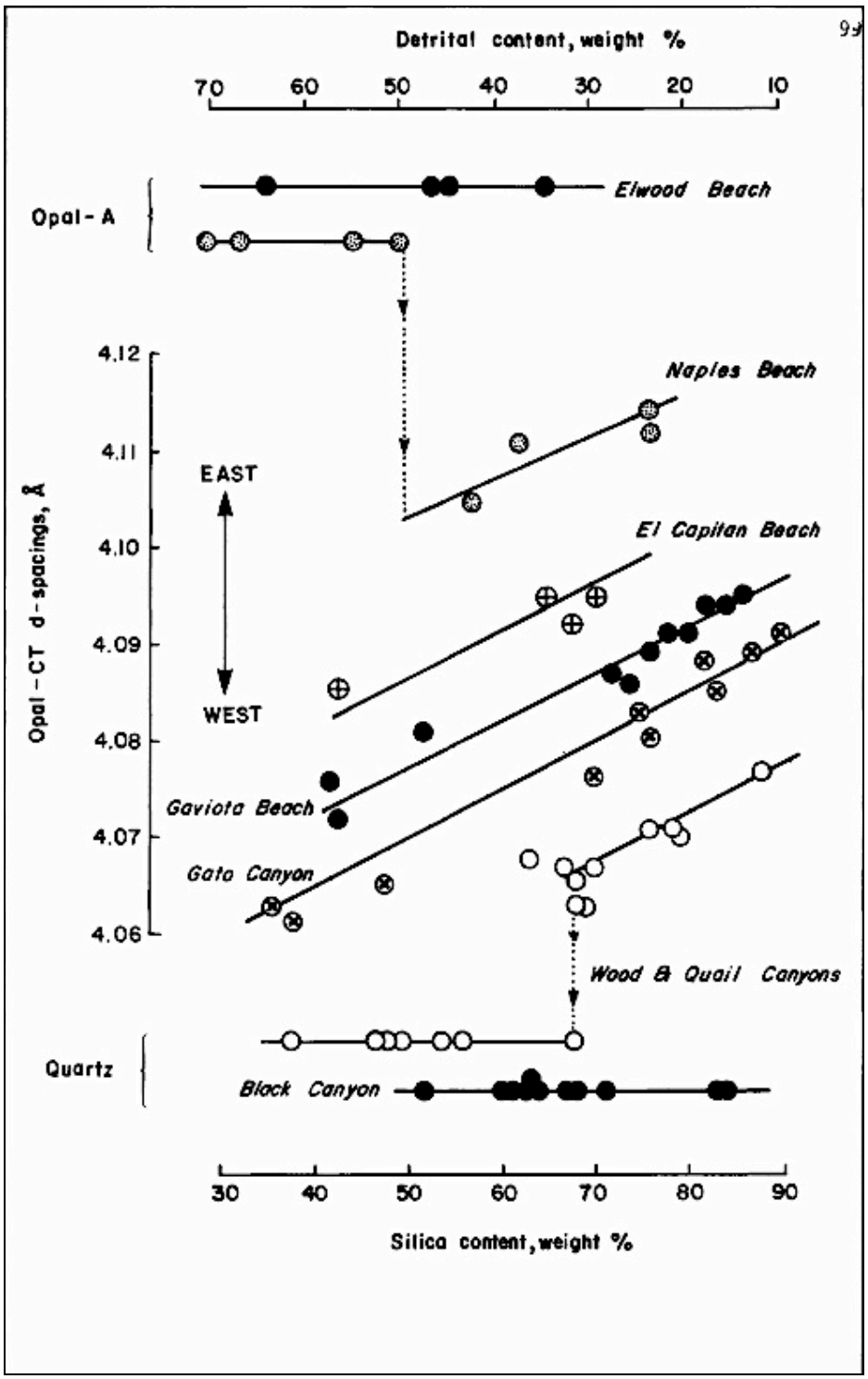

FIGURE 43. Data showing the relationship between composition and opal-CT d_{101}-spacing for closely spaced rock from different sites in the siliceous member. From Isaacs (1980).

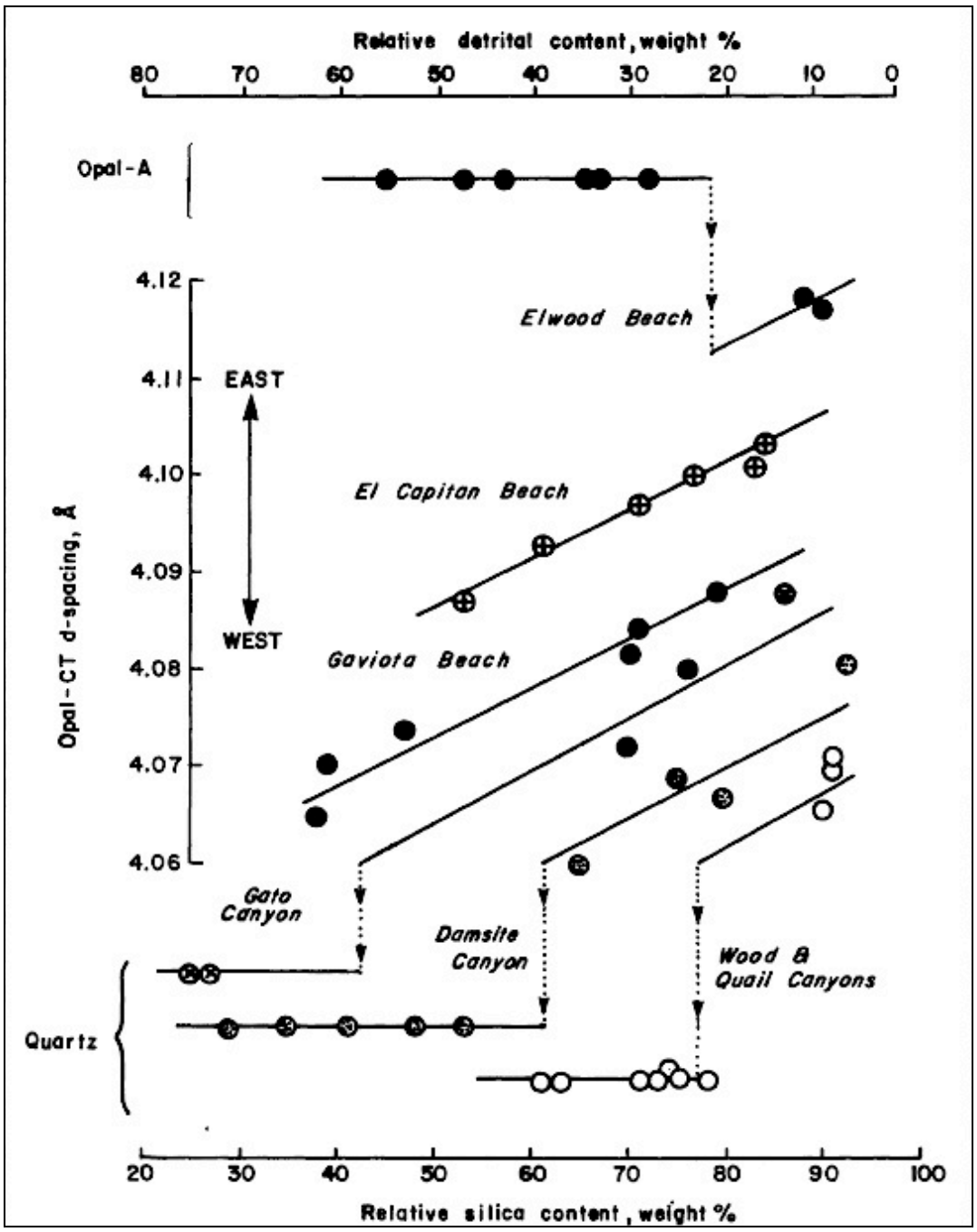

FIGURE 44. Data showing the relationship between composition and opal-CT d_{101}-spacing in closely spaced rocks from different sites in the transition and upper calcareous shale members. From Isaacs (1980).

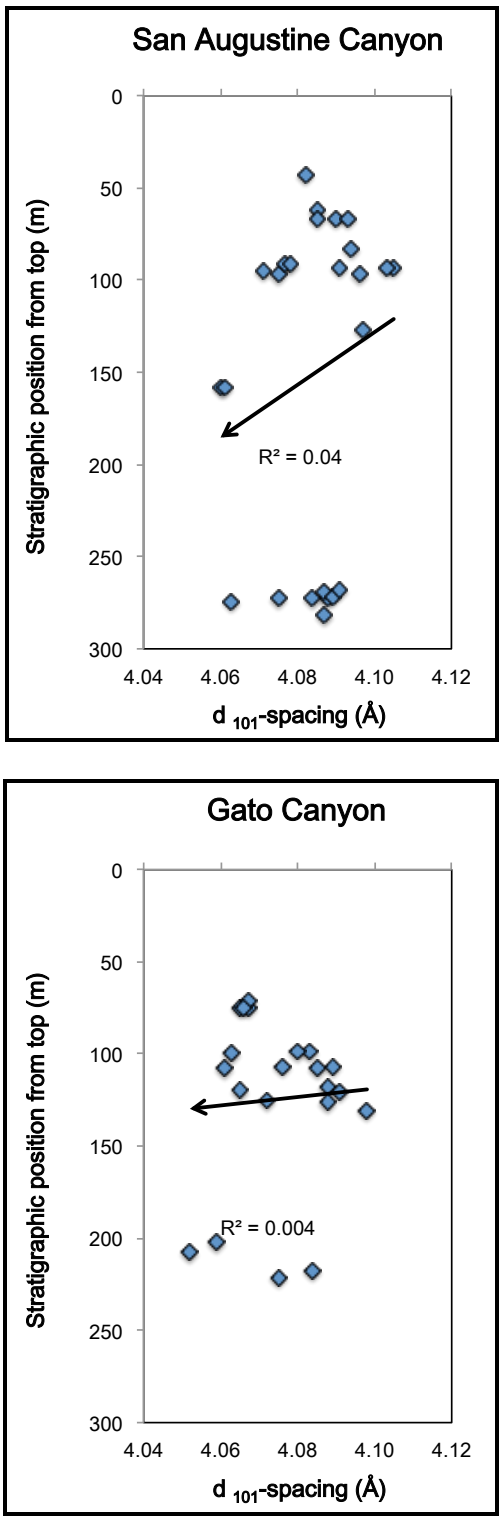

FIGURE 45. Data showing the relationship between composition and opal-CT d_{101}-spacing for closely spaced rock from the Gato and San Augustine Canyon sections. From Isaacs (1980).

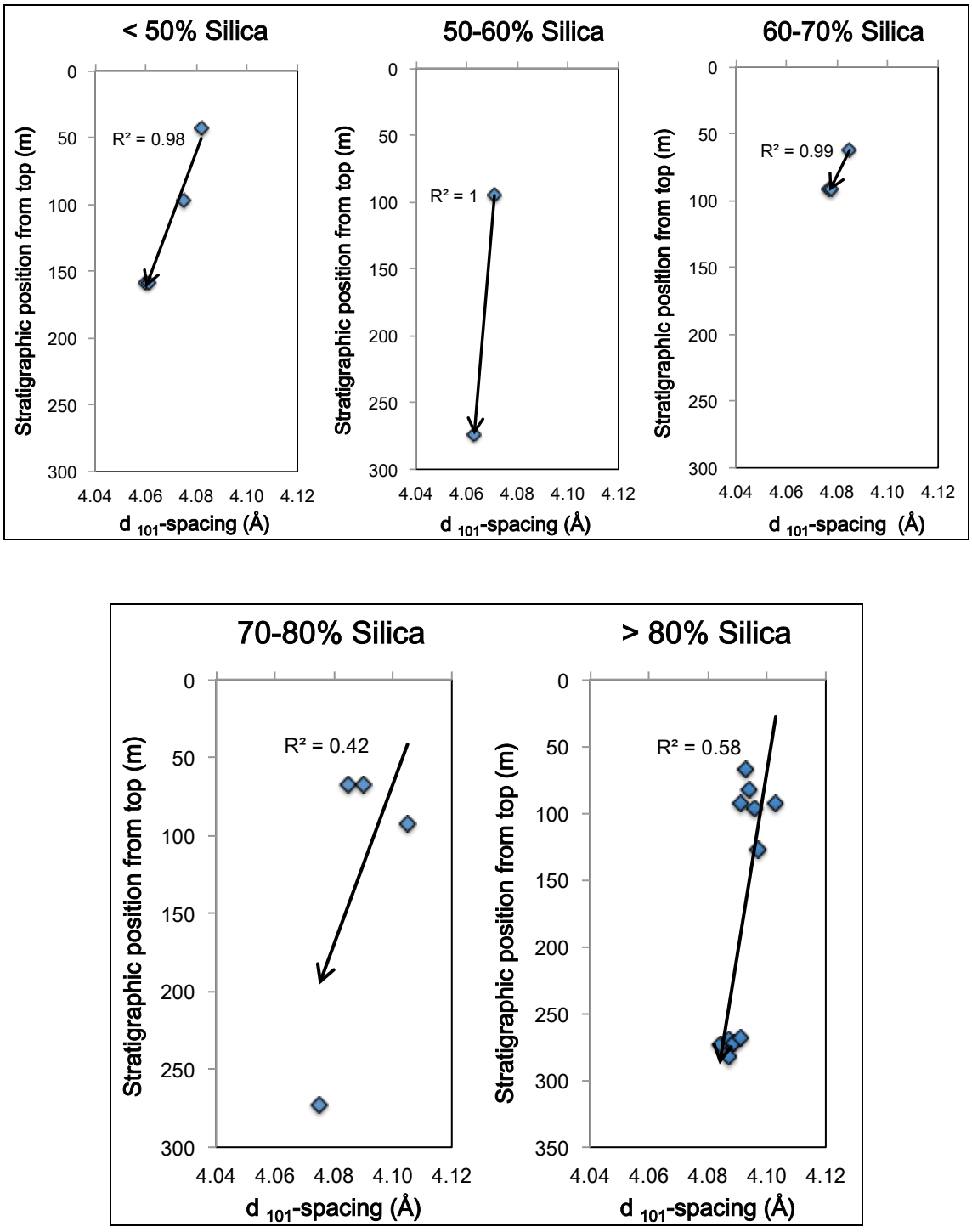

FIGURE 46. Data from the San Augustine Canyon section showing opal-CT d_{101}-spacing plotted versus stratigraphic depth in meters for narrow 10 percent silica ranges on a carbonate-, apatite-, and organic matter-free basis. Data from Isaacs (1980).

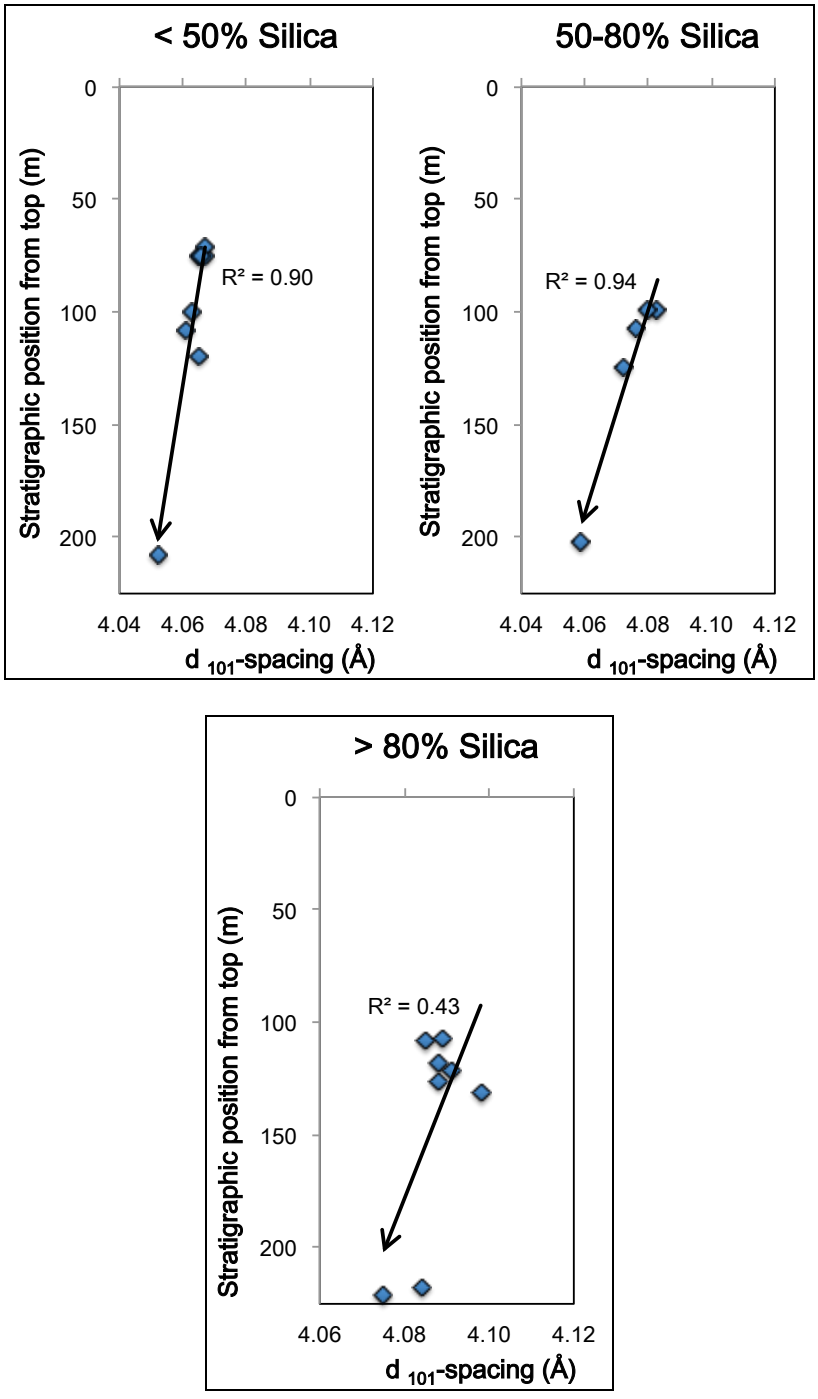

FIGURE 47. Data from the Gato Canyon section showing opal-CT d_{101}-spacing plotted versus stratigraphic depth in meters for narrow 10 to 30 percent silica ranges on a carbonate-, apatite-, and organic matter-free basis. Data from Isaacs (1980).

Assessment of Inconsistencies and Possible Explanations

Pore water chemistry has a major effect on silica diagenesis because it influences dissolution of existing phases and helps inhibit or provide nucleation sites for precipitation of diagenetic phases (Kastner et al., 1977; Hesse and Schacht, 2011). Experimental data shows the influence of water chemistry on the rate of silica diagenetic transformation (Kastner et al., 1977) and the initial ordering of opal-CT (Hinman, 1990). Kastner et al. (1977) showed the effect of alkalinity from carbonate, which increases the rate of silica diagenesis (Kastner et al., 1977) by providing part of the MgOH compound that serves as a nucleating agent for opal-CT. These workers and others also theoretically linked decreased activity of Mg^{+2} in pore waters to the presence of smectitic clays. Organic acids produced by the breakdown of organic matter, have a similar affect on opal-CT formation and d_{101} ordering as detrital clays (Hinman, 1990). This apparently occurs because organic acids lower the pH of the solution by consuming alkalinity, which reduces the rate of opal-CT nucleation (Hinman, 1990).

Previous workers have presumed that the chemistry of pore waters are primarily controlled by solubility relationships with the sedimentary components within individual beds for these kind of low-permeability sediments (c.f., Isaacs, 1980). Consequently, the mineralogic or chemical composition of the rock can be taken as a proxy for pore water chemistry during diagenesis. However, neither dissolved silica (silicic acid) nor other ions are necessarily restricted to single beds on geologic time scales as they can be transported by diffusion or advection over both short and longer distances. At a multi-bed scale, pore-water chemistry in a single layer may change when it is interbedded with strata of different clay, carbonate, phosphate, or organic-matter content. Ions from these

substances can diffuse into a bed lacking any of these components to influence the dissolution or precipitation of silica. Therefore, the timing of silica phase transitions and the ordering of opal-CT in one bed may be impacted by diffusion of ions from surrounding beds that influence alkalinity, pH or the presence of catalytic or inhibiting ions. The pore water conditions of diagenesis in any one bed may be more accurately defined by the integrated solid composition of all beds within diffusional radius–possibly centimeters to meters away–than by its composition alone.

Dissolved silica itself can also be transported within and between beds. Opal-A or opal-CT silica in the form of small, poorly ordered crystallites can dissolve and be transported via diffusion through the pore water to re-precipitate as larger, better-ordered opal-CT or quartz crystallites (c.f., Williams and Crerar, 1985) in another location if the chemistry is more favorable for nucleation or if lower solubility phases of silica already exist. This short-distance diffusion can take place within or between beds (Tada, 1991), over scales of microns to 10's of centimeters (Hesse and Schacht, 2011; Fig. 50). Localized growth of better-ordered opal-CT supplied by dissolution of poorly ordered opal-CT would necessarily decrease the whole-rock opal-CT d_{101}-spacing while increasing silica content in single beds or parts thereof (Fig. 36). A test of the variability of opal-CT d_{101}-spacing and silica content between two closely spaced, apparently similar, porcelanite beds (Fig. 23) showed results quite different from Isaacs (1980), where she analyzed a number of samples that were within about 20 meters stratigraphic distance. Being from just two beds, this should have been a better test of natural diagenetic variation. We expected the silica content and opal-CT d_{101}-spacing of the samples from each bed to have been quite similar and not as varied as found. A suspected reason for

this variability is that our sampling was not restricted to the middle of the bed where it is most silicified, but included samples from different places on the bed that have lower silica:detritus ratios. Most individual porcelanite beds display a compositional zonation of being more detrital-rich at the upper and lower edges and being more siliceous in the center. Additionally, some beds display lateral variation in "chertiness" resulting from localized migration and silicification.

The timing of most active silica dissolution, migration and re-precipitation ultimately depends on temperature, which is mainly determined by the geothermal gradient of the area (Hesse and Schacht, 2011). Complex burial and uplift histories can cause strata to deform before physiochemical equilibrium is reached with respect to the diagenetic process (Mizutani, 1977). As a result of folding and differential uplift, there can be differences in opal-CT d_{101}-ordering in beds that are in the same stratigraphic horizon (Mizutani, 1977) or at the same burial depth.

The previously reviewed studies indicate that pore water chemistry, compositionally complex interbedding, and silica migration may be the three most significant factors affecting the timing of silica phase transitions, opal-CT d_{101}-spacing and silica content. Favorable conditions for the smooth progressive ordering (decreasing d_{101}-spacing with burial depth) of opal-CT are where the composition of the sediments and pore waters are fairly homogeneous, and they reach physicochemical equilibrium with respect to the diagenetic process before uplift and tilting, or have been uplifted but maintain a mostly original depositional geometry. These favorable conditions were present in the hydrothermal experiments of Mizutani (1977), where the chemistry was kept constant with changes in temperature and in the study area of Murata et al. (1974,

1975, 1977) where the Antelope Shale has a relatively consistent composition of silica and detritus with relatively minimal carbonate, phosphate, and organic matter content.

The data produced by this study support a hypothesis that the influence of pore water chemistry and silica migration at and beyond the bed-scale is important for silica diagenesis. This modification to the general understanding is significant in how opal-CT d_{101}-spacing may be useful as a tool for geologic investigation. The basis of these models are: (1) the timing of formation and initial ordering of opal-CT at one location are influenced by pore-water composition controlled by the integrated water-rock interactions within the maximum diffusional radius of the bed; and (2) the final whole-rock opal-CT d_{101}-spacing is controlled by progressive dissolution of disordered, high d_{101}-spacing opal-CT crystallites and new precipitation of better-ordered opal-CT. The latter involves silica migration on both the submicron scale of lepispheres and a larger scale migration between beds. Evidence for bedding-scale silica mobility is displayed by increased silica content at cherty centers of porcelanite beds and lateral compositional variability in nodular or pinch-and-swell strata (Tada, 1991; Behl et al., 2003). Behl and Meike (1990) documented variation in opal-CT crystallographic ordering on the sub-millimeter scale within beds or laminations, and observed difference in crystal size and shape between inner and outer portions of opal-CT lepispheres. Kassa & Behl (2014) observed increased porosity in lepisphere centers and increased precipitation/ cementation towards outer parts of lepispheres. These features could result in the development of micro-diffusional gradients between smaller, less ordered, more-soluble crystallites and larger, more ordered, less-soluble ones. Dissolution related to these gradients would contribute to the formation of secondary porosity in the centers of

lepispheres and other locations of poorly ordered, more-soluble opal-CT (Kassa, thesis in prep; Fig. 48).

The data presented within this thesis suggest that opal-CT-phase silica can be initially precipitated with a large range of d_{101}-spacings within any one stratigraphic interval and for any silica: detritus ratio. With the increased temperature of further burial, opal-CT crystallites with higher d_{101}-spacings dissolve and silica is diffusionally transported to precipitate as new crystals or on pre-existing less-soluble, better-ordered crystals (Fig. 49). This transport, reprecipitation and reordering of diagenetic silica may take within a single bed or lamination, resulting in no change in whole-rock composition (Fig. 50), or may occur between beds, removing silica from one and adding it to the other. Removal of the least ordered, most-soluble silica (high opal-CT d_{101}-spacing) is shown by the general absence of samples above the sloping upper limit-line (Fig. 49).

The variability of opal-CT d_{101}-spacing for any composition at any depth under the limit-line may be attributed to the heterogeneity of the interbedded rocks and pore fluid influences that are not considered in models of Isaacs (1980) or Williams and Crerar (1985). Isaacs's (1980) summary diagram (Fig. 10) only displays the relationship of d_{101}-spacing on a plot of depth/temperature vs. silica:detritus-a two-dimensional perspective. This portrayal does not account for the affects of other potentially important variables, such as carbonate and organic matter. Hinman (1990) showed that concentration of organic acids have a similar, but independent, effect to smectitic clays in retarding opal-CT formation and initial d_{101}-spacing–i.e., samples with low organic content will form opal-CT earlier than those with high organic content. The initially wide scatter of the new data suggests that the relationship cannot be displayed in two dimensions alone, but

must be multidimensional to account for the different variables (carbonate, organic matter, etc.). For example, a sample of a particular silica:detritus ratio will also be influenced by organic content which defines its own sloping stability boundary between opal-A and opal-CT and influences the opal-CT d_{101}-spacing, consequently the initial opal-CT d_{101}-spacing may be higher or lower than that predicted from silica:detritus ratio alone. Likewise, high carbonate and increased alkalinity will cause earlier formation of opal-CT and this trend must also be applied to relationships determined from silica:detritus ratios. Because each member or stratigraphic interval of the Monterey and lower Sisquoc have different gross lithologic compositions, their pore-water chemistry would also vary and initial opal-CT formation will occurs at different burial depths (temperature) and d_{101}-spacings. The middle and lower Monterey have a particularly complex lithologic variability, with more carbonate, phosphate, and organic material than the other members, so their diagenetic pathways are likely to be different than the other members.

In spite of these complexities and variability, opal-CT d_{101}-spacing may still be useful as a geothermometer. Each of the stratigraphic members (Lower Sisquoc and Upper, Middle, Lower Monterey) have distinct upper limits of opal-CT d_{101}-spacing with somewhat different slopes (Fig. 44). Whereas the opal-CT d_{101}-spacing of an individual sample may have too complex diagenetic origin to permit it alone to be used as a geothermometer as attempted by Behl and Morita (2007), the maximum opal-CT d_{101}-spacing in a stratigraphic interval may still have significance as a geothermometer. We suggest the only the maximum opal-CT d_{101}-spacing for a given composition in a stratigraphic interval be used to determine maximum burial depth and temperature for tectonic reconstructions.

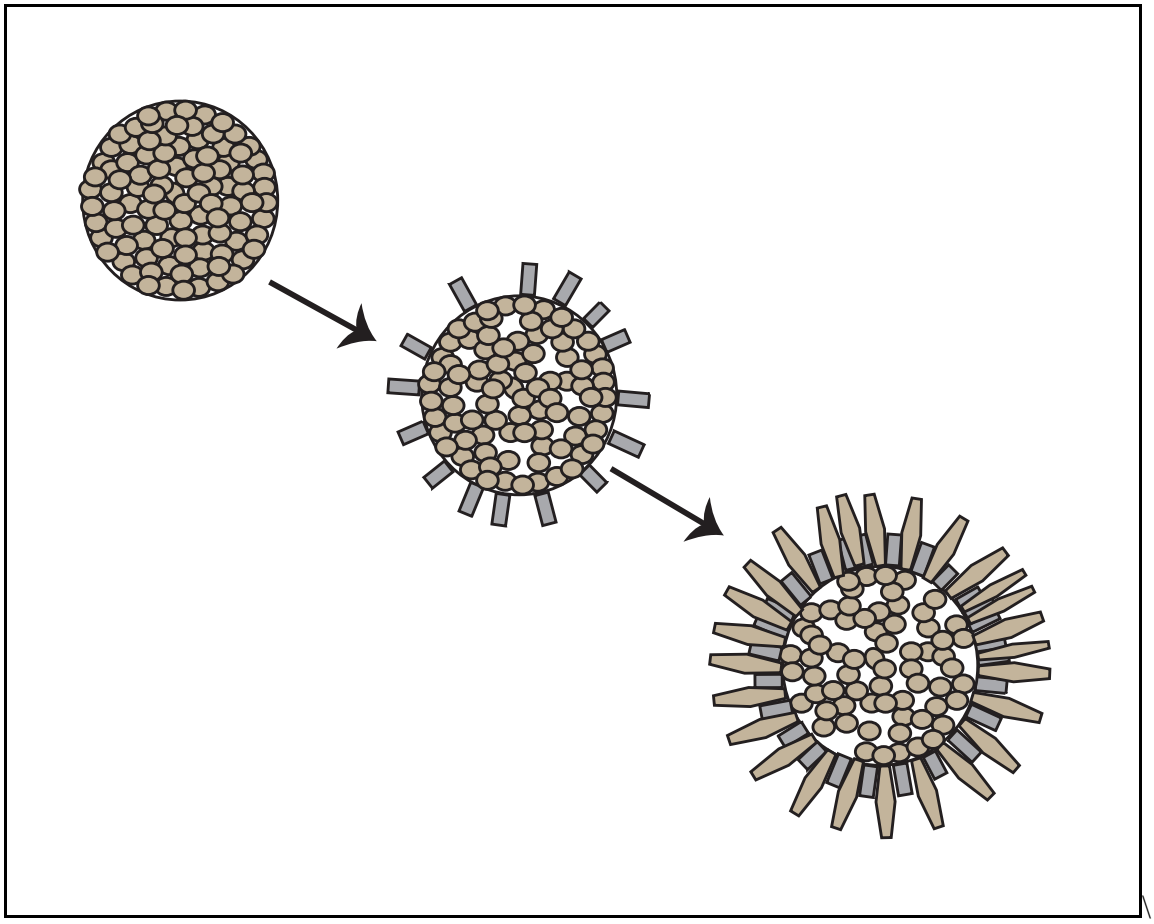

FIGURE 48. Model for diagenetic ordering with growth of opal-CT lepispheres. With burial the lepispheres grow and transition to smaller d_{101}-spacing by dissolving the inner poorly ordered crystals and re-precipitating as larger, better ordered crystals on the outer perimeter.

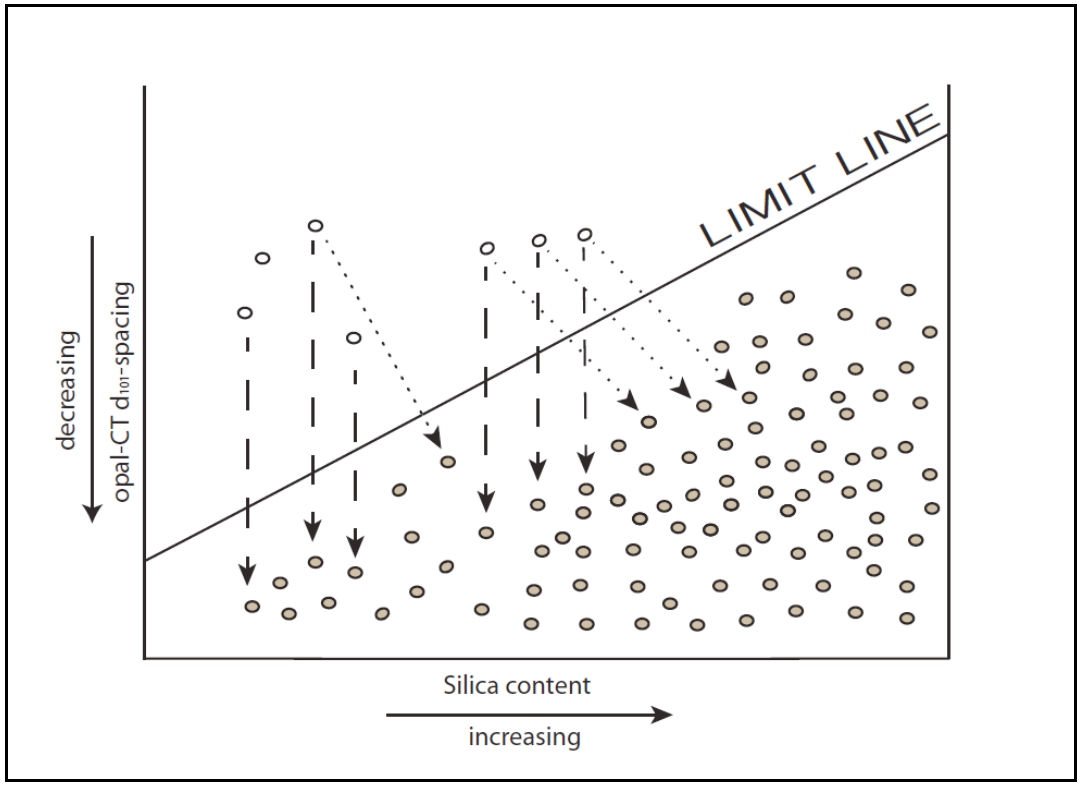

FIGURE 49. With increased burial higher opal-CT d_{101}-spacing values dissolve and re-precipitate as more ordered opal-CT with increased silica content. The unfilled in circles are the poorly ordered crystals that are being removed from the system. The dashed arrows show the reprecipitation of opal-CT crystals in lepispheres, while the dotted arrows show the migration of silica and opal-CT between beds.

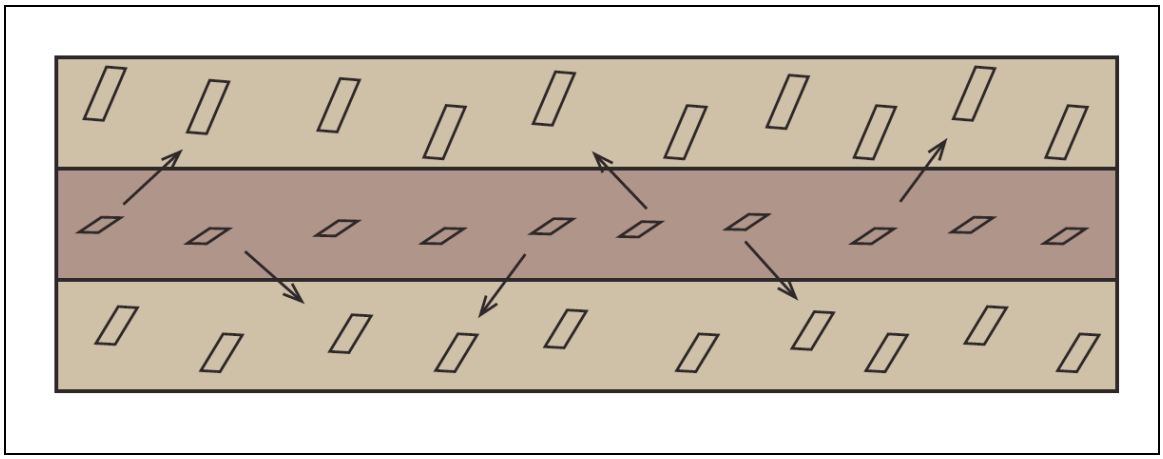

FIGURE 50. Silica migration and reprecipitation between layers at lamination to bed scale results in changes in silica concentration and opal-CT d_{101}-spacing.

CHAPTER 6

CONCLUSIONS

This study set out to test the diagenetic models of Isaacs (1980), Murata et al., (1974, 1975, 1977) and Pisciotto (1978) in a new field area, and to test natural variability in crystallographic ordering of opal-CT at high spatial resolution. This study presents and evaluates data from more samples in a single stratigraphic succession than has ever been published before. Analytical techniques (Combined EDX/XRF and XRD) were used to obtain information of the diagenetic ordering and composition of 230 samples from a complete siliceous section of the Monterey Formation. Although silica diagenesis has been studied for over 60 years in the Monterey Formation in California, Miocene-Pliocene formations in Japan and in the Bering Sea and West Pacific, a complete understanding of all the processes that effect its progression is still incomplete. The data from this study has led to the following new findings and conclusions:

1. The presented data does not support the concept that the ordering of opal-CT d_{101}-spacing is universally a simple linear progression with depth, as found by Murata and Larson (1975) and predicted by Isaacs (1980). The expected linear trend is rarely present or well developed even when composition is controlled by evaluating only sets of rocks from narrow composition ranges or when the data is plotted and evaluated in other restricted fashions (i.e., by single beds, by members).

2. Opal-CT phase silica can be initially precipitated with a large range of d_{101}-spacings within any one stratigraphic interval and for any silica:detritus ratio. With the increased temperature of further burial, opal-CT with higher d_{101}-spacings preferentially dissolve and silica is diffusionally transported to precipitate as new crystals or on pre-existing less-soluble, better-ordered crystals.
3. Favorable conditions for the simple progressive ordering (decreasing d_{101}-spacing with burial depth or temperature) are likely restricted to those environments where the composition of the sediments and pore waters are fairly homogeneous, and sediments have reached physicochemical equilibrium with respect to the diagenetic process before uplift and structural deformation or have been uplifted, still buried in a mostly vertical position.
4. Dissolved silica and other ions from carbonate, phosphate, organic matter, etc. are likely transported within and between beds by diffusion, thereby similarly influencing diagenesis in multiple adjacent beds, even those with different sediment compositions.
5. The initially wide scatter of opal-CT d_{101}-spacing with burial depth and silica:detritus suggests that the relationship cannot be portrayed in a 2-D graph with these variables alone, but must be considered in a multidimensional perspective to account for other variables (carbonate, organic matter, etc.) that can influence the timing of opal-CT precipitation or degree of crystal ordering.
6. The opal-CT d_{101}-spacing of any individual sample may have too complex diagenetic influences to permit it to be used as a geothermometer, but the maximum opal-CT d_{101}-spacing for a specific composition rock in a stratigraphic interval may still have significance as a geothermometer.

CHAPTER 7

RECOMMENDATIONS FOR FUTURE WORK

The results of this study have fueled a reevaluation of previous assumptions about silica diagenesis progression and more work needs to be done to further evaluate and refine our conclusions. Recommendations for future work include:

1. Identify and characterize geologic areas where there are favorable conditions for the progressive ordering seen in Murata et al., (1974, 1975, 1977) and Mizutani (1977) studies and also the settings where our study's results are more likely to occur.
2. Develop a multidimensional model that shows all the variables (temperature, silica: detritus, carbonate, organic matter) effecting silica diagenesis and crystallographic ordering, because the results of this study prove the 2D model of Isaacs is not sufficient to predict data in a compositionally heterogeneous stratigraphic setting.
3. Analyze multiple samples from one small stratigraphic interval and test the compositional and opal-CT d_{101}-spacing variability at high spatial resolution, to determine the effects of pore water chemistry and silica migration and their spatial distribution.
4. Perform ultra-high-resolution electron microscopy and electron diffraction to establish relationships between opal-CT crystallite size and position in lepispheres with degree of crystallographic ordering to test the hypothesis of localized silica migration and re-ordering.

5. Revisit the study by Schwalbach et al. (2009), that measured the change in facture density with proximity to the South Branch of the Santa Ynez fault on the Santa Barbara coast, and take d_{101}-spacing measurements from the same outcrops to test the effects fracture-related fluid- or heat-flow on opal-CT progression.

APPENDICES

APPENDIX A

X-RAY DIFFRACTION AND COMBINED ELECTRON SPECTROSCOPY/X-RAY FLUORESCENCE DATA TABLES

Major Oxides Measured by Combined EDX/XRF, in % Weight for Lower Sisquoc Formation.

Stratigraphic Depth (m)	Na_2O	MgO	Al_2O_3	SiO_2	P_2O_5	K_2O	CaO	TiO_2	MnO_2	Fe_2O_3
0	0.25	1.89	8.92	85.10	0.11	1.09	0.36	0.38	0.01	1.90
169	0.88	1.68	7.20	82.02	2.58	0.98	0.75	0.49	0.03	3.39
182	0.95	1.71	10.19	83.25	0.05	1.13	0.26	0.41	0.02	2.02
194	0.31	1.58	6.20	84.45	0.09	1.12	0.67	0.56	0.02	5.00
195	0.21	1.25	5.87	85.40	0.02	0.96	0.30	0.32	0.01	5.66
204	0.31	1.58	6.20	84.45	0.09	1.12	0.67	0.56	0.02	5.00
205	0.57	1.66	8.19	83.41	1.46	1.18	0.36	0.44	0.02	2.72
211	0.31	1.99	7.66	84.26	0.10	1.60	0.60	0.66	0.03	2.80
211	2.17	2.05	12.90	71.14	5.81	2.38	1.24	0.51	0.01	1.79
226	0.89	1.62	6.93	80.41	4.92	1.18	0.34	0.47	0.02	3.23

Major Oxides Measured by Combined EDX/XRF, in % Weight for Upper Monterey Formation.

Stratigraphic Depth (m)	Na_2O	MgO	Al_2O_3	SiO_2	P_2O_5	K_2O	CaO	TiO_2	MnO_2	Fe_2O_3
252	0.12	1.41	9.49	78.48	7.14	0.71	1.01	0.23	0.00	1.41
257	0.09	1.33	9.06	78.02	8.19	0.55	0.70	0.27	0.01	1.78
261	0.64	1.55	8.18	85.08	0.13	1.10	0.58	0.39	0.02	2.33
264	0.79	1.94	12.29	78.60	0.27	1.91	0.96	0.58	0.01	2.64
266	0.33	1.02	5.04	87.19	1.20	0.91	0.41	0.34	0.15	3.42
279	0.65	1.14	5.48	86.06	3.28	0.86	0.32	0.36	0.01	1.84
281	0.71	1.46	9.05	84.64	0.09	1.19	0.48	0.43	0.01	1.93
286	0.18	1.35	6.24	88.75	0.13	0.94	0.35	0.34	0.01	1.73
297	0.55	1.47	7.04	83.60	1.39	1.23	0.56	0.42	0.01	3.74
297	0.54	1.63	8.78	82.44	1.45	1.16	0.42	0.52	0.02	3.04
297	0.41	2.16	9.96	82.00	0.16	1.24	0.77	0.48	0.03	2.80
297	0.28	1.30	5.84	88.22	0.02	1.34	0.53	0.38	0.01	2.09
310	0.15	1.25	5.28	83.65	0.09	0.75	0.34	0.28	0.01	8.21
314	0.23	1.90	9.39	83.65	0.07	1.58	0.41	0.56	0.01	2.20
326	0.30	1.63	9.35	84.76	0.13	1.08	0.37	0.42	0.02	1.94
328	0.18	2.34	8.62	83.90	0.09	1.36	0.44	0.58	0.01	2.49
329	0.27	1.63	6.37	87.27	0.01	1.30	0.48	0.43	0.01	2.23
334	0.59	2.68	11.38	78.40	0.33	2.44	0.82	0.78	0.01	2.57
350	3.25	2.28	14.91	74.89	0.44	1.54	0.51	0.57	0.02	1.60
357	0.27	1.65	8.67	85.00	0.23	1.19	0.40	0.46	0.01	2.14
365	0.18	1.21	4.80	89.62	0.09	0.54	0.30	0.21	0.01	3.05
370	0.27	1.07	4.31	87.28	0.19	0.60	0.30	0.21	0.03	5.76
372	0.41	6.96	17.15	70.81	0.04	1.60	0.59	0.69	0.01	1.74
374	0.44	2.26	12.27	80.73	0.21	1.53	0.45	0.61	0.00	1.51
388	0.34	1.38	6.22	90.22	0.02	0.35	0.25	0.12	0.00	1.11
398	0.60	1.19	5.58	88.47	1.10	0.90	0.32	0.27	0.02	1.56
404	1.22	2.14	11.55	79.58	0.22	1.64	0.47	0.57	0.02	2.60
406	0.32	1.35	7.04	87.00	0.02	1.28	0.24	0.36	0.02	2.38
407	0.49	1.03	4.84	90.68	0.04	0.69	0.45	0.21	0.02	1.55
408	0.93	1.30	7.81	79.92	0.03	1.46	0.51	0.42	0.03	7.60
408	0.40	1.38	6.38	88.91	0.03	0.96	0.22	0.30	0.02	1.41
409	0.36	1.02	3.28	92.50	0.03	1.03	0.41	0.22	0.01	1.15
410	0.32	1.30	5.29	90.17	0.20	1.09	0.31	0.27	0.02	1.03
410	0.18	0.94	3.44	93.93	0.05	0.63	0.25	0.14	0.02	0.41
411	0.32	1.08	4.91	89.88	0.07	1.38	0.26	0.32	0.01	1.75
411	0.66	1.05	5.05	88.95	0.06	1.24	0.35	0.82	0.02	1.79

Major Oxides Measured by Combined EDX/XRF, in % Weight for Upper Monterey Formation Continued.

Stratigraphic Depth (m)	Na_2O	MgO	Al_2O_3	SiO_2	P_2O_5	K_2O	CaO	TiO_2	MnO_2	Fe_2O_3
411	0.29	1.04	4.15	91.26	0.57	0.95	0.30	0.24	0.01	1.20
411	0.30	0.93	3.23	93.16	0.07	0.69	0.28	0.20	0.01	1.13
419	0.15	1.12	5.14	90.06	0.19	1.41	0.34	0.43	0.01	1.16
419	2.80	1.67	6.27	86.17	0.02	1.73	0.46	0.12	0.02	0.75
422	0.55	2.20	9.24	82.66	0.15	1.87	0.74	0.57	0.01	2.01
422	1.06	1.28	17.37	76.34	0.51	1.56	0.50	0.34	0.01	1.04
423	0.26	1.02	4.12	92.11	0.24	0.76	0.38	0.16	0.01	0.94
426	0.46	1.08	5.54	89.25	0.26	1.01	0.41	0.32	0.01	1.66
430	0.32	1.12	5.82	88.20	0.13	2.02	0.54	0.51	0.01	1.34
430	2.49	1.61	12.48	78.68	0.67	1.47	0.60	0.40	0.00	1.61
430	0.36	1.27	5.29	89.37	0.16	1.38	0.32	0.36	0.01	1.48
430	0.34	0.97	5.30	91.53	0.05	0.77	0.23	0.29	0.01	0.51
430	0.35	1.12	7.46	85.35	0.93	1.69	0.99	0.39	0.00	1.71
434	0.41	1.45	7.24	86.68	0.03	1.79	0.49	0.66	0.02	1.23
434	0.45	1.23	5.22	89.55	0.03	1.24	0.37	0.30	0.02	1.60
434	0.28	0.80	2.49	94.98	0.03	0.44	0.27	0.10	0.00	0.61
440	0.29	0.95	3.40	94.25	0.10	0.40	0.17	0.06	0.00	0.38
442	5.44	0.91	17.11	71.38	0.07	2.08	0.67	0.45	0.00	1.90
442	0.85	1.17	6.87	87.55	0.04	1.55	0.42	0.50	0.01	1.06
442	0.65	1.32	8.14	86.79	0.10	1.10	0.42	0.33	0.01	1.15
442	0.48	1.26	5.54	90.19	0.03	0.88	0.24	0.27	0.01	1.11
443	0.27	1.12	3.99	91.82	0.04	0.65	0.24	0.38	0.02	1.48
445	0.21	1.11	4.16	92.61	0.06	0.62	0.33	0.23	0.01	0.66
450	0.38	1.32	6.16	86.01	0.18	1.79	0.23	0.40	0.02	3.51
450	0.79	1.57	4.79	90.08	0.01	1.01	0.34	0.27	0.02	1.12
450	0.83	1.05	4.71	89.98	0.05	1.14	0.19	0.34	0.02	1.71
450	0.36	1.09	4.38	91.88	0.05	0.53	0.20	0.21	0.02	1.29
450	2.74	1.17	5.58	88.48	0.07	0.60	0.22	0.23	0.00	0.91
450	0.45	1.28	5.93	88.41	0.04	0.81	0.21	1.21	0.01	1.66
450	0.60	1.15	5.26	89.23	0.56	0.86	0.25	0.30	0.01	1.76
450	1.10	0.81	4.42	85.85	6.05	0.61	0.15	0.19	0.01	0.79
450	1.08	1.27	7.02	84.99	1.47	1.02	0.20	0.34	0.02	2.60
450	0.87	1.06	4.59	86.08	2.66	1.03	0.19	0.76	0.02	2.74
450	0.63	1.01	5.06	90.52	1.11	0.54	0.19	0.23	0.01	0.71
450	0.64	0.95	5.53	81.67	3.13	2.04	0.19	0.33	0.01	5.51
451	0.53	0.86	3.05	91.79	2.69	0.34	0.16	0.13	0.01	0.43

Major Oxides Measured by Combined EDX/XRF, in % Weight for Upper Monterey Formation Continued.

Stratigraphic Depth (m)	Na_2O	MgO	Al_2O_3	SiO_2	P_2O_5	K_2O	CaO	TiO_2	MnO_2	Fe_2O_3
451	0.52	0.99	4.09	90.11	2.42	0.64	0.17	0.34	0.01	0.72
451	0.45	0.93	5.34	88.28	3.09	0.59	0.20	0.19	0.01	0.93
451	0.46	1.17	6.40	85.90	3.18	0.89	0.25	0.34	0.01	1.42
451	0.47	1.24	7.47	85.09	3.10	0.83	0.22	0.39	0.01	1.18
451	1.01	1.16	6.78	80.61	5.36	1.06	0.22	0.37	0.01	3.43
451	0.48	1.06	5.87	88.44	1.57	0.69	0.20	0.33	0.02	1.35
451	0.37	1.08	5.91	87.41	2.53	0.84	0.22	0.42	0.01	1.22
451	0.38	1.84	11.96	78.75	0.27	1.07	0.21	3.69	0.02	1.82
451	0.45	1.58	7.69	84.55	0.05	3.18	0.26	0.53	0.01	1.70
451	0.33	1.22	4.94	90.57	0.03	1.35	0.22	0.38	0.01	0.97
460	0.28	1.00	4.68	91.97	0.14	0.60	0.17	0.24	0.01	0.92
460	0.44	1.11	4.81	91.95	0.05	0.60	0.18	0.22	0.01	0.65
460	0.55	1.02	4.42	93.03	0.03	0.31	0.13	0.08	0.01	0.43
460	0.51	0.91	4.33	93.04	0.05	0.36	0.13	0.13	0.01	0.53
469	0.24	1.19	4.93	91.20	0.03	1.69	0.34	0.14	0.01	0.24
469	0.77	1.13	4.64	91.09	0.02	0.87	0.19	0.27	0.01	1.02
470	0.29	1.16	7.43	86.78	1.07	1.21	0.29	0.34	0.01	1.44
470	3.76	0.86	10.53	79.70	1.41	0.94	0.22	0.42	0.01	2.15
472	0.32	1.02	3.67	91.08	0.03	1.31	0.27	0.30	0.02	2.00
473	0.39	1.71	8.51	81.87	0.07	0.96	0.26	0.43	0.02	5.78
474	0.85	1.38	8.13	85.99	0.08	1.20	0.24	0.60	0.01	1.52
474	0.73	1.02	5.52	90.76	0.02	0.80	0.22	0.21	0.01	0.71
476	0.17	1.26	4.58	91.56	0.04	0.65	0.27	0.27	0.02	1.18
477	0.42	1.11	4.95	86.24	3.42	0.70	0.20	0.35	0.02	2.58
478	0.87	0.96	5.41	86.93	3.34	1.00	0.19	0.34	0.01	0.96
478	0.62	1.87	7.72	86.17	0.77	1.03	0.21	0.53	0.01	1.07
479	0.78	1.32	6.38	84.42	3.92	0.78	0.20	0.39	0.02	1.80
479	0.40	1.02	4.58	88.11	2.44	0.96	0.18	0.38	0.02	1.93
481	0.30	0.70	2.74	93.84	0.95	0.34	0.17	0.16	0.01	0.79
481	0.23	0.92	3.35	90.84	1.93	0.86	0.25	0.23	0.01	1.38
483	0.20	1.27	5.33	89.95	0.05	0.92	0.23	0.32	0.01	1.71
484	0.18	1.11	4.49	91.06	0.44	0.49	0.23	0.24	0.01	1.76
485	0.24	0.90	1.94	96.27	0.02	0.07	0.18	0.02	0.00	0.38
486	0.18	1.77	9.52	83.59	0.04	1.75	0.26	0.58	0.02	2.30
486	0.23	1.12	3.97	91.49	0.10	0.59	0.44	0.24	0.02	1.79
487	0.20	1.21	4.70	90.98	0.07	0.61	0.25	0.26	0.01	1.72
487	0.27	1.32	4.62	91.17	0.13	0.55	0.24	0.24	0.01	1.46

Major Oxides Measured by Combined EDX/XRF, in % Weight for Upper Monterey Formation Continued.

Stratigraphic Depth (m)	Na_2O	MgO	Al_2O_3	SiO_2	P_2O_5	K_2O	CaO	TiO_2	MnO_2	Fe_2O_3
488	0.21	1.14	4.78	91.76	0.07	0.51	0.16	0.18	0.01	1.19
490	0.55	0.90	3.79	91.06	1.46	0.46	0.44	0.19	0.01	1.14
490	0.73	0.78	2.73	91.41	2.76	0.31	0.52	0.13	0.00	0.64
490	0.86	1.98	13.04	76.29	2.14	1.17	0.47	0.59	0.02	3.45
490	0.50	2.06	8.02	83.37	4.00	0.33	0.76	0.10	0.01	0.87
491	0.22	1.08	4.86	92.59	0.01	0.32	0.17	0.08	0.01	0.67
491	0.26	1.89	10.61	83.55	0.05	1.46	0.19	0.52	0.01	1.48
491	0.34	1.17	7.30	88.80	0.06	0.91	0.16	0.26	0.01	1.00
491	0.82	1.46	4.66	87.95	2.50	0.38	0.42	0.18	0.03	1.60
493	0.23	1.03	3.56	92.28	0.11	0.44	0.24	0.14	0.01	1.96
493	0.20	0.84	2.05	95.99	0.08	0.11	0.29	0.00	0.00	0.43
493	0.22	0.97	3.06	93.93	0.06	0.29	0.25	0.07	0.01	1.13
493	0.59	0.64	3.09	91.80	2.58	0.26	0.19	0.39	0.00	0.46
493	0.37	0.87	3.69	89.90	2.84	0.45	0.20	0.19	0.01	1.49
494	0.67	1.37	6.22	87.87	0.03	1.13	0.22	0.41	0.02	2.07
494	0.36	1.72	9.48	82.10	0.06	1.86	0.22	0.62	0.02	3.56

Major Oxides Measured by Combined EDX/XRF, in % Weight for Middle Monterey Formation.

Stratigraphic Depth (m)	Na_2O	MgO	Al_2O_3	SiO_2	P_2O_5	K_2O	CaO	TiO_2	MnO_2	Fe_2O_3
503	0.51	1.17	16.40	26.01	29.79	0.26	24.67	0.23	0.01	0.95
504	0.59	1.60	7.37	84.98	0.13	1.15	0.41	0.47	0.00	3.31
504	0.60	0.99	4.64	88.32	1.37	0.64	0.61	0.56	0.01	2.26
504	0.40	1.60	6.91	84.91	0.09	1.41	0.88	0.39	0.01	3.42
504	0.24	0.86	1.95	96.05	0.00	0.05	0.28	0.29	0.00	0.29
504	0.26	1.64	7.07	86.35	0.13	1.76	0.39	0.42	0.01	1.97
504	0.33	1.17	4.53	89.80	0.02	0.63	0.24	0.20	0.01	3.09
509	0.27	0.91	2.46	69.41	0.66	0.36	25.21	0.05	0.00	0.68
509	0.83	1.07	2.90	93.63	0.03	0.19	0.36	0.14	0.01	0.84
512	0.52	1.66	9.52	80.34	0.78	1.64	0.37	0.61	0.02	4.53
512	0.60	1.48	6.25	88.56	0.15	0.89	0.24	0.35	0.01	1.47
512	1.03	1.68	8.07	84.43	0.17	1.76	0.28	0.49	0.03	2.06
512	0.22	1.02	3.08	93.73	0.01	0.49	0.26	0.14	0.01	1.04
512	0.18	0.83	2.61	95.57	0.03	0.18	0.24	0.03	0.00	0.33
512	0.17	0.78	2.84	95.28	0.04	0.11	0.29	0.01	0.00	0.48
512	0.04	0.38	2.99	95.67	0.00	0.10	0.09	0.09	0.00	0.64
512	0.18	0.91	5.18	92.18	0.30	0.21	0.24	0.06	0.00	0.74
512	0.18	0.87	2.76	93.34	0.01	0.37	0.38	0.18	0.01	1.88
512	0.53	0.90	3.56	90.16	3.40	0.30	0.25	0.14	0.00	0.76
512	0.18	0.90	2.55	94.79	0.02	0.32	0.27	0.07	0.00	0.90
514	0.23	0.91	3.55	92.81	0.05	0.50	0.26	0.21	0.01	1.47
514	1.18	0.91	5.27	89.70	0.08	0.26	0.22	0.14	0.01	2.25
515	0.20	1.25	6.34	90.04	0.03	0.52	0.15	0.21	0.01	1.26
518	0.31	1.01	3.47	92.80	0.18	0.38	0.32	0.21	0.01	1.32
518	0.32	1.15	4.33	89.91	0.47	0.51	0.37	0.29	0.02	2.64
519	0.33	0.92	4.81	92.77	0.26	0.22	0.19	0.04	0.00	0.45
520	0.79	1.67	6.60	86.41	0.08	1.10	0.60	0.44	0.03	2.29
521	0.39	1.07	4.27	90.38	0.65	0.45	0.38	0.20	0.01	2.22
522	0.34	0.62	1.98	88.79	1.62	0.18	5.43	0.09	0.01	0.95
523	0.27	0.69	2.33	94.76	0.00	0.28	0.40	0.13	0.01	1.14
524	0.29	0.74	2.54	93.01	0.41	0.19	1.96	0.09	0.01	0.76
524	0.46	0.85	3.58	87.81	1.46	0.40	3.01	0.22	0.02	2.20
524	0.46	1.27	5.00	81.46	2.40	0.94	5.23	0.30	0.03	2.93
527	0.40	2.43	3.22	82.80	0.18	0.78	8.07	0.29	0.03	1.79
528	0.46	1.47	4.52	92.44	0.11	0.13	0.28	0.08	0.01	0.50
530	0.80	1.13	6.94	87.49	0.02	1.53	0.29	0.45	0.01	1.35

Major Oxides Measured by Combined EDX/XRF, in % Weight for Lower Monterey Formation.

Stratigraphic Depth (m)	Na_2O	MgO	Al_2O_3	SiO_2	P_2O_5	K_2O	CaO	TiO_2	MnO_2	Fe_2O_3
532	0.49	0.67	2.36	73.56	3.39	0.37	17.58	0.13	0.01	1.45
533	0.66	1.33	3.89	88.43	0.54	0.30	3.07	0.16	0.01	1.61
533	0.40	1.33	5.77	78.19	6.21	1.57	2.09	0.49	0.01	3.95
536	0.74	0.93	3.11	81.26	4.11	0.50	6.56	0.34	0.01	2.44
536	0.51	0.78	3.10	87.12	1.97	0.38	4.39	0.17	0.01	1.58
537	0.48	1.31	5.77	87.49	0.19	0.99	0.56	0.37	0.01	2.83
538	0.38	0.84	2.77	92.05	1.17	0.13	1.90	0.05	0.01	0.72
538	0.35	0.68	2.22	91.49	1.86	0.20	1.47	0.14	0.02	1.59
539	0.25	2.35	1.39	60.11	0.31	0.15	34.74	0.02	0.04	0.63
540	0.23	0.75	2.10	96.10	0.04	0.10	0.20	0.00	0.00	0.48
540	0.24	0.88	2.16	74.88	2.50	0.24	18.45	0.03	0.00	0.63
543	0.24	0.72	1.51	67.42	0.61	0.20	28.80	0.01	0.01	0.48
547	0.60	1.35	5.80	66.53	5.41	1.24	15.65	0.43	0.01	2.98
549	0.33	0.77	1.61	74.16	0.48	0.15	21.83	0.02	0.01	0.66
553	0.33	0.85	1.94	72.18	1.72	0.26	22.17	0.02	0.00	0.53
554	0.24	0.74	1.75	71.38	2.21	0.10	23.06	0.02	0.00	0.50
555	1.40	0.79	3.51	55.58	4.13	0.29	33.62	0.05	0.01	0.63
560	0.23	0.80	1.82	48.10	5.76	0.48	42.03	0.10	0.01	0.68
576	0.65	0.74	2.83	84.43	5.38	0.60	3.14	0.21	0.01	1.99
586	0.68	0.88	3.34	67.93	0.92	0.43	24.57	0.17	0.00	1.08
591	0.50	0.68	1.56	91.06	1.83	0.21	3.21	0.06	0.02	0.88
597	0.74	0.89	3.38	86.28	3.34	0.58	3.09	0.27	0.02	1.42
619	0.61	0.85	2.63	80.08	3.74	0.52	8.50	0.21	0.01	2.85
626	0.70	0.86	3.11	82.89	6.35	0.68	3.81	0.30	0.02	1.28
640	0.29	3.79	4.97	73.01	0.76	1.75	12.51	0.32	0.02	2.58
647	0.50	0.92	5.84	81.08	6.10	0.89	0.84	0.38	0.01	3.44
652	0.35	0.75	2.81	92.51	1.21	0.27	0.28	0.10	0.01	1.70
660	0.43	0.83	3.10	88.98	0.59	0.59	3.20	0.29	0.02	1.98
660	0.60	1.19	5.79	86.14	0.35	0.65	2.91	0.24	0.06	2.08
664	0.39	1.67	9.83	79.27	0.27	1.79	0.37	0.62	0.02	5.78
665	0.47	1.41	6.81	87.77	0.27	0.50	0.25	0.27	0.01	2.25
667	0.52	1.15	5.82	87.32	0.47	0.98	0.34	0.41	0.01	2.97
669	0.74	0.91	4.12	82.34	1.21	1.86	8.11	0.21	0.04	0.46
671	0.60	0.93	4.13	89.44	0.13	0.52	2.11	0.22	0.01	1.91
675	0.98	1.25	5.28	87.59	0.15	0.70	1.22	0.22	0.01	2.60
675	0.70	1.03	1.03	86.41	0.85	0.91	2.11	0.38	0.02	2.81
675	1.13	1.96	7.58	75.30	1.66	1.74	2.68	1.18	0.46	6.32
678	2.44	2.14	10.80	81.18	0.04	1.08	0.40	0.41	0.01	1.49
679	0.48	1.04	4.19	89.27	0.89	0.64	1.42	0.27	0.01	1.81
680	1.33	1.93	8.28	79.07	0.46	1.71	1.75	0.53	0.01	4.94
680	0.45	1.19	5.63	89.23	0.43	0.70	0.28	0.29	0.01	1.79
683	0.40	0.84	3.27	90.51	0.39	0.37	2.06	0.16	0.01	1.99

Sedimentary Components Measured by Combined EDX/XRF in % Weight and Opal-CT d_{101}-spacing Measured by XRD in Angstroms (Å) for Lower Sisquoc Formation.

Stratigraphic Depth (m)	Raw Detritus	Raw Silica (biogenic & diagenetic)	Raw Calcite	Normalized Silica	opal-CT d_{101}-spacing (Å)
0	49.97	53.86	0.51	51.87	4.05
169	40.33	56.82	-0.45	58.49	4.04
182	57.08	47.57	-1.33	45.46	4.07
194	34.74	62.74	0.75	64.36	4.07
195	32.86	64.86	0.34	66.37	4.08
204	34.74	62.74	0.75	64.36	4.07
205	45.84	54.76	-0.33	54.43	4.06
211	42.92	57.44	0.72	57.23	4.05
211	72.23	26.00	-2.45	26.47	4.05
226	38.80	56.16	-1.21	59.14	4.06

Sedimentary Components Measured by Combined EDX/XRF in % Weight and Opal-CT d_{101}-spacing Measured by XRD in Angstroms (Å) for Upper Monterey Formation.

Stratigraphic Depth (m)	Raw Detritus	Raw Silica (biogenic & diagenetic)	Raw Calcite	Normalized Silica	opal-CT d_{101}-spacing (Å)
252	53.13	45.28	2.01	46.01	4.00
257	50.72	46.32	1.53	47.73	4.07
261	45.82	56.44	-0.09	55.19	4.09
264	68.84	35.58	0.43	34.07	4.00
266	28.23	69.54	0.20	71.13	4.08
279	30.67	66.89	-0.75	68.56	4.09
281	50.69	52.96	-0.41	51.09	4.04
286	34.94	66.91	0.52	65.69	4.05
297	39.41	58.97	0.03	59.94	4.09
297	49.19	51.69	-0.10	51.24	4.06
297	55.79	47.13	0.91	45.79	4.04
297	32.69	67.79	0.56	67.47	4.09
310	29.57	65.17	0.54	68.79	4.09
314	52.60	50.78	0.68	49.12	4.10
326	52.38	52.02	0.44	49.83	4.07
328	48.25	53.74	0.83	52.69	4.06
329	35.66	64.98	0.53	64.57	4.09
334	63.73	38.57	0.62	37.70	4.07
350	83.51	22.70	-6.33	21.37	4.06
357	48.52	54.67	0.53	52.98	4.05
365	26.87	72.83	0.36	73.04	4.09
370	24.11	72.21	0.09	74.97	4.08
372	96.04	10.79	0.98	10.10	4.07
374	68.68	37.81	0.41	35.50	4.04
388	34.82	68.46	-0.03	66.28	4.06
398	31.27	68.93	-0.59	68.79	4.06
404	64.66	39.16	-1.53	37.72	4.08
406	39.41	62.37	0.03	61.28	4.07
407	27.11	73.74	-0.15	73.12	4.05
408	43.74	52.58	-0.97	54.59	4.04
408	35.73	66.58	-0.25	65.08	4.08
409	18.35	81.03	0.03	81.54	4.10
410	29.64	71.65	0.04	70.74	4.08
410	19.26	81.89	0.20	80.96	4.04
411	27.52	72.68	-0.06	72.54	4.09
411	28.29	71.26	-0.74	71.58	4.09

Sedimentary Components Measured by Combined EDX/XRF in % Weight and Opal-CT d_{101}-spacing Measured by XRD in Angstroms (Å) for Upper Monterey Formation Continued.

Stratigraphic Depth (m)	Raw Detritus	Raw Silica (biogenic & diagenetic)	Raw Calcite	Normalized Silica	opal-CT d_{101}-spacing (Å)
411	23.21	76.76	0.03	76.78	4.10
411	18.10	81.85	-0.06	81.89	4.08
419	28.77	72.08	0.52	71.47	4.09
419	35.12	64.22	-5.79	64.65	4.07
422	51.74	50.32	0.47	49.31	4.06
422	97.27	15.54	-0.77	13.78	4.07
423	23.06	77.70	0.26	77.11	4.07
426	31.00	69.88	-0.11	69.27	4.05
430	32.58	67.84	0.50	67.56	4.06
430	69.87	35.01	-4.43	33.38	4.00
430	29.60	70.87	-0.04	70.54	4.05
430	29.69	72.98	-0.13	71.08	4.07
430	41.79	59.23	1.30	58.63	4.00
434	40.54	61.34	0.26	60.21	4.06
434	29.24	71.27	-0.17	70.91	4.09
434	13.95	86.27	-0.07	86.08	4.09
440	19.06	82.34	-0.22	81.20	4.07
442	95.84	11.48	-11.36	10.69	4.11
442	38.46	63.51	-0.97	62.29	4.04
442	45.58	58.30	-0.40	56.12	4.06
442	31.01	70.81	-0.46	69.54	4.09
443	22.35	77.85	-0.01	77.70	4.08
445	23.29	78.05	0.31	77.02	4.09
450	34.51	64.44	-0.18	65.13	4.07
450	26.84	73.31	-1.09	73.20	4.08
450	26.36	73.51	-1.45	73.61	4.07
450	24.52	76.56	-0.28	75.74	4.06
450	31.25	68.95	-6.10	68.81	4.07
450	33.23	67.64	-0.40	67.06	4.10
450	29.47	70.81	-0.75	70.61	4.06
450	24.77	70.37	-2.22	73.96	4.08
450	39.31	60.42	-1.92	60.58	4.09
450	25.71	70.01	-1.58	73.14	4.05
450	28.32	72.82	-0.93	72.00	4.08
450	30.98	62.31	-0.94	66.79	4.06
451	17.09	81.11	-0.85	82.60	4.08

Sedimentary Components Measured by Combined EDX/XRF in % Weight and Opal-CT d_{101}-spacing Measured by XRD in Angstroms (Å) for Upper Monterey Formation Continued.

Stratigraphic Depth (m)	Raw Detritus	Raw Silica (biogenic & diagenetic)	Raw Calcite	Normalized Silica	opal-CT d_{101}-spacing (Å)
451	22.90	75.80	-0.75	76.80	4.07
451	29.92	69.58	-0.45	69.93	4.08
451	35.81	63.51	-0.33	63.94	4.07
451	41.83	58.95	-0.38	58.49	4.10
451	37.95	56.89	-1.72	59.98	4.05
451	32.87	67.89	-0.52	67.38	4.05
451	33.08	66.74	-0.19	66.86	4.07
451	66.99	36.87	0.09	35.50	4.05
451	43.07	57.63	-0.24	57.23	4.09
451	27.64	73.29	-0.16	72.62	4.09
460	26.18	75.61	-0.14	74.28	4.08
460	26.95	75.10	-0.50	73.59	4.08
460	24.74	77.57	-0.88	75.82	4.07
460	24.25	77.88	-0.80	76.26	4.06
469	27.61	73.95	0.29	72.81	4.07
469	25.99	74.84	-1.32	74.22	4.08
470	41.61	60.77	0.20	59.36	4.06
470	58.96	42.84	-8.34	42.08	4.08
472	20.55	78.23	-0.11	79.19	4.05
473	47.63	52.10	-0.02	52.24	4.08
474	45.50	57.55	-1.23	55.85	4.00
474	30.90	71.45	-1.12	69.81	4.06
476	25.67	75.52	0.32	74.63	4.08
477	27.73	68.91	-0.42	71.31	4.07
478	30.30	67.99	-1.52	69.18	4.07
478	43.21	59.16	-0.74	57.79	4.07
479	35.72	62.09	-1.21	63.48	4.07
479	25.63	72.10	-0.41	73.78	4.06
481	15.32	84.27	-0.28	84.62	4.07
481	18.77	79.11	0.07	80.82	4.07
483	29.85	71.30	0.21	70.49	4.07
484	25.14	75.34	0.22	74.98	4.08
485	10.84	89.49	-0.16	89.20	4.05
486	53.32	50.27	0.56	48.53	4.06
486	22.22	77.60	0.43	77.74	4.08
487	26.33	74.52	0.21	73.89	4.09
487	25.87	75.01	0.02	74.36	4.06

Sedimentary Components Measured by Combined EDX/XRF in % Weight and Opal-CT d_{101}-spacing Measured by XRD in Angstroms (Å) for Upper Monterey Formation Continued.

Stratigraphic Depth (m)	Raw Detritus	Raw Silica (biogenic & diagenetic)	Raw Calcite	Normalized Silica	opal-CT d_{101}-spacing (Å)
488	26.76	75.03	0.04	73.71	4.07
490	21.24	77.79	-0.37	78.56	4.10
490	15.28	81.86	-0.73	84.27	4.07
490	73.01	30.66	-0.58	29.57	4.08
490	44.91	55.30	0.56	55.19	4.09
491	27.23	75.57	0.02	73.51	4.04
491	59.39	46.43	0.30	43.87	4.04
491	40.87	63.25	-0.16	60.75	4.07
491	26.12	71.62	-1.03	73.28	4.08
493	19.92	79.83	0.05	80.03	4.10
493	11.50	88.81	0.13	88.54	4.08
493	17.11	83.24	0.07	82.95	4.07
493	17.30	80.99	-0.96	82.40	4.05
493	20.65	76.99	-0.35	78.85	4.09
494	34.82	66.11	-0.93	65.50	4.08
494	53.07	48.94	0.02	47.98	4.05

Sedimentary Components Measured by Combined EDX/XRF in % Weight and Opal-CT d_{101}-spacing Measured by XRD in Angstroms (Å) for Middle Monterey Formation.

Stratigraphic Depth (m)	Raw Detritus	Raw Silica (biogenic & diagenetic)	Raw Calcite	Normalized Silica	opal-CT d_{101}-spacing (Å)
503	91.85	-31.40	43.69	-51.94	4.00
504	41.26	59.20	-0.33	58.93	4.08
504	25.97	72.09	-0.14	73.51	4.08
504	38.67	60.74	0.95	61.10	4.00
504	10.90	89.23	0.01	89.11	4.00
504	39.61	61.60	0.43	60.86	4.07
504	25.34	73.96	-0.14	74.48	4.07
509	13.78	60.80	44.47	81.53	4.07
509	16.23	83.48	-1.25	83.72	4.08
512	53.32	47.02	-0.10	46.86	4.06
512	35.02	66.67	-0.73	65.56	4.08
512	45.19	56.19	-1.60	55.43	4.07
512	17.25	82.94	0.09	82.78	4.10
512	14.62	86.43	0.14	85.53	4.07
512	15.90	85.34	0.26	84.29	4.06
512	16.73	85.22	0.23	83.59	4.09
512	28.99	74.06	0.27	71.87	4.09
512	15.44	83.69	0.39	84.43	4.08
512	19.93	77.70	-0.67	79.59	4.10
512	14.25	85.88	0.17	85.77	4.10
514	19.87	80.40	0.09	80.18	4.10
514	29.50	71.26	-2.23	70.72	4.08
515	35.48	67.86	0.12	65.67	4.09
518	19.40	80.67	-0.01	80.61	4.10
518	24.26	74.74	0.12	75.50	4.06
519	26.95	75.92	-0.21	73.80	4.00
520	36.97	63.30	-0.54	63.13	4.07
521	23.89	75.45	-0.05	75.95	4.06
522	11.08	81.86	8.95	88.08	4.08
523	13.02	86.62	0.18	86.93	4.08
524	14.24	84.12	2.91	85.53	4.06
524	20.05	75.28	4.45	78.97	4.08
524	27.98	63.97	8.48	69.57	4.05
527	18.03	71.53	13.58	79.87	4.05
528	25.33	76.61	-0.39	75.15	4.10
530	38.86	63.20	-1.09	61.92	4.00

Sedimentary Components Measured by Combined EDX/XRF in % Weight and Opal-CT d_{101}-spacing Measured by XRD in Angstroms (Å) for Lower Monterey Formation.

Stratigraphic Depth (m)	Raw Detritus	Raw Silica (biogenic & diagenetic)	Raw Calcite	Normalized Silica	opal-CT d_{101}-spacing (Å)
532	13.21	65.30	30.30	83.17	4.07
533	21.78	74.82	4.08	77.45	4.07
533	32.31	57.99	3.08	64.22	4.06
536	17.42	70.37	10.06	80.16	4.07
536	17.36	76.27	6.75	81.46	4.08
537	32.33	67.29	0.15	67.54	4.00
538	15.53	82.34	2.62	84.13	4.09
538	12.43	83.72	1.88	87.07	4.07
539	7.80	55.24	61.49	87.63	4.07
540	11.77	88.74	-0.10	88.29	4.10
540	12.10	67.32	32.47	84.77	4.09
543	8.46	62.13	50.91	88.01	4.08
547	32.49	46.22	26.78	58.73	4.06
549	9.02	68.52	38.25	88.36	4.09
553	10.89	65.38	38.88	85.72	4.09
554	9.79	65.26	40.67	86.96	4.08
555	19.63	43.31	56.75	68.81	4.07
560	10.19	41.73	74.59	80.37	4.06
576	15.86	74.52	4.14	82.45	4.08
586	18.70	56.24	42.35	75.04	4.06
591	8.74	85.60	4.58	90.74	4.07
597	18.94	74.44	3.88	79.71	4.07
619	14.73	70.87	13.81	82.79	4.07
626	17.39	72.02	5.24	80.55	4.05
640	27.83	55.61	21.90	66.65	4.00
647	32.70	60.64	0.59	64.97	4.08
652	15.71	82.69	-0.20	84.04	4.08
660	17.35	78.13	4.81	81.82	4.05
660	32.44	65.87	4.04	67.00	4.05
664	55.03	44.88	0.24	44.92	4.00
665	38.11	63.95	-0.34	62.66	4.04
667	32.59	66.96	-0.35	67.26	4.06
669	23.07	67.93	12.87	74.65	4.06
671	23.15	74.97	2.49	76.41	4.04
675	29.57	69.10	0.05	70.03	4.06
675	5.75	82.82	2.09	93.51	4.04
675	42.43	48.78	2.41	53.48	4.05

Sedimentary Components Measured by Combined EDX/XRF in % Weight and Opal-CT d_{101}-spacing Measured by XRD in Angstroms (Å) for Lower Monterey Formation Continued.

Stratigraphic Depth (m)	Raw Detritus	Raw Silica (biogenic & diagenetic)	Raw Calcite	Normalized Silica	opal-CT d_{101}-spacing (Å)
679	23.48	74.59	1.59	76.06	4.04
680	46.35	50.11	0.29	51.95	4.00
680	31.54	69.52	-0.29	68.79	4.06
683	18.31	79.07	2.86	81.20	4.06

APPENDIX B

COMBINED ELECTRON SPECTROSCOPY/X-RAY FLUORESCENCE METHOD

This section explains in detail the calibration process of the combined EDS/XRF method using IXRF Iridium Ultra Software and FEI Quanta 200 scanning electron microscope (SEM).

Setup instrument and warm-up

- Make sure the detector is cooled with liquid nitrogen and has time to cool (~ 4 hours prior to operation)
- Start up FEI xT microscope control
- Turn on iXRF Model 550i control box
- Open Iridium Ultra software

Load sample of crushed and pressed standard (USGS or other certified standard)

- Vent sample chamber to release vacuum
  - When vented, place sample pellet on vitreous carbon planchet, then place inside chamber
  - Pump the chamber to high vacuum

Sample adjustment

- Once the chamber is under vacuum, activate the High Voltage (HV)
  - Zoom in on the sample to about 4000x – 5000x magnification, focus and fix Z to sample
  - Adjust coordinate Z until it is 10mm (this is the depth or distance of the surface of the sample from the detector)
- This is good time to warm up the IXRF Systems X-Beam Controller
  - Turn the key to position 1 and press the x-ray button, but do not open the shutter yet!!

Least Squares Calibration

Using Iridium Ultra Software

- Open a new combined SEM/XRF spectrum
  - Adjust spot size on the xT microscope control until the dead time is ~27-30% in the green zone

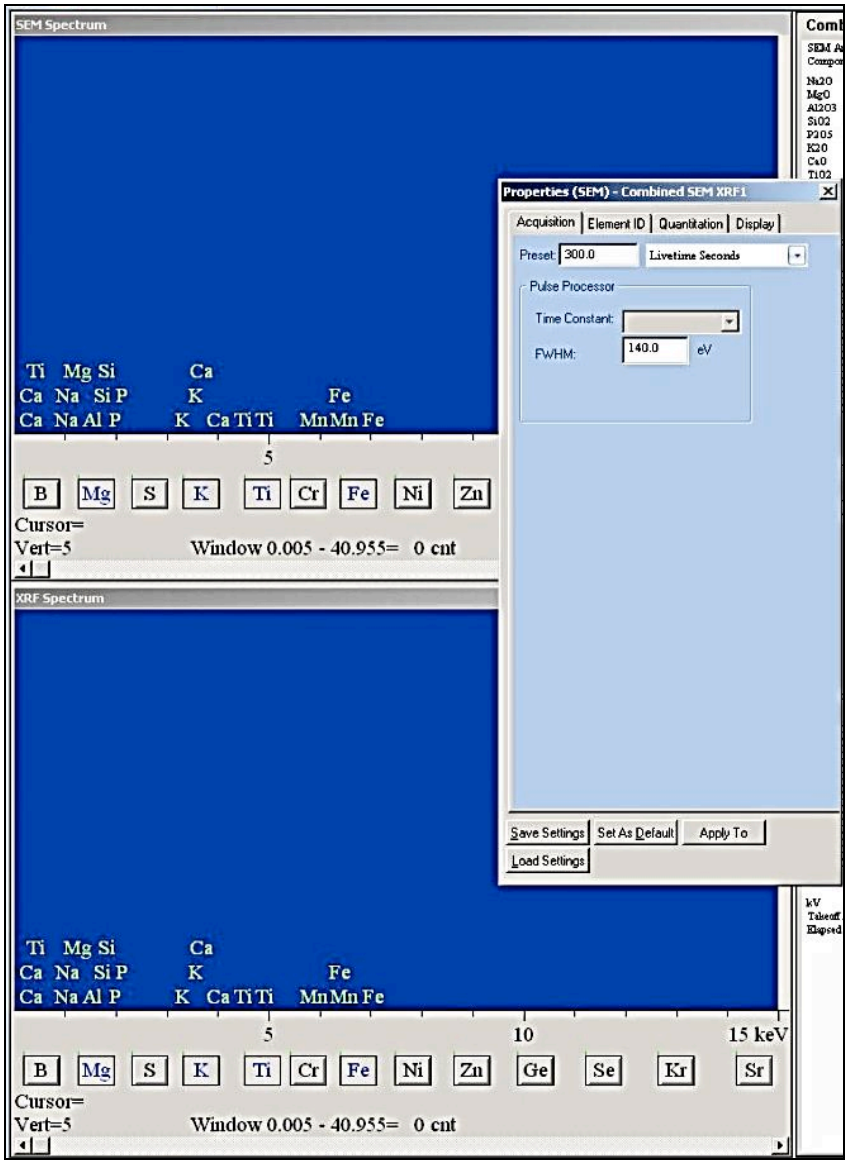

Right click on the SEM spectrum window (upper window).

- Select properties
- Click on Acquisition tab
- Enter 300.0 in preset for livetime seconds

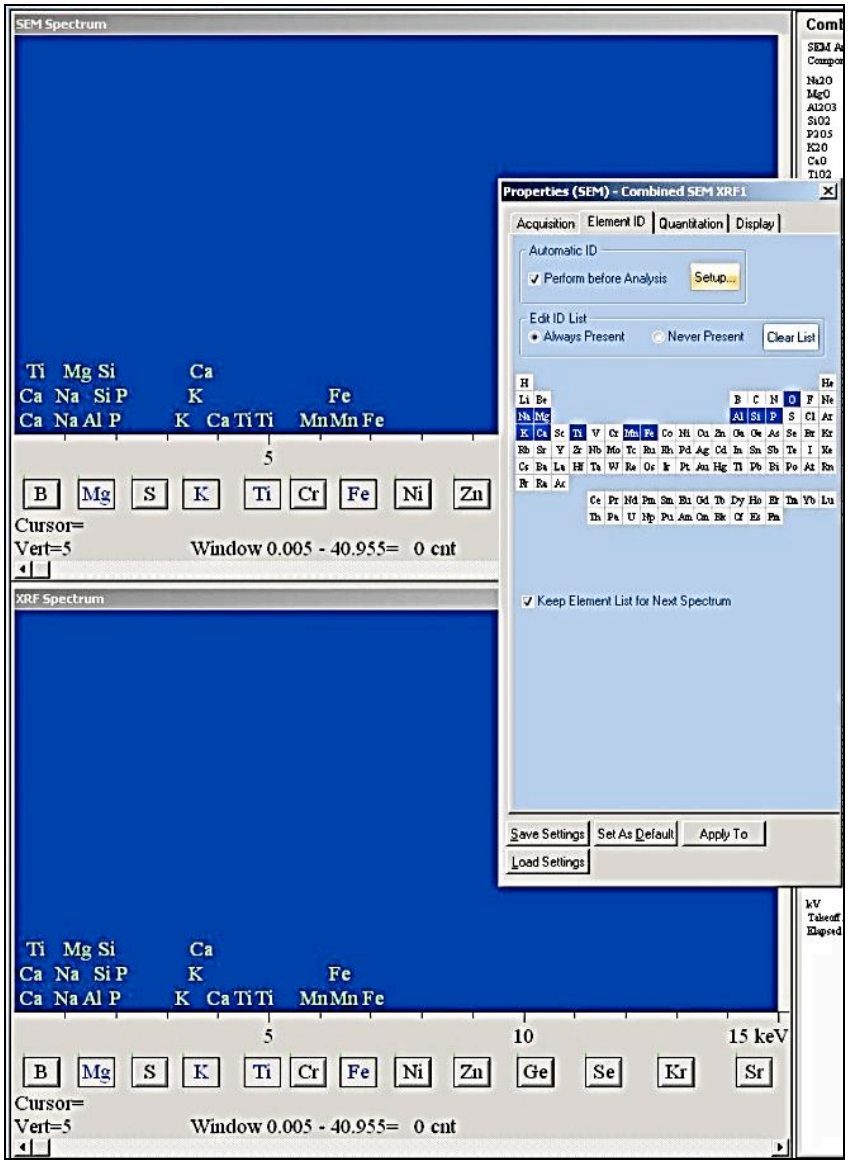

Click on Element ID tab

- Select desired elements on the periodic table

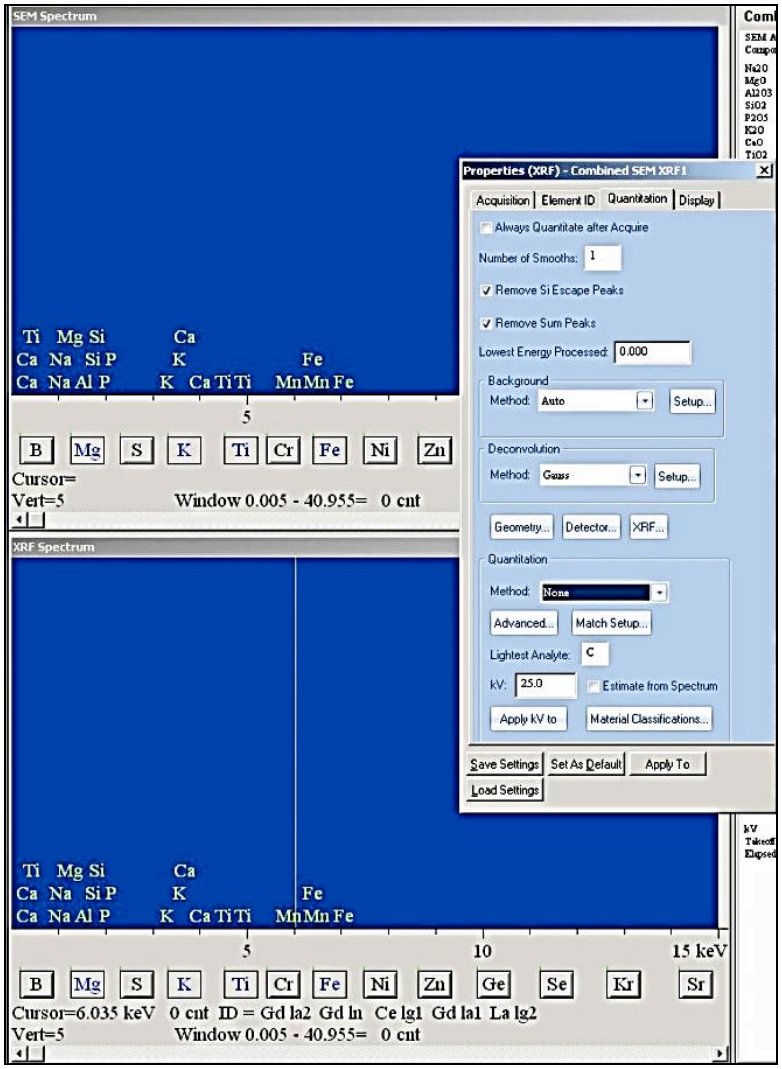

Click on Quantitation tab

- Choose none as the method
- Enter 25 as kv
- Then close

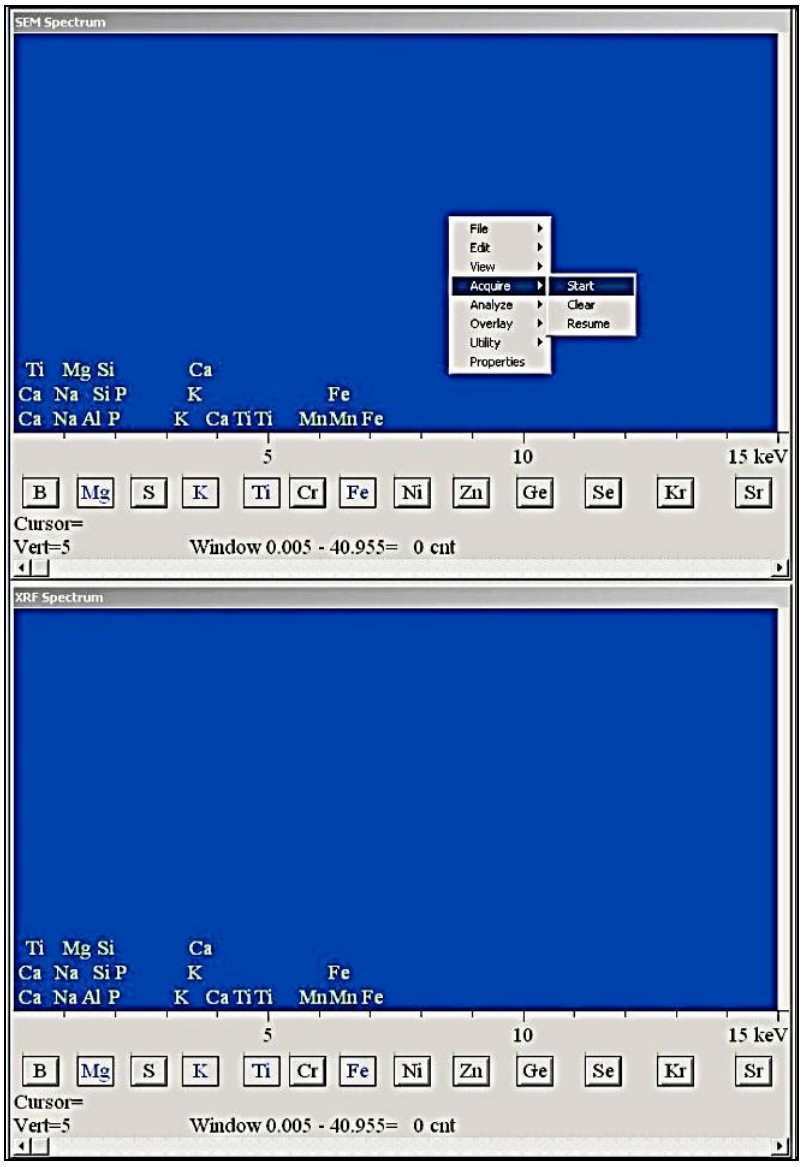

Right click on SEM spectrum window

- Select Acquire
- Click start

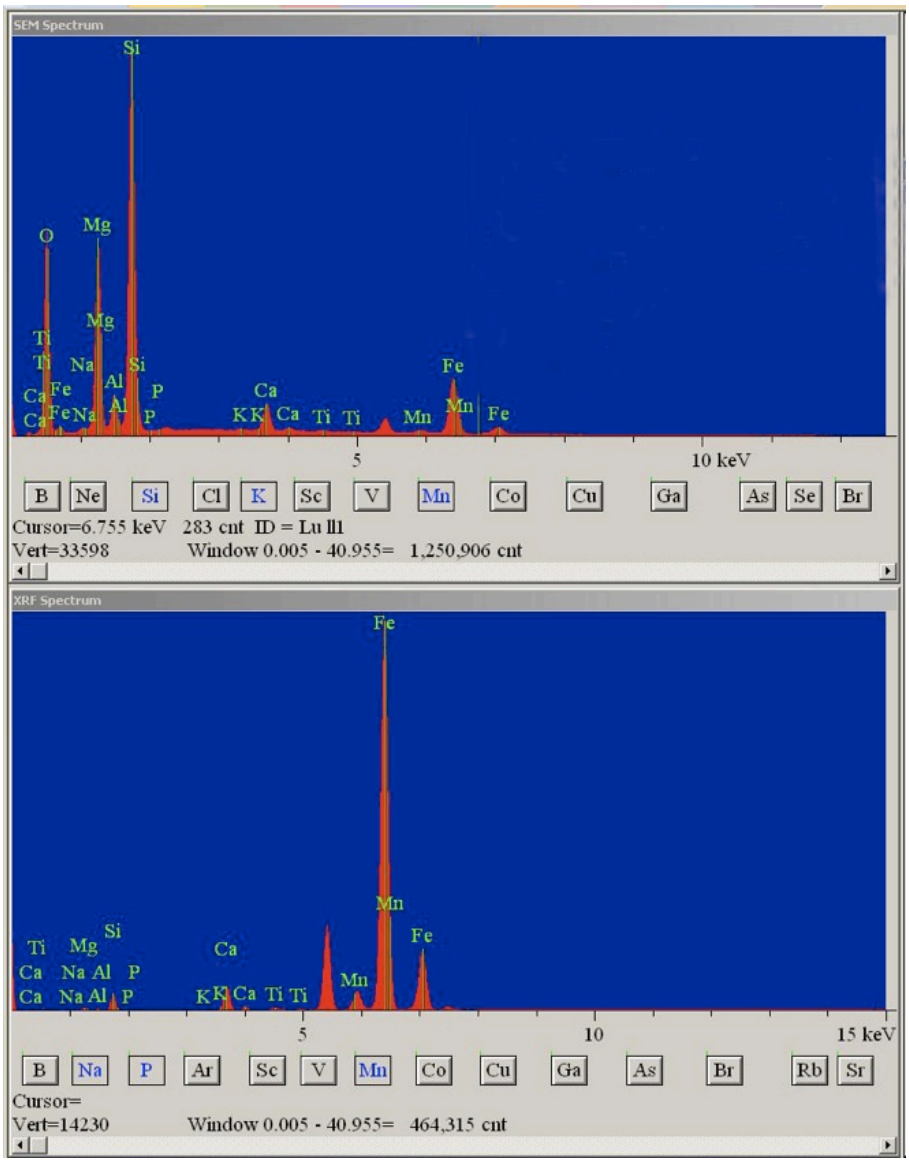

After the acquisition is complete

- Turn off the HV and make sure all windows are paused (CCTV)
- Activate and open the X-ray shutter
- Right click the XRF spectrum window
    - Follow same steps for properties as was done for SEM spectrum window

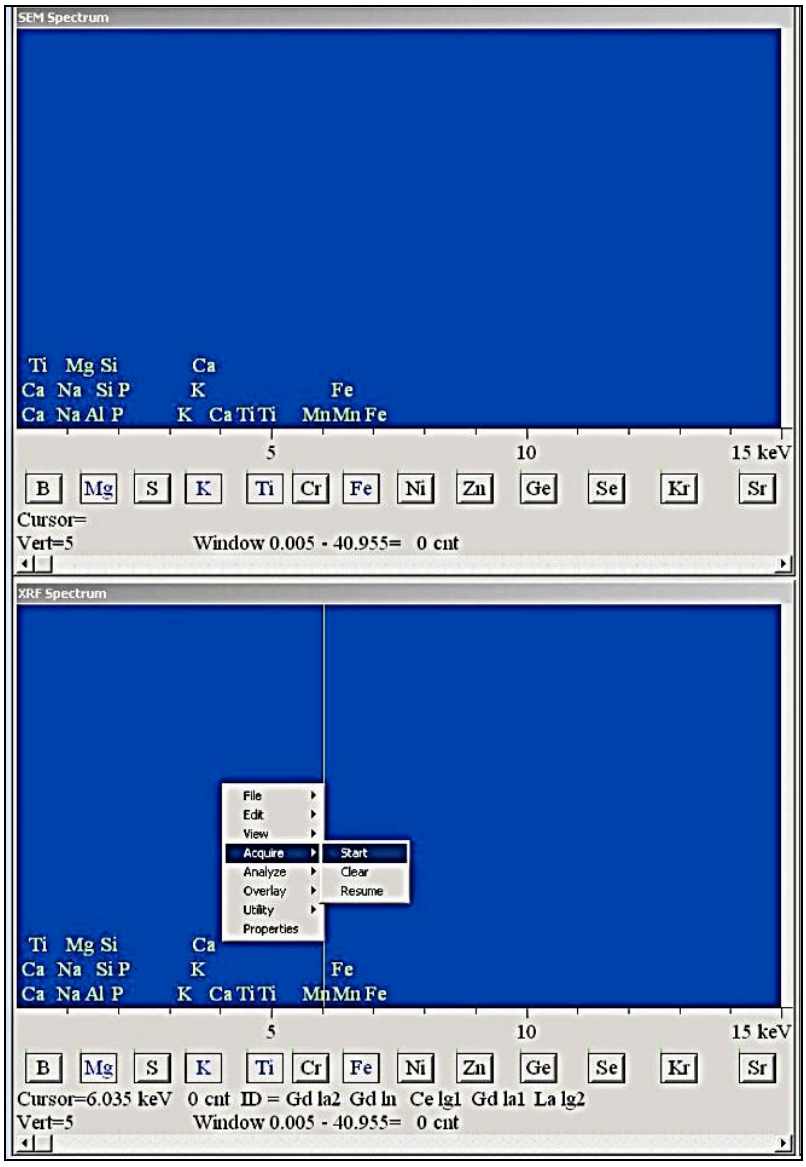

Right click on XRF spectrum window

- Select Acquire
- Click start

Make sure to close X-ray shutter when the run is done

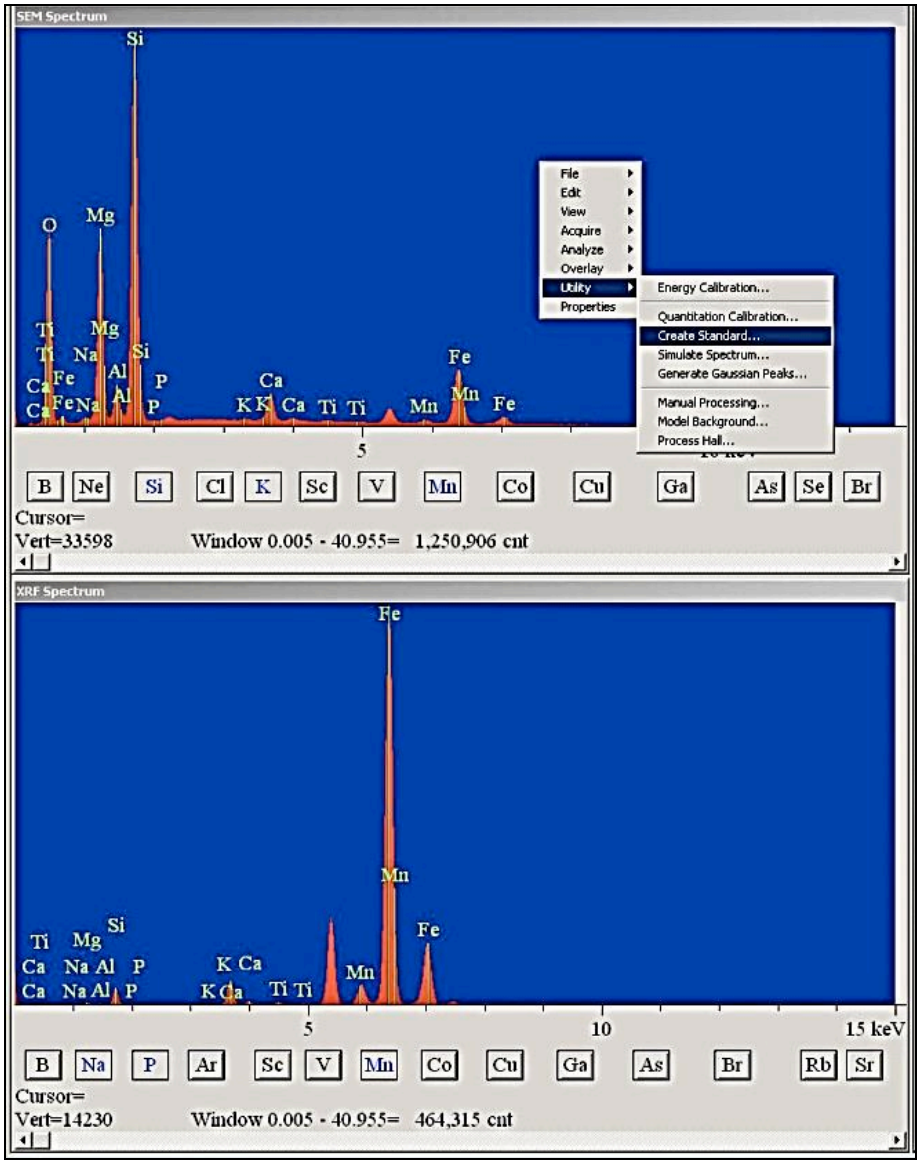

After all of the standard spectrums have been acquired, open them one by one and do the following to each of them:

- Right click SEM spectrum window
- Select Utility
- Select create standard
    - Add components and known normalized concentrations
    - Save as standard name_SEM.std and save as standard name_XRF.std
    - Do this for all of the standards

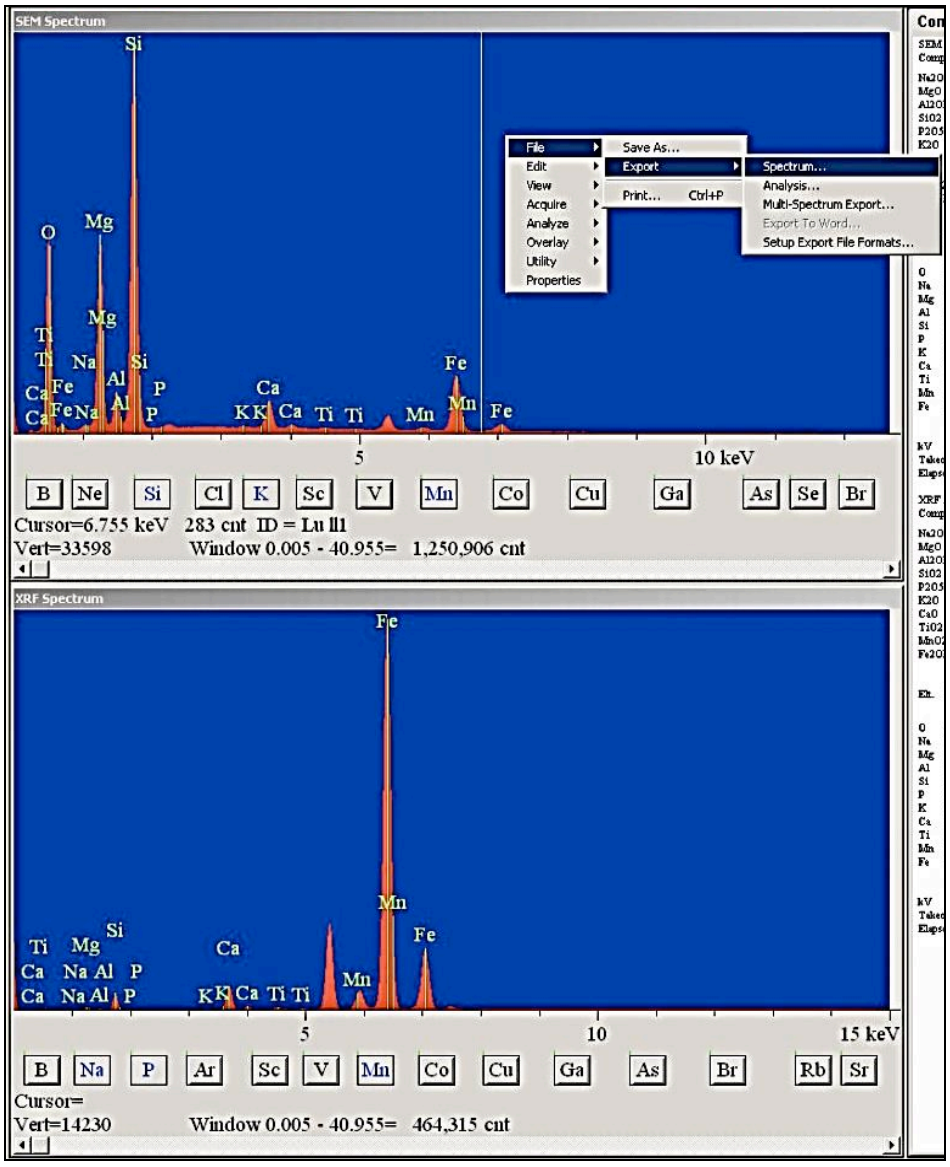

When done, right click SEM spectrum window

- Select file
  - Export
    - Spectrum

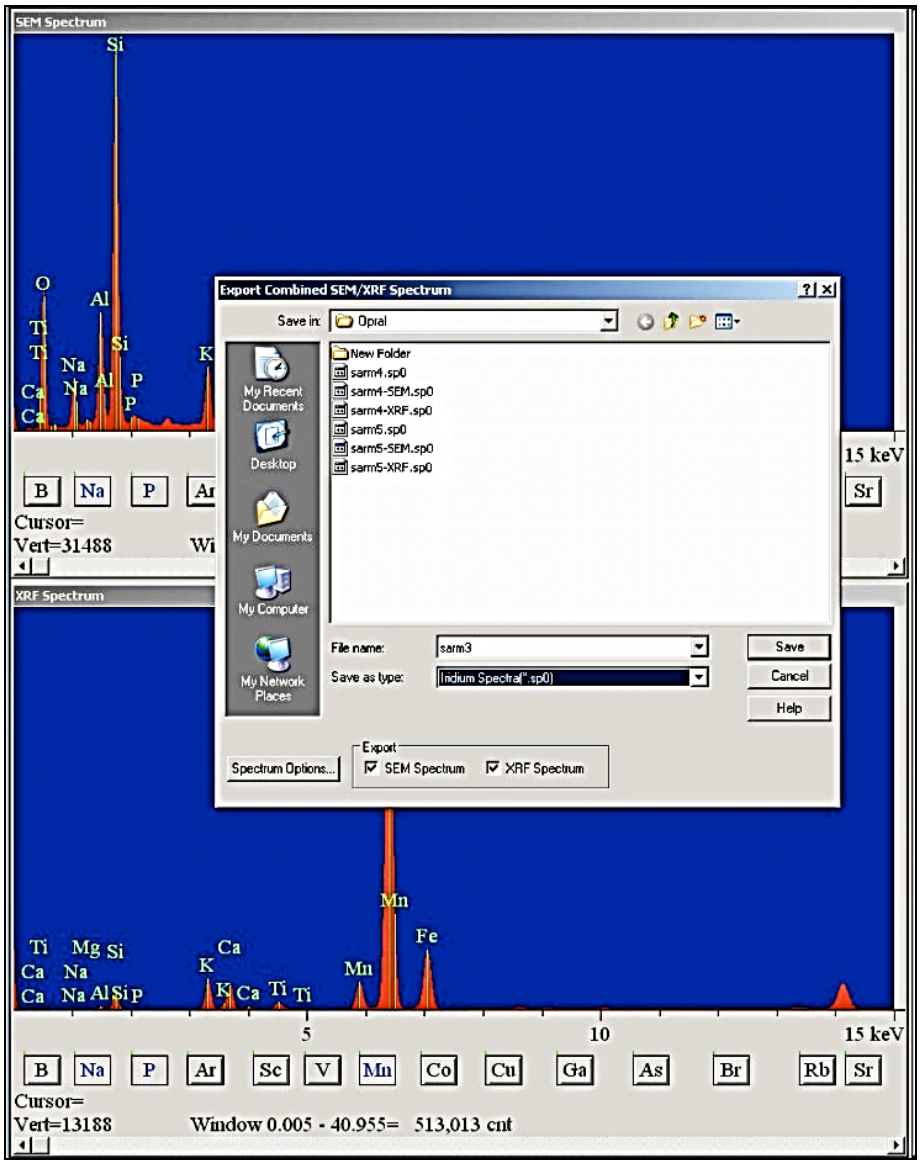

Save as

- Standard name
- Save as type: Iridium spectrum (*.spo)
- Select SEM spectrum and XRF spectrum under export
- Do this for all standards

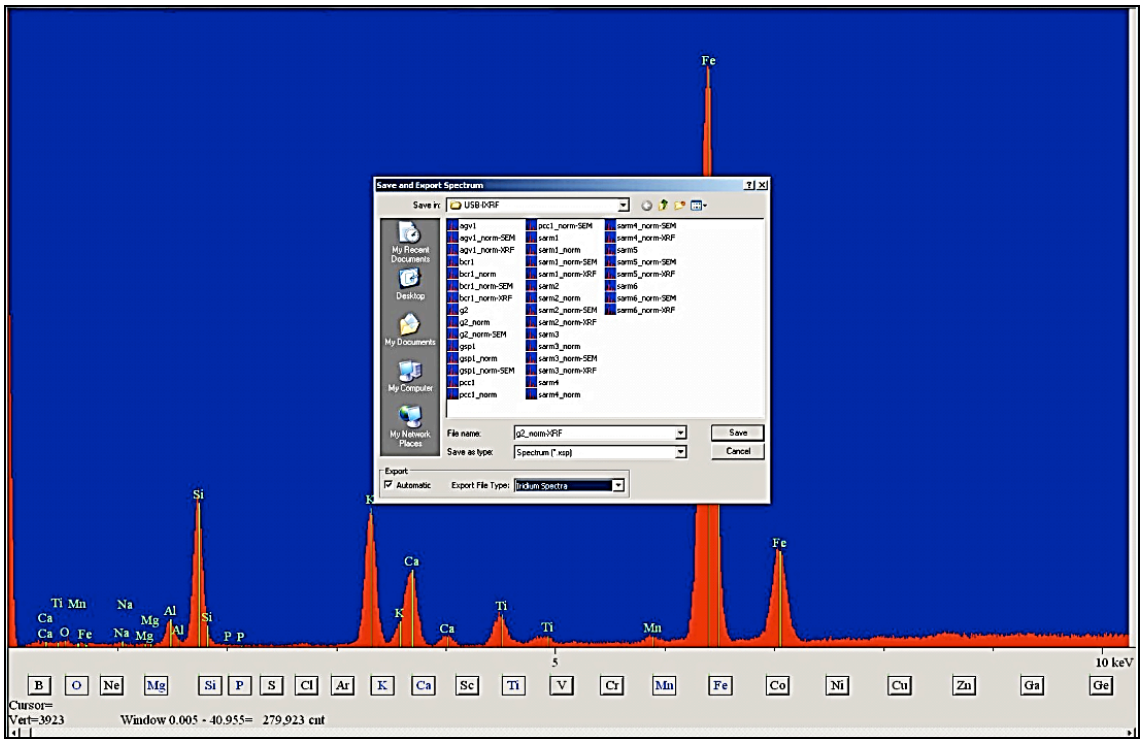

Open all SEM and XRF .spo files as spectrum one by one

- Right click spectrum and select properties
- Under quantitation tab
- Select none for method
- Enter (F) for lightest Analyte
- Enter 25.0 for kV
- Close properties, then right click spectrum
- Select Analyze, then select quantify
- Save as spectrum (*.xsp) files
- Do this for all standard SEM and XRF spectrums

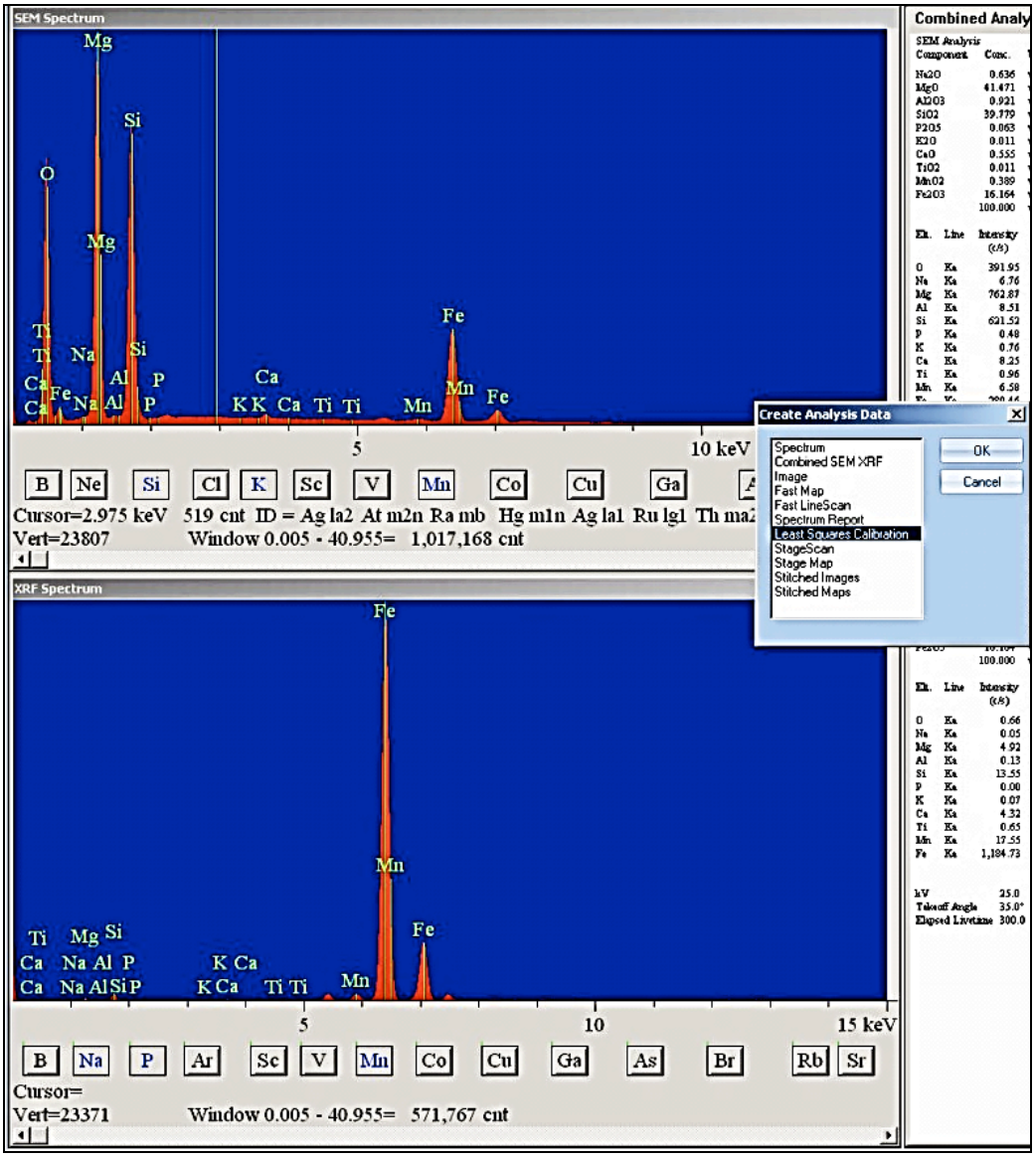

When done, open new Least Squares Calibration

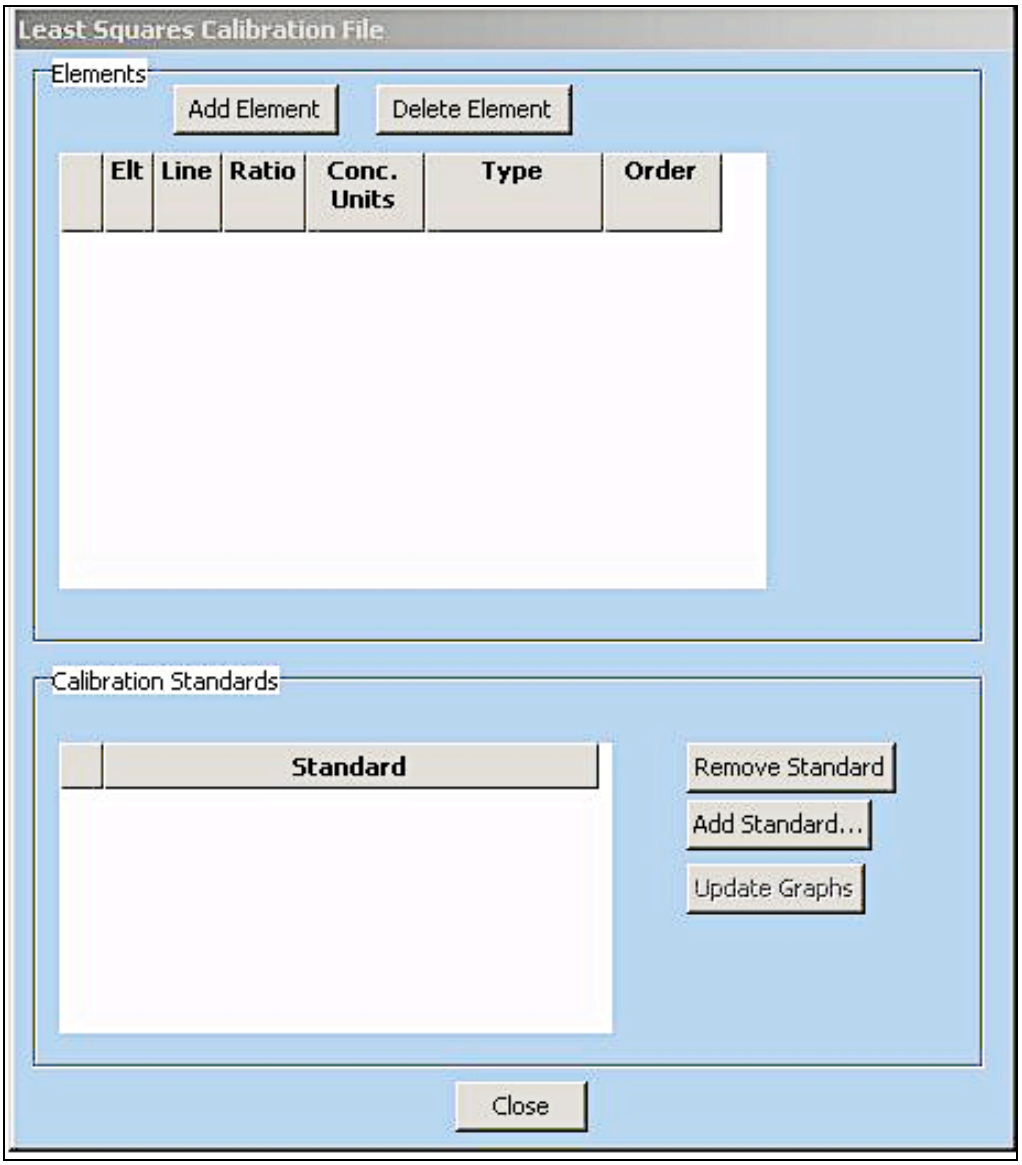

Add standards for SEM or XRF

- Add or delete elements according to the calibration preferences
- Ex. SEM elements – Na, Mg, Al, Si, P
- Ex. XRF elements – K, Ca, Mn, Fe, Ti
- Crossover of maximum sensitivity between EDS and XRF is at about 2 keV (or at Phosphorous)

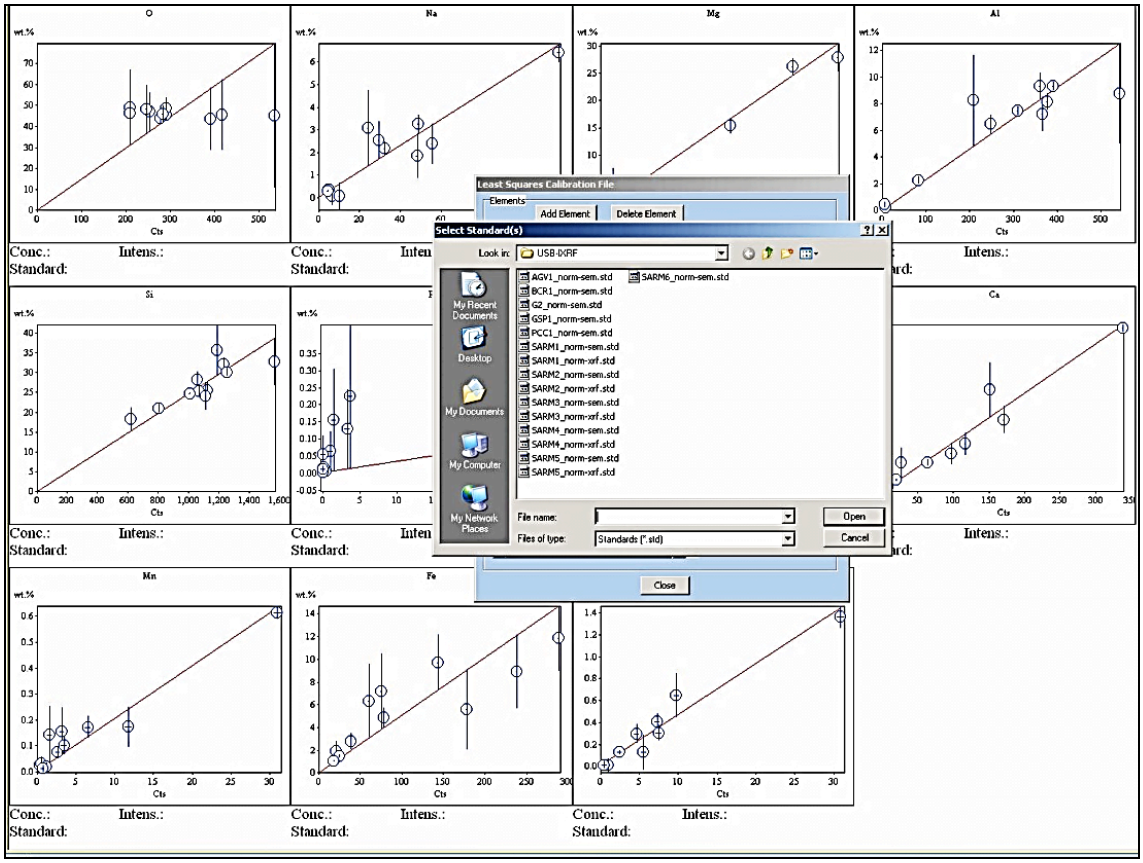

Save Least Squares Calibration

- One for SEM and for XRF

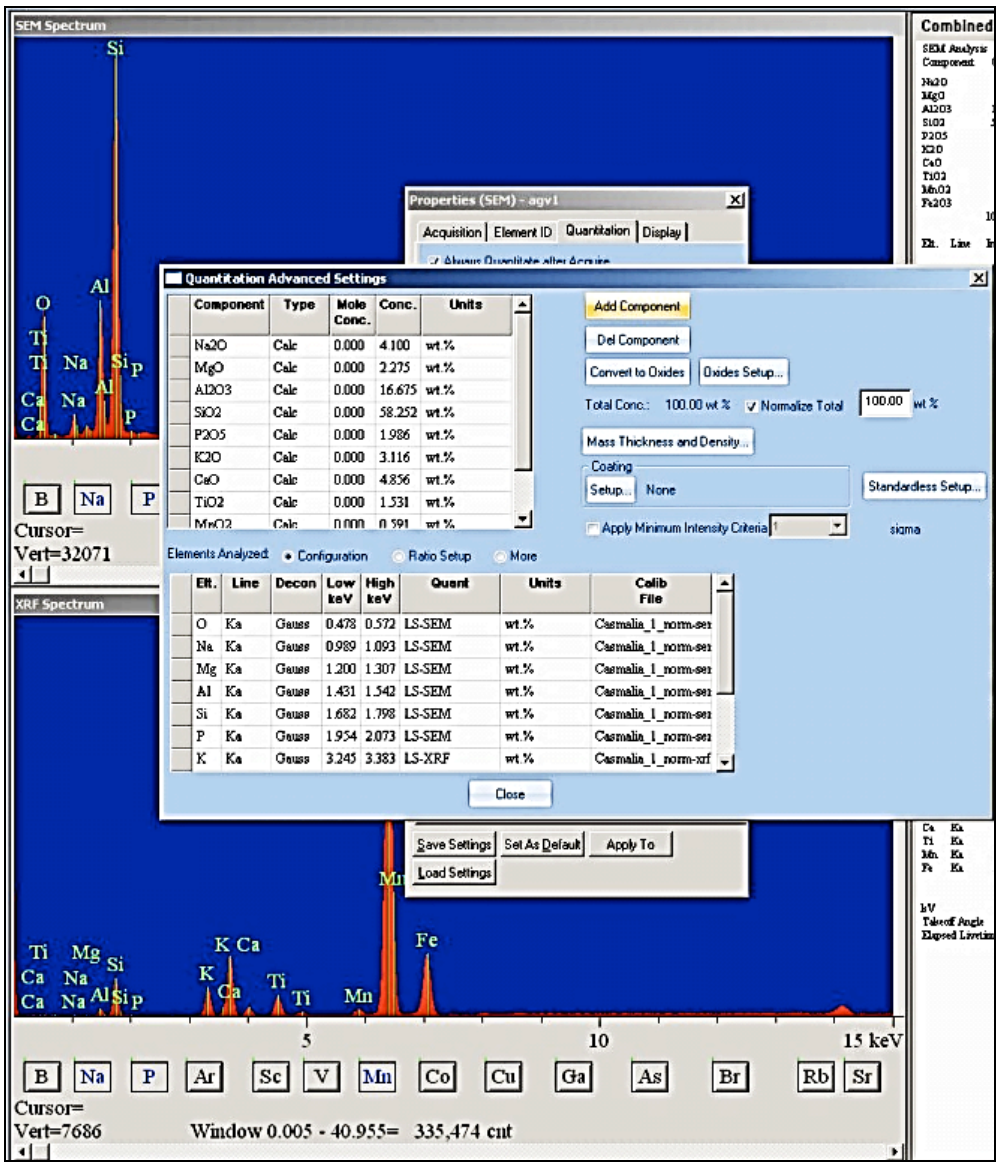

Close Least Squares Calibration window

- Open a standard spectrum
- Right click spectrum, select properties
- Click quantitation tab
- Select LS-SEM for method
- Open Advanced under method
- For each element select LS-SEM or LS-XRF and select the corresponding least squares calibration file
- Select none for the element Oxygen
    - Since elemental concentrations will be converted to oxides
- When done close and click save setting as
- Chose a file name

To Analyze unknown samples with new Least Squares Calibration

Using Iridium Ultra Software

Open a new combined SEM/XRF spectrum (Make sure all adjustments have been made on the xT microscope Control and the High Voltage is activated)
Adjust spot size on the xT microscope control until the dead time is ~27-30% in the green zone

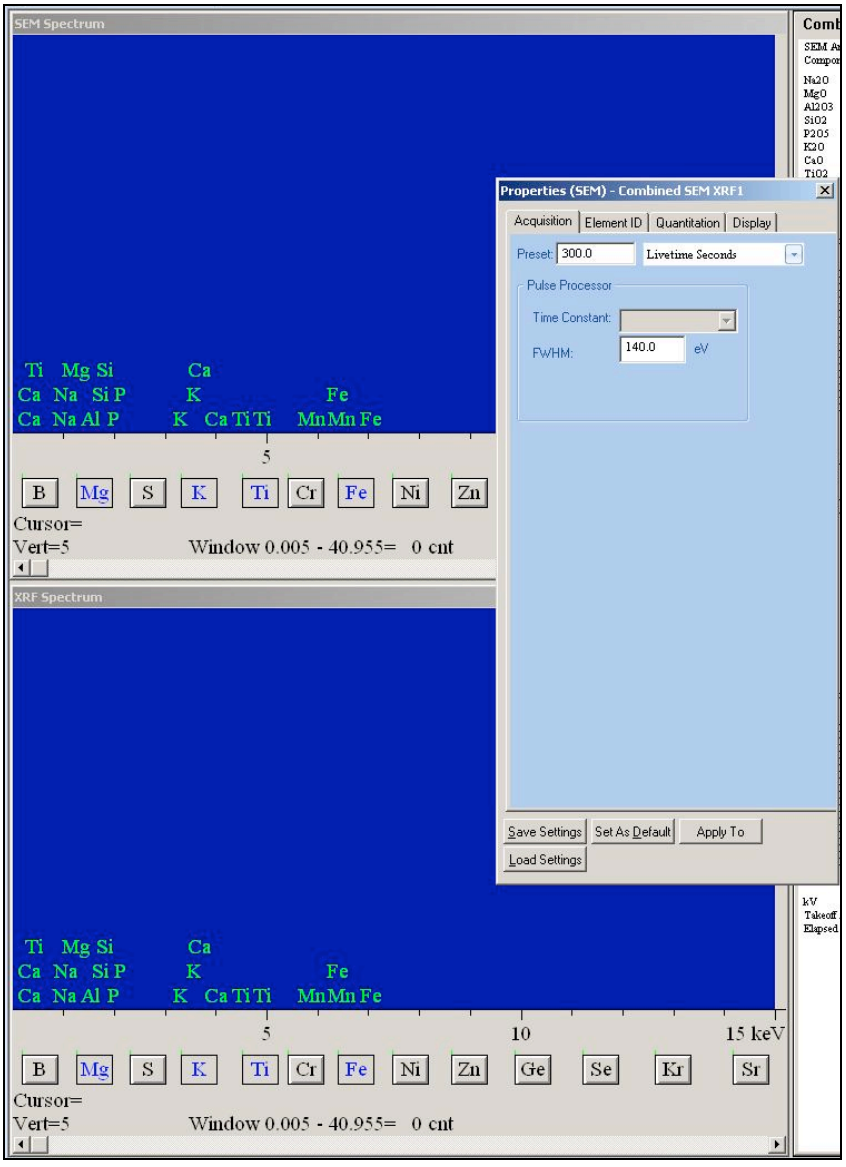

Right click on the SEM spectrum window.

- Select properties
- Click on Acquisition tab
- Enter 300.0 in preset for livetime seconds

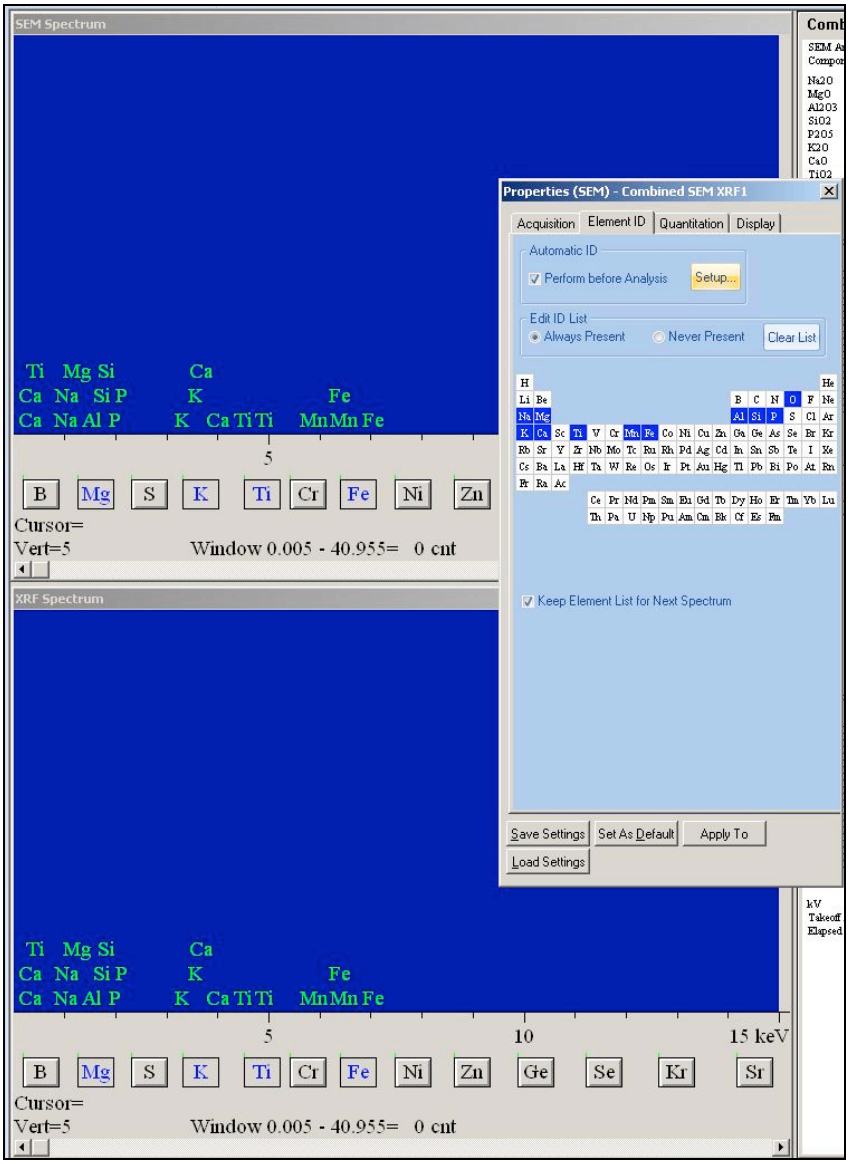

Click on Element ID tab

- Select desired elements on the periodic table

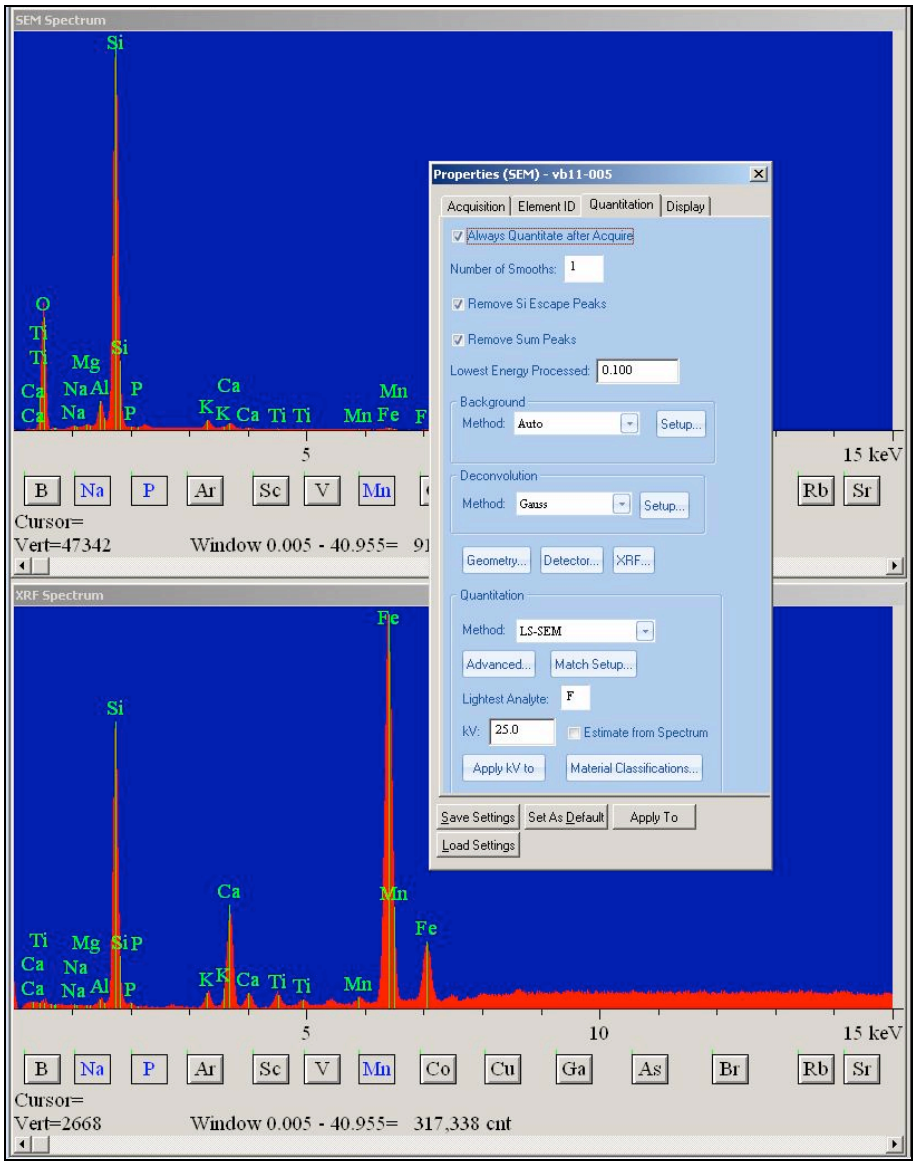

Click on Quantitation tab

- Select LS-SEM for method
- Enter (F) for Lightest Analyte
- 25.0 for kv
- Select Load settings
    - Open newly created setting file
- Close properties
- Do the same for the XRF spectrum window

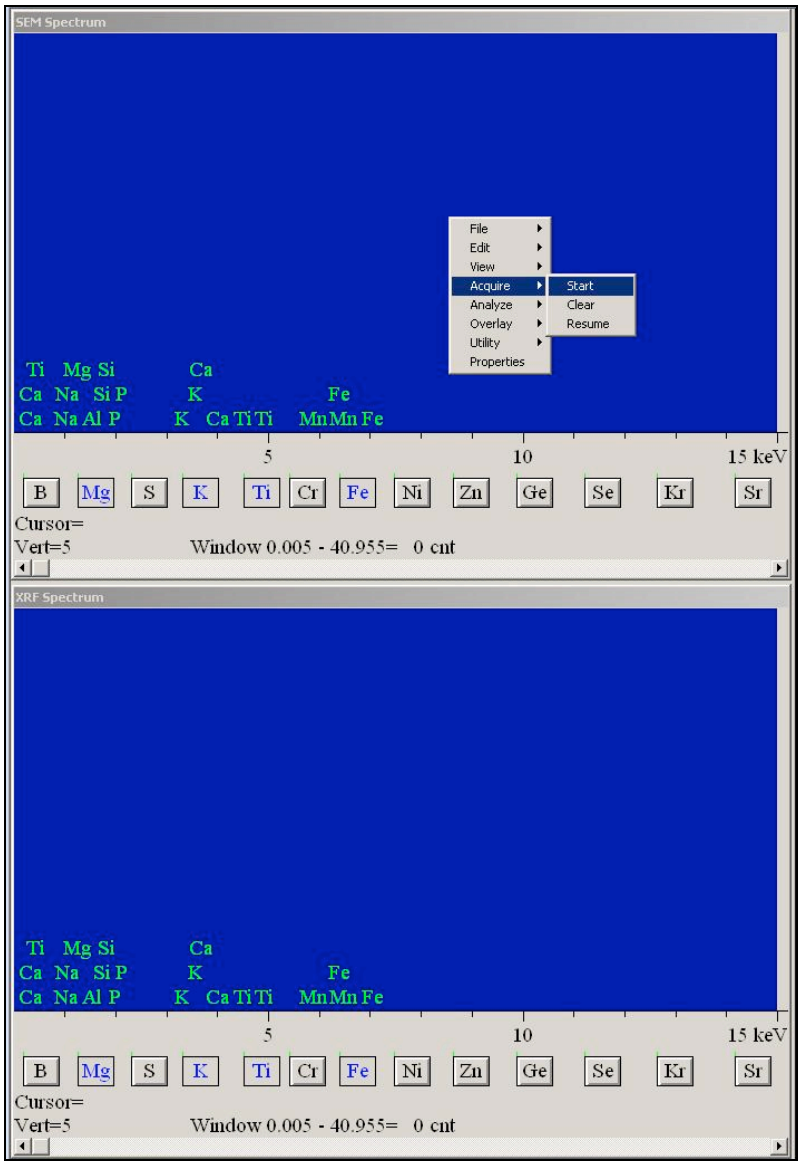

Right click on SEM spectrum window

- Select Acquire
- Click start

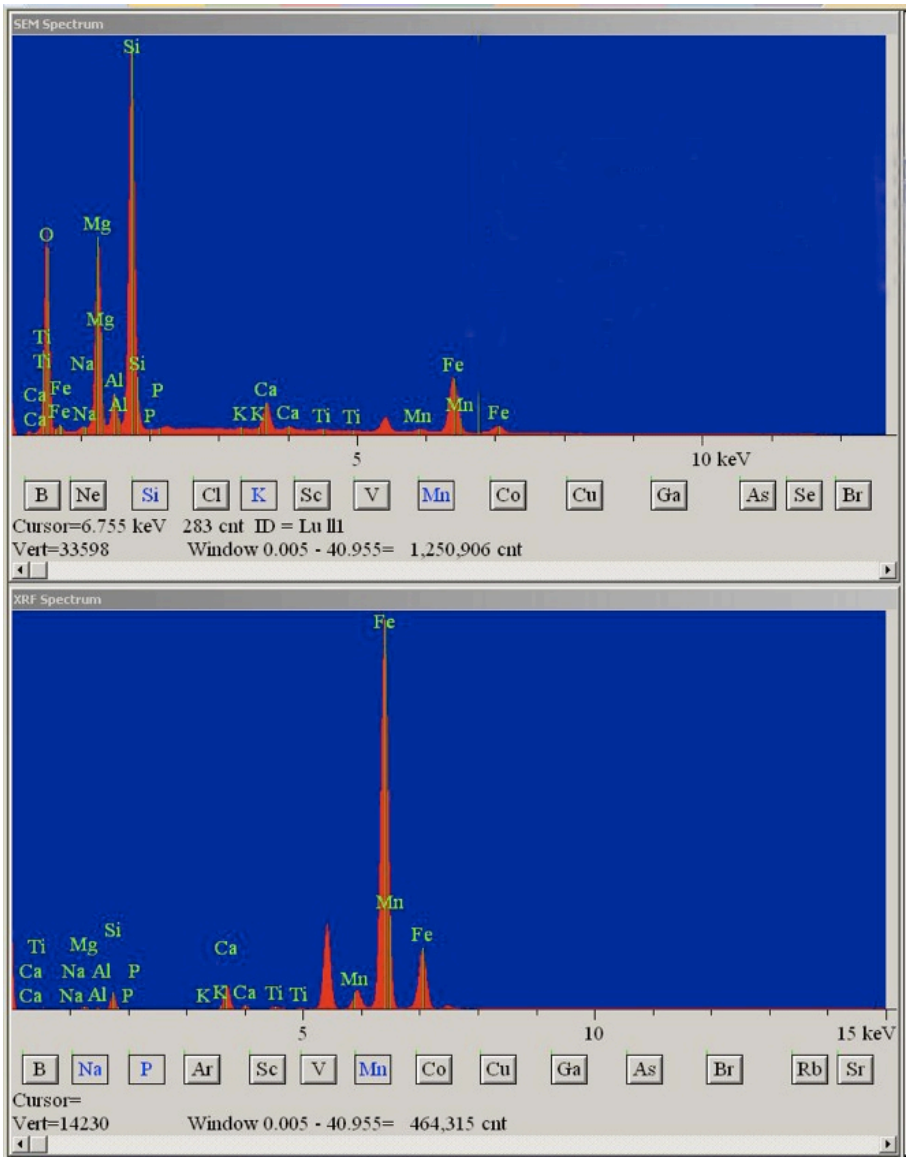

After the acquisition is complete

- Turn off the HV and make sure all windows are paused (CCTV)
- Open the X-ray shutter
- Right click the XRF spectrum window
    - Select Acquire
    - Click start

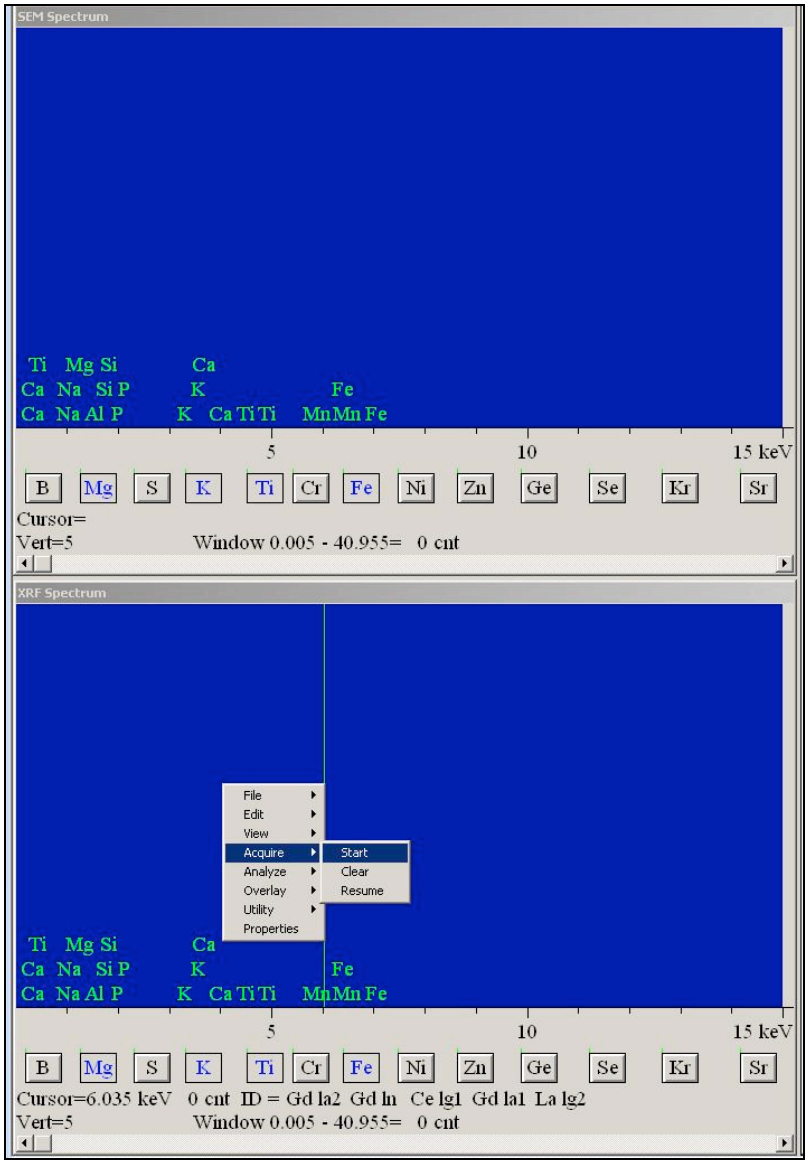

Right click on XRF spectrum window

- Select Acquire
- Click start
- When done close X-ray shutter

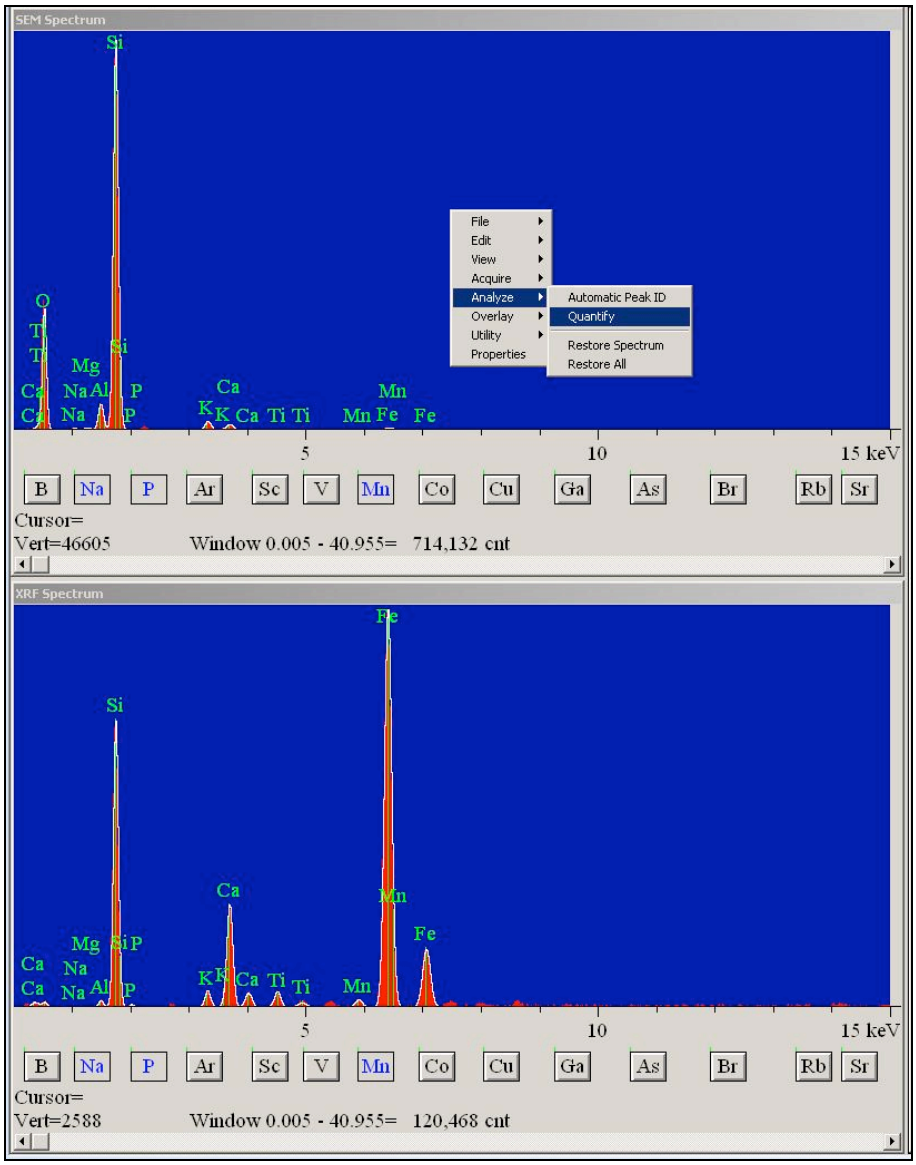

When done right click spectrum

- Select Analyze
- Select Quantify

APPENDIX C

CALIBRATION ERROR

The follow section shows calibration quality control graphs of CSULB combined EDS/XRF results blind tested by comparison with independent ICP analysis by Activation Laboratories Ltd., Canada (Actilabs).

Samples and Standards (Note Scales Vary)

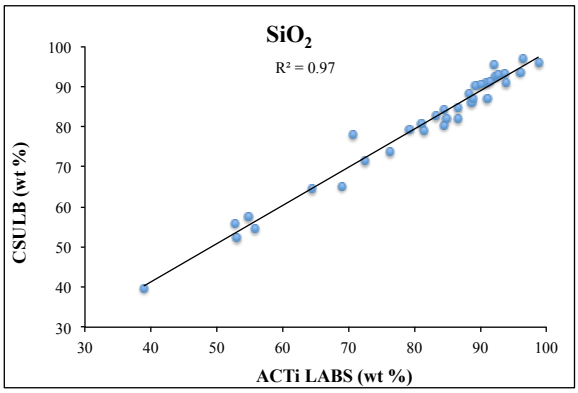

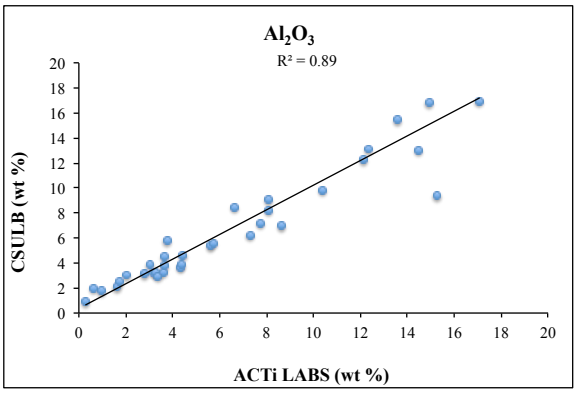

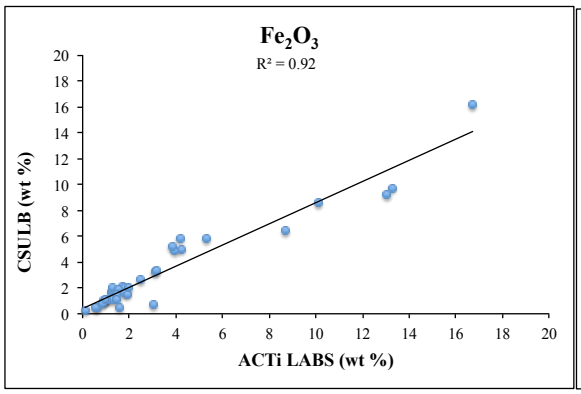

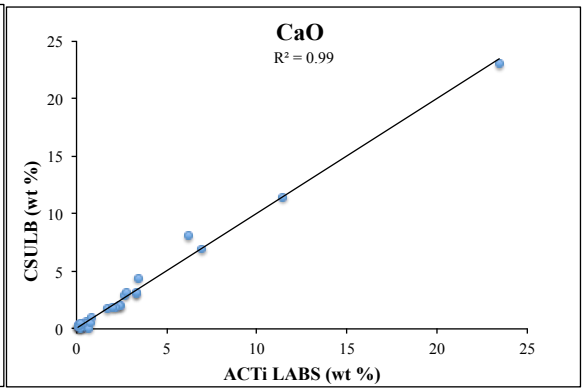

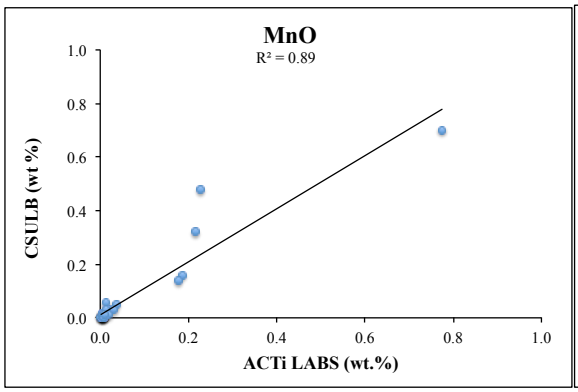

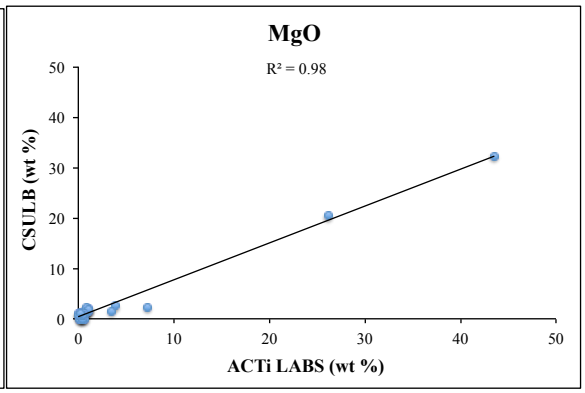

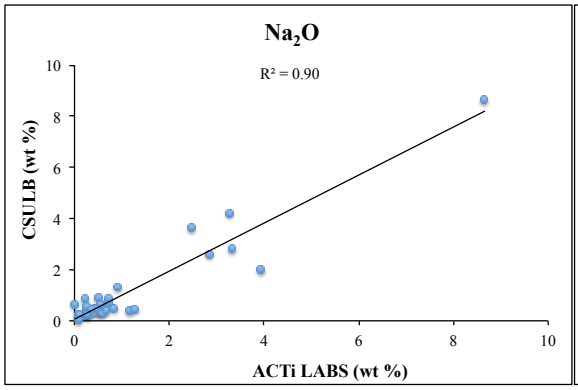
Na2O
R² = 0.90
CSULB (wt %)
ACTi LABS (wt %)
0
2
4
6
8
10

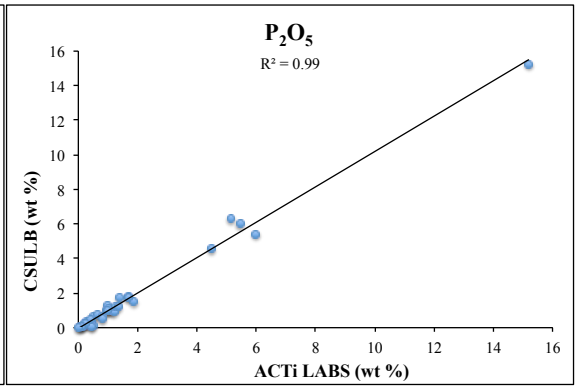
P2O5
R² = 0.99
CSULB (wt %)
ACTi LABS (wt %)
0
2
4
6
8
10
12
14
16

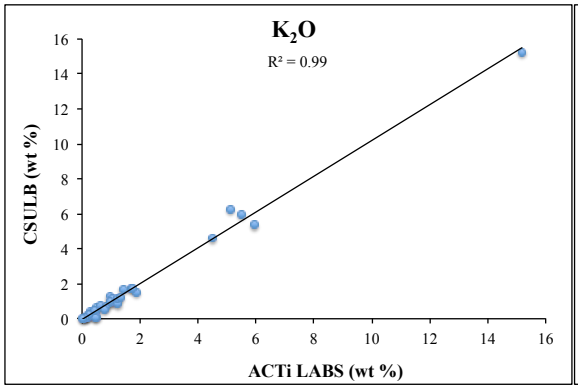
K2O
R² = 0.99
CSULB (wt %)
ACTi LABS (wt %)
0
2
4
6
8
10
12
14
16

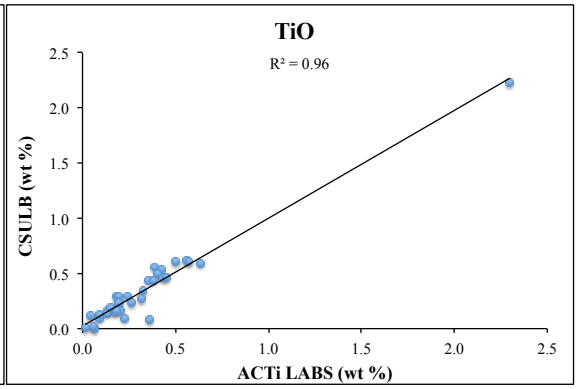
TiO
R² = 0.96
CSULB (wt %)
ACTi LABS (wt %)
0.0
0.5
1.0
1.5
2.0
2.5

REFERENCES

REFERENCES

Activation Laboratories Ltd., 2013, Code 4B ICP http://www.Actlabs.com, (accessed 07/2013)

Arnold, R., and Anderson, R., 1907, Geology and Oil Resources of the Santa Maria Oil District, Santa Barbara County, California, No. 322, US Government Printing Office

Atwater, T.M., 1970, Implications of Plate Tectonics for the Cenozoic Tectonic Evolution of Western North America, Geological Society of America Bulletin, V. 81, p. 3513-3536.

Barron, J.A., 1986; Paleooceanographic and Tectonic Controls on Deposition of the Monterey Formation and Related Siliceous Rocks in California, Palaeogeography, Palaeoclimatology, Palaeoecology, V. 53, p. 27-45

Behl, R.J., Herzig, C.T., Singley, S.P., Deason, C.T., Hill, P.S., and Katsuk, O.K., 2003, The Monterey Formation of Coastal Orange County, California: Preliminary Sedimentologic and Diagenetic Findings, AAPG Pacific Section/SPE Western Regional Joint Meeting, Long Beach, California

Behl, R. J. and Garrison, R.E., 1994, The Origin of Chert in the Monterey Formation of California (USA), Siliceous, Phosphatic and Glauconitic Sediments of the Tertiary and Mesozoic: Proceedings of the 29th International Geological Congress, Part C, p. 101-132

Behl, R.J. and Ramirez, P.C., 2000, Field Guide to the Geology of the Neogene Santa Maria Basin, From Rift to Uplift, the Pacific Section SEPM, Book 86, p. 1-26

Behl, R.J. and Smith, B.M., 1992, Silicification of Deep-Sea sediments and the Oxygen Isotope composition of Diagenetic Siliceous rocks from the Western Pacific, Pigafetta and East Mariana basins, Leg 129, *in Proceedings of the Ocean Drilling Program, Scientific Results*, V. 129, p. 81-117

Behl, R J. and Meike, A., 1990, Cryptocrystalline Relationships of Silica Phases in Cherts, Particulate Science and Technology, V. 8, p. 111-122

Behl, R.J. and Morita, S., 2007, The Monterey Formation of the Palos Verdes Hills, California: Stratigraphy and Diagenetic Implications for Burial and Uplift History, p.1-22

Bramlette, M.N., 1946, The Monterey Formation of California and the Origin of its Siliceous Rocks, Geological Survey, Professional Paper 212, p. 1-55

Brueckner, H.K., and Snyder, W.S., 1985, Chemical and Sr-Isotopic Variations During Diagenesis of Miocene Siliceous Sediments of the Monterey Formation, California, Journal of Sedimentary Petrology, V. 55, No. 4, p. 553-568

Dibblee, T.W., 1989a, Geologic Map of the Point Sal and Guadalupe Quadrangles, Santa Barbara County, California, Dibble Geological Foundation Map DF-25, scale 1:24,000

Dibblee, T.W., 1989b, Geologic Map of the Casmalia and Orcutt Quadrangles, Santa Barbara County, California, Dibble Geological Foundation Map DF-24, scale 1:24,000

Dunham, J.B. and Blake, G.H., 1987, Guide to Coastal Outcrops of the Monterey Formation of Western Santa Barbara County, California; Pacific Section SEPM, Book 53, p. 1-36

Ernst, W.G. and Calvert, S.E., 1969, An Experimental Study of the Recrystallization of Porcelanite and its Bearing on the Origin of some Bedded Cherts, Am. Jour. Sci., V. 267A, p. 114-133

Eichhubl, P. and Behl, R. J., 1998, Diagenesis, Deformation, and Fluid Flow in the Miocene Monterey Formation, *In* Eichhubl, P., ed., 1998, Diagenesis, Deformation, and Fluid Flow in the Miocene Monterey Formation: Pacific Section SEPM Special Publication, Book 83, p. 5-13

Hein, J.R., 1978, Fine-Grained Siliceous Deposits: Hosts for Multifarious Mineral Deposits, *In* Siliceous Sedimentary Rock-Hosted Ores and Petroleum, p. 3-9

Hein, J.R. and Scholl, D.W., 1978, Diagenesis and Distribution of Late Cenozoic Volcanic Sediment in the Southern Bering Sea, Geological Society of America Bulletin, V. 89, p. 197-210

Hein, J.R. and Parrish, J.T., 1987, Distribution of Siliceous Deposits in Space and Time, *In* Siliceous Sedimentary Rock-Hosted Ores and Petroleum, p. 10-25

Hesse, R., 1988, Diagenesis #13. Origin of Chert: Diagenesis of Biogenic Siliceous Sediment, Geoscience Canada, V. 15, Number 3, p. 171- 92

Hesse, R. and Schacht, 2011, Early Diagenesis of Deep-Sea Sediments, *In* Heiko Hüneke and Thierry Mulder, editors: *Developments in Sedimentology*, V. 63, p. 557-713

Hinman, N.W., 1990, Chemical Factors Influencing the Rates and Sequences of Silica Phase Transitions: Effects of Organic Constituents *Geochemimica et Cosmochimica Acta*, V. 54, p. 1563-1574

Hinman, N.W., 1998, Sequences of Silica Phase Transitions: Effects of Na, Mg, K, Al, and Fe ions, Marine Geology, V. 147, p. 13-24

Hurst, R.W., 1992, Geochemical and Isotopic Constraints on Silica and Carbonate Diagenesis in the Miocene Monterey Formation, Santa Maria and Ventura basins, California, In Diagenesis III: Developments in Sedimentology, V. 47, p. 387-425

Iijima, A. and Tada, R., 1981, Silica Diagenesis of Neogene Diatomaceous and Volcaniclastic Sediments in Northern Japan, Sedimentology, V. 28, p. 185-200

Iijima, A., Hein, J.R, and Siever R., 1983, An Introduction to Siliceous Deposits in the Pacific Region, in Siliceous Deposits in the Pacific Region, Developments in Sedimentology, V. 36, p. 1-6

Iijima, A. and Tada, R., 1983, Petrology and Diagenetic changes of Neogene Siliceous Rocks in Northern Japan, Journal of Sedimentary Petrology, V. 53, No. 3, p. 0911-0930

Iijima, A., 1988, Diagenetic Transformations of Minerals as Exemplified by Zeolites and Silica Minerals–Japanese, Part II. Silica Diagenesis, In Diagenesis II: Developments in Sedimentology, V. 43, p. 189-211

Iler, R.K, 1979, Chemistry of Silica: New York, Wiley-Interscience, p. 866

Isaacs, C.M., 1980, Diagenesis in the Monterey Formation Examined Laterally Along the Coast near Santa Barbara, California United States Department of the Interior-Geological Survey, Open-File Report 80-606, p. 1-308

Isaacs, C.M., 1981a, Lithostratigraphy of the Monterey Formation, Goleta to Point Conception, Santa Barbara Coast, California, Pacific Section AAPG, V. 52, p. 9-23

Isaacs, C.M., 1981b, Outline of Diagenesis in the Monterey Formation Examined Laterally Along the Santa Barbara Coast, California, Pacific Section AAPG, V. 52, p. 25-38

Isaacs, C.M., 1981c, Field Characterization of Rocks in the Monterey Formation Along the Coast near Santa Barbara, California, Pacific Section AAPG, V. 52, p. 39-53

Isaacs, C.M., 1983, Compositional Variation and Sequence in the Miocene Monterey Formation, Santa Barbara Coastal Area, California: *in* Larue, D.K. and Steel, R.J., eds., Cenozoic Marine Sedimentation, Pacific Margin, USA. Pacific Section Society for Sedimentary Geology Special Publication, p. 117-132.

Isaacs, C.M., Garrison, R.E., Graham, S.A., and Jensky, W.A. II, 1983, Preliminary Evaluation of Miocene Lithostratigraphy in the Point Conception Cost Well OCS-CAL 78-164 No.1, Off Southern California, in Petroleum Generation and Occurrence in the Miocene Monterey Formation, California, PS-SEPM, p. 99-110

Isaacs, C M. and Petersen, N.F., 1987, Petroleum in the Miocene Monterey Formation, California, (In Hein, James R, et al. Siliceous Sedimentary Rock-Hosted Ores and Petroleum), p. 83-116

Ingle, J .C.Jr., 1973, Neogene Foraminifera from the Northeastern Pacific Ocean, Leg l8, Deep Sea Drilling Project, Initial Report Deep Sea Drilling Project, V. l8, p. 517-567

Ingle, J. C.Jr., 1981, Cenozoic Depositional History of the Northern Continental Borderland of Southern California and the Origin of Associated Miocene Diatomites, Pacific Section AAPG, V. 52, p. 1-8

Jones, J.B. and Segnit, E.R., 1971, The Nature of Opal I. Nomenclature and Constituent Phases, Journal of the Geological Society of Australia, V. 18, Issue 1, p. 57-68

Jones, J.B. and Segnit, E.R., 1972, Genesis of Cristobalite and Tridymite at Low Temperatures, Journal of the Geological Society of Australia, V. 18, Pt. 4, p. 419-422

Kamatani, A. and Riley, J.P., 1979, Rate of Dissolution of Diatom Silica Walls in Seawater, *Mar Biol*, V. 55, p. 29-35

Kamatani, A. and Riley, J.P., and Skirrow, G., 1980, The Dissolution of Opaline Silica of Diatom Tests in Seawater, *J Oceanogr Soc Jpn*, V. 36, p. 201-208

Kamatani, A., 1982, Dissolution Rates of Silica from Diatoms Decomposing at Various Temperatures, *Mar Biol*, V. 68, p. 91-96

Kassa, T. and Behl, R.J., 2014, Pore Structure of Opal-CT and Quartz Phase Porcelanites, Monterey Formation, California, *in* Pacific Section AAPG, SPE, and SEPM Joint Technical Conference, Bakersfield, California

Kastner, M., Keene, J.B., and Gieskes, J.M., 1977, Diagenesis of siliceous oozes-I. Chemical Controls on the Rate of Opal-A to Opal-CT Transformation–an Experimental Study, Geochimica et Cosmochimica Acta, V. 41, p. 1041-1059

Kastner, M., 1979, Silica Polymorphs, in Marine Minerals, Mineralogic Society of America- Short course notes, V. 6, p. 99-109

Kastner, M. and Gieskes, J.M., 1983, Opal-A to Opal-CT Transformation: A Kinetic Study, in Siliceous Deposits in the Pacific Region, Developments in Sedimentology, V. 36, p. 211-227

Keller, M.A. and Isaacs, C.M., 1985, An Evaluation of Temperature Scales for Silica Diagenesis in Diatomaceous Sequences Including a New Approach Based on the Miocene Monterey Formation, California, Geo-Marine Letters, V. 5, p. 31-35

Keene, J.B., 1975, Cherts and Porcelanites from the North Pacific, Deep Sea Drilling Project Leg 32, in Larson, R.L., and others, eds., Initial Reports of the Deep Sea Drilling Project: Washington, D.C., U.S. Government Printing Office, V. 32, p. 429-507

Keene, J.B., 1976, Distribution, mineralogy and petrography of biogenic and authigenic silica in the Pacific Basin, unpub. Ph,d thesis, University of California at San Diego

Lawson, D. S., Hurd, D. C., and Pankratz, H. S., 1978, Silica Dissolution Rates of Phytoplankton Assemblages at Various Temperatures, *Am J Sci,* V. 278, p. 1373-1393.

Loucaides, S., 2009, Dissolution of Biogenic Silica: Roles of pH, Salinity, Pressure, Electrical Charging and Reverse Weathering Dissertation at Utrecht University, p. 13-125

MacKinnon, T.C., 1989, Petroleum geology of the Monterey Formation in the Santa Maria, *in: Oil in the California Monterey Formation, Field Trip Guidebook,* T.C. MacKinnon (Ed.), V. T311, p. 11-27

Martinez, R. and Caro, R.T., 1980, Microfosiles Siliceousde las Diatomitas de Tongoy, Provincia de Coquimbo, Chilei su Significado Biochronogeologica, Paleoecologico, Paleoecologico, y Paleogeografico, Rev. Geologica de Chila, no. 10, p. 33-53

McCrory, P.A., Barron, J.A., and Dumont, M.P., 1995, Neogene Geohistory Analysis of Santa Maria Basin, California, and its Relationship to Transfer of Central California to the Pacific Plate, U.S. Geological Survey Bulletin, Chapter J, p. 1-38

McLean, Hugh, 1991, Distribution and Juxtaposition of Mesozoic Lithotectonic Elements in the Basement of the Santa Maria Basin, California, U.S. Geological Survey Bulletin, 1995-B, p. 12

Mizutani, S., 1970, Silica Minerals in the Early Stage of Diagenesis, Sedimentology, V. 15, p. 419-436

Mizutani, S., 1977, Progressive Ordering of Cristobalitic Silica in the Early Stage of Diagenesis, Contributions to Mineralogy and Petrology, V. 61, p. 129-140

Murata, K.J. and Nakata, J.K, 1974, Cristobalitic Stage in the Diagenesis of Diatomaceous Shale, Science, V. 184, No. 4136, p. 567-568

Murata, K.J. and Larson, R.R., 1975, Diagenesis of Miocene Siliceous Shales, Temblor Range, California, Journal of Research of the U.S. Geological Survey, V. 3, No. 5, p. 553-566

Murata, K.J., Friedman, I., and Gleason, J.D., 1977, Oxygen Isotope Relations Between Diagenetic Silica Minerals in Monterey Shale, Temblor Range, California, American Journal of Science, V. 277, p. 259-272

Pisciotto, K.A, 1978, Basinal Sedimentary Facies and Diagenetic Aspects of the Monterey Shale, California, University of California, Santa Cruz, Unpublished Dissertation, p. 1-450

Pisciotto, K.A., 1981a, Notes on Monterey Rocks near Santa Maria, California, Pacific Section AAPG, Vol. 52, pg. 73-81

Pisciotto, K.A., 1981b, Diagenetic Trends in the Siliceous Facies of the Monterey Shale in the Santa Maria region, California, Sedimentology, V. 28, p. 547-571

Pisciotto, K.A., and Garrison, R.E., 1981, Lithofacies and Depositional Environments of the Monterey Formation, California, *in* Garrison, R. E., and Douglas, R. G., eds., The Monterey Formation and related siliceous Rocks of California: Los Angeles, Pacific Section, Society of Economic Paleontologists and Mineralogists, p. 97–122.

Schwalbach, J.R., Gordon, S.A., O'Brien, C.P., Lockman, D.F., Benmore, W.C., and Huggins, C.A, 2009, Reservoir Characterization of Monterey Formation Siliceous Shales: Tools and Applications, I*n* Contributions To The Geology Of The San Joaquin Basin, California, L. C. Knauer & A. Britton (eds.), Miscellaneous Publications 48, p. 233

Siever, R and Scott, R.A., 1963, Organic Geochemistry: Pergamin, New York

Siever, R., 1983, Evolution of Chert at Active and Passive Continental Margins, in Siliceous Deposits in the Pacific Region, Developments in Sedimentology, V. 36, p. 7-24

Stanley, R.G., Johnson, S.Y., Cole, R.B., Mason, M.A., Swisher, C.C., III, M.L., Thornton, Filewicz, M.V., Vork, D.R., Tuttle, M.C., and Obradovich, J.D., 1992, Origin of the Santa Maria basin, California, V.E. McKelvey Forum on Mineral and Energy Resources, U.S. Geological Survey Circular C-1074, p. 73.

Stamatakis, M.G., Kanaria-Sotiriou, R., and Spears, D.A., 1991, Authigenic Silica Polymorphs and the Geochemistry of Pliocene Siliceous Swamp Sediments of the Aridea Volcanic Province, Greece Canadian Mineralogist, V. 29, p. 587-598

Stein, C.L. and Kirkpatrick, R.J., 1976, Experimental Porcelanite Recrystallization Kinetics: A Nucleation and Growth Model, Jour. Sed. Petrology, V. 46, p. 430-435

Supko, P.R., 1971, Initial Reports of the Deep Sea Drilling Project, Volume 19-covering Leg 19 of the Cruises of the Drilling Vessel *Glomar Challenger*, p. 93-558

Tada, R., 1991, Origin of Rhythmical Bedding in Middle Miocene Siliceous Rocks of the Onnagawa Formation, Northern Japan, *Journal of Sedimentary Research,* V.61.7, p. 1123-1145.

Tucker, M.E., 2010, Sedimentary Petrology –An Introduction to the Origin of Sedimentary Rocks, Blackwell Science Ltd., Third Edition, p. 212-220

Tennyson, M.E. and Isaacs, C.M., 2001, Geologic Setting and Petroleum Geology of Santa Maria and Santa Barbara Basins, Coastal California, In the Monterey Formation from Rocks to Molecules, Columbia University Press, p. 207-240

Walther, J.V. and Helgeson, H.C., 1977, Calculation of the Thermodynamic Properties of Aqueous Silica and the Solubility of Quartz and its Polymorphs at High Pressures and Temperatures: Am. Jour. Sci., V. 277, p. 1315-1351

Willey, J.D., 1974, The Effect of Pressure on the Solubility of Silica in Seawater at 0°C: Marine Chem., V. 2, p. 239-250

Williams, L.A., Parks, G.A, and Crerar, D.A, 1985, Silica Diagenesis, I. Solubility Controls, Journal of Sedimentary Petrology, V. 55, No. 3, p. 0301-0311

Williams, L.A. and Crerar, D.A, 1985, Silica Diagenesis, II. General Mechanisms, Journal of Sedimentary Petrology, V. 55, No. 3, p. 0312-0321

Wise, S.W. and Kelts, K.R., 1972, Inferred Diagenetic History of a Weakly Silicified Deep-Sea Chalk, Trans. Gulf Coast. Assoc. Geol. Soc., V. 22, p. 177-203

Woodring and Bramlette, 1950, Geology and Paleontology to the Santa Maria District California, Geological Survey Professional Paper 222, p. 1-197

Van Cappellen, P. and Qiu, L., 1997a, Biogenic Silica Dissolution in Sediments of the Southern Ocean. I. Solubility, *Deep Sea Res* II 44, p. 1109-1128

Van Cappellen, P. and Qiu, L., 1997b, Biogenic Silica Dissolution in Sediments of the Southern Ocean. II. Kinetics, *Deep Sea Res II* 44, p. 1129-1149

Volosov, A.G., Khodakovskiy, I.L., and Ryzhenko, B.N., 1972, Equilibria in the System SiO_2-H_2O at Elevated Temperature Along the Lower Three-Phase Curve, Geochem. Internatl., V. 9, p. 362-377